# MASTER OF SCIENCE

## Profiling the activity of GPR55 antagonists against recombinant and endogenous GPR55

Haugh, Orla

*Award date:*
2015

# Profiling the activity of GPR55 antagonists against recombinant and endogenous GPR55

**Orla Haugh**

A thesis submitted to the University of Dundee for the degree of Master of Science by Research in Medicine, April 2015.

## Table of Contents

## List of Tables and Figures

# Acknowledgments

I would like to express my utmost gratitude to my supervisor Dr. Andrew Irving for his expertise, guidance and encouragement throughout this very engaging project.

A special thank you goes to Professor Veronica Campbell of Trinity College Dublin, Ireland, who provided me with a placement opportunity within her lab during this research project. This placement proved to be an invaluable learning experience. I look forward to working with her again during the next stage of my postgraduate career.

I wish to express my gratitude to Professor Tapio Nevalainen of the University of Eastern Finland and his research group for providing me with the synthetic GPR55 agonist used in this study.

The assistance provided by Cullen McCulloch in obtaining some of the results detailed in this thesis is gratefully acknowledged and appreciated.

I would like to express my sincere gratitude to my present and past colleagues in the Irving lab, Dr. June Penman and Dr. Mónica Tapia Pacheco respectively. Their support and guidance throughout this research project has been invaluable and very much appreciated.

A special thank you extends to members of Dr. Jenni Harvey's lab – Gemma McGregor, Yasaman Malekizadeh and Dr. Mary Palmer. Your company has been an absolute pleasure.

Lastly, I would like to thank my family for their never-ending support while I engaged in this new venture.

# Declaration

I declare that I am the author of this thesis. All references cited have been consulted by me unless otherwise stated. I have conducted all of the work that is described in this thesis and this work has not been previously accepted for a higher degree.

Signed

Orla Haugh

# Summary

GPR55 is a putative novel cannabinoid receptor that is capable of being activated by a subset of cannabinoid ligands and the endogenous lipid, L-α-lysophosphatidylinositol (LPI). GPR55 mRNA is expressed widely throughout the body, particularly in the brain, bone and immune tissue, and is also expressed at high levels in certain types of tumour. Understanding the physiological and pathological role of GPR55 has been challenging due to the absence of selective pharmacological tools. However, novel antagonists have recently been developed, allowing for the determination of GPR55-selective effects. The objective of the present study was to utilise molecular imaging techniques to evaluate the effectiveness of two previously published novel GPR55 antagonists on LPI-mediated GPR55 responses, in a HEK293 cell line stably expressing GPR55 (hGPR55-HEK293) and also in a prostate cancer cell line that expresses GPR55 endogenously at high levels (DU145). Antagonist effectiveness was also examined in a neuronal model of Alzheimer's disease (AD). The effects of the antagonists on LPI-mediated calcium ($Ca^{2+}$) responses and cAMP-response element-binding protein (CREB) phosphorylation were evaluated. In hGPR55-HEK293 cells, treatment with antagonists at varying concentrations did not have an effect on intracellular $Ca^{2+}$ levels or alter CREB phosphorylation when applied alone. However, both inhibited increases in $Ca^{2+}$ signal induced by GPR55 agonists when applied at 3 $\mu$M. Overall, this data suggests that the GPR55 antagonists are active in *in vitro* models that over-express GPR55. Such pharmacological tools will help to advance the research on the physiological function of GPR55.

# Abbreviations

| | |
|---|---|
| **$\mu$M** | micromolar |
| **Aβ** | β-amyloid |
| **AD** | Alzheimer's disease |
| **AM251** | 1-(2,4-dichlorophenyl)5-(4-iodophenyl)-4-methyl-*n*-(1-piperidyl)pyrazole-3-carboxamide |
| **ARA-S** | N-arachidonoyl-serine |
| **C390-0219 (CID16020046)** | 4-[4-(3-hydroxyphenyl)-3-(4-methylphenyl)-6-oxo-1H,4H,5H,6H-pyrrolo[3,4-c]pyrazol-5-yl] benzoic acid |
| **$Ca^{2+}$** | calcium |
| **$[Ca^{2+}]_i$** | intracellular calcium |
| **CaMK** | $Ca^{2+}$-calmodulin-dependent protein kinase |
| **$CB_1$** | Cannabinoid receptor type 1 |
| **$CB_1^{-/-}$** | Cannabinoid receptor type 1 knockout |
| **$CB_2$** | Cannabinoid receptor type 2 |
| **$CB_2^{-/-}$** | Cannabinoid receptor type 2 knockout |
| **CBD** | cannabidiol |
| **$CO_2$** | carbon dioxide |
| **$cPLA_2$** | cytosolic phospholipase $A_2$ |
| **CP55,940** | 2-[(1r,2r,5r)-5-hydroxy-2-(3-hydroxypropyl) cyclohexyl]-5-(2-methyloctan-2-yl)phenol |
| **CRE** | cyclic-AMP binding response element |
| **CREB** | cyclic-AMP binding response element binding protein |

| | |
|---|---|
| **D327-0013 (ML191/ CID23612552)** | (3-[1-[1-(4-methylphenyl)cyclopropanecarbonyl]piperidin-4-yl]-5-phenyl-1,3,4-oxadiazol-2-one), |
| **DAG** | diacylglycerol |
| **DMEM/F-12** | Dulbecco's modified eagle medium: nutrient mixture F-12 |
| **DMSO** | dimethyl sulphoxide |
| **DU145** | *Homo sapiens,* human prostate carcinoma cell line |
| **ER** | endoplasmic reticulum |
| **ERK** | extracellular signal-regulated kinase |
| **Fura 2-AM** | acetoxymethyl 2-[5-[bis[(acetoxymethoxy-oxo-methyl)methyl]amino]-4-[2-[2 [bis[(acetoxymethoxy-oxo-methyl)methyl]amino]-5-methyl-phenoxy]ethoxy]benzofuran-2-yl]oxazole-5-carboxylate |
| **GDP** | gunanosine diphosphate |
| **GPCR** | G protein-coupled receptor |
| **GPR18** | G protein-coupled receptor 18 |
| **GPR23** | G protein-coupled receptor 23 |
| **GPR35** | G protein-coupled receptor 35 |
| **GPR55** | G protein-coupled receptor 55 |
| **GPR92** | G protein-coupled receptor 92 |
| **GPR119** | G protein-coupled receptor 119 |
| **G-protein** | Guanine nucleotide-binding protein |
| **GTPγS** | guanosine 5'-O-[gamma-thio] triphosphate |

| | |
|---|---|
| **GTP** | gunanosine triphosphate |
| **HA** | haemagglutinin |
| **HBS** | HEPES buffered saline |
| **HEK293** | *Homo sapiens,* human embryonic kidney 293 cell line |
| **HEPES** | (4-(2-hydroxyethyl)-1-piperazineethanesulfonic acid) |
| **hGPR55-HEK293** | HEK293 cell line that stably overexpresses recombinant human GPR55 protein with a triple HA tag on N-terminus |
| **$IP_3$** | inositol 1,4,5-triphosphate |
| **JNK** | c-Jun N-terminal kinase |
| **JWH015** | (2-Methyl-1-propyl-1H-indol-3-yl)-1-naphthalenylmethanone |
| **LPI** | L-α-lysophosphatidylinositol |
| **MAPK** | mitogen activated protein kinase |
| **MEA** | methanandamide |
| **min** | minute |
| **mM** | millimolar |
| **NAGly** | N-arachidonoyl-glycine |
| **NBM** | neurobasal medium |
| **NFAT** | Nuclear factor of activated T-cells |
| **nM** | nanomolar |
| **PEA** | palmitoylethanolamide |
| **PBS** | phosphate buffered saline |
| **pCREB** | phosphorylated CREB |
| **PFA** | paraformaldehyde |

| | |
|---|---|
| **$PIP_2$** | phosphatidylinositol 4,5-bisphosphate |
| **PKA** | protein kinase A |
| **PKC** | protein kinase C |
| **PLC** | phospholipase C |
| **RhoA** | ras homolog gene, family member A |
| **ROCK** | Rho associated protein kinase |
| **S1P** | sphingosine-1-phosphate |
| **SEM** | standard error of the mean |
| **siRNA** | small/short interfering RNA |
| **TPA** | Phorbol 12-myristate 13-acetate/12-O-Tetradecanoylphorbol-13-acetate |
| **Triton™ X-100** | 4-(1,1,3,3-Tetramethylbutyl)phenyl-polyethylene glycol |
| **$\Delta^9$-THC** | $\Delta^9$-tetrahydrocannabinol |

# Chapter One

## Introduction

### *1.1. Cannabinoid signalling*

The hemp plant *Cannabis sativa* was thought to originate from Central Asia thousands of years ago and has since been associated with many uses, with one of the most well-known being recreational consumption (Iversen, 2000; Leonard, 2003). Cannabinoids occur naturally in *Cannabis sativa* and were originally described as a family of oxygen-containing 21-carbon aromatic hydrocarbon compounds. The principal psychoactive constituent of the plant is $\Delta^9$-tetrahydrocannabinol ($\Delta^9$-THC), which was first isolated by Gaoni and Mechoulam in 1964. However, cannabinoids no longer encompass compounds that are derived solely from the hemp plant. The term now refers to substances that are capable of either mimicking the pharmacological effects of plant-derived cannabinoids, or have similar chemical structures to plant-derived cannabinoids. As a result, cannabinoids that are expressed endogenously are referred to as "endocannabinoids" whereas naturally occurring cannabinoids sourced from the cannabis plant, such as $\Delta^9$-THC and cannabidiol (CBD), are now referred to as "phytocannabinoids" (Irving *et al.,* 2002; Pertwee, 2005, 2010). There are also "synthetic cannabinoid" compounds (Iversen, 2000).

Cannabinoids exert their primary effects through cannabinoid receptors (Pacher & Kunos, 2013). To date, two types of endogenously expressed cannabinoid receptor have been identified. $CB_1$ receptor was first cloned in 1990 by Matsuda *et al.* and $CB_2$ receptor by Munro *et al.* in 1993. The two principal endocannabinoids that interact with these receptors are anandamide (N-arachidonylethanolamine; AEA) and 2-arachidonylglycerol (2-AG). AEA and $\Delta^9$-THC bind with higher affinity to $CB_1$, whereas 2-AG binds primarily to $CB_2$ (Pacher & Kunos, 2013; Pertwee *et al.* 2010). Both receptors belong to the family of G protein-coupled receptors (GPCR). Upon ligand binding, both of these receptors mediate a signalling system that results in the inhibition of adneylate cyclase and the activation of mitogen-activated protein kinase (MAPK) through $G\alpha_{i/o}$ protein coupling. Inhibitory effects of G protein beta-gamma ($\beta\gamma$) subunits on voltage-gated $Ca^{2+}$ channels have also been reported following $CB_1$ receptor activation (Guo & Ikeda, 2004). However, $CB_1$ receptors have also been reported to couple to stimulatory $G\alpha_s$ proteins (Pertwee *et al.,* 2010).

$CB_1$ receptors are abundantly expressed in the brain, whereas $CB_2$ receptors are expressed at high levels peripherally (e.g. on immune cells) with lower levels found in the CNS. For this reason $CB_1$ receptors are thought to mediate the main psychoactive effects of cannabis. $CB_1$ receptors are expressed by central and peripheral neurons, along with some non-neuronal cells such as microglia

(Cabral & Marciano-Cabral, 2005; Pertwee, 2005). Recent evidence has suggested that $CB_1$ receptor expression can also occur peripherally in almost all tissues and cell types (Di Marzo, 2008; Pacher & Mechoulam, 2011; Pacher *et al.* 2006). It has been suggested that $CB_2$ receptors can also be expressed by some types of neurons (Rodríguez-Cueto *et al.,* 2013; Ross *et al.,* 2001; Van Sickle *et al.,* 2005), as well as being found on CNS-resident immune cells (e.g. microglia; Pertwee, 2005).

Despite the apparent abundance with which cannabinoid receptors are expressed in various tissues and cell types, there is evidence that these receptors are not the only ones responsible for mediating the physiological effects of cannabinoid ligands. Studies conducted with $CB_1^{-/-}$ and $CB_2^{-/-}$ mice have aided in the identification of additional cannabinoid-sensitive targets (Mackie & Stella, 2006). It is now believed that certain orphan receptors which couple to heterotrimeric guanine nucleotide-binding proteins (G-proteins) are capable of responding to cannabinoid ligands. One such example is the orphan G-protein coupled receptor, GPR55.

### *1.2. The structure of GPR55*

GPR55 was first identified by Sawzdargo *et al.* (1999) using cloning experiments and was found to be expressed at high levels in the human striatum. Its structural characteristics were found to be consistent with other GPCRs, including its possession of seven hydrophobic regions corresponding to seven putative transmembrane regions; conserved first and second extracellular loop cysteines; and a DRY motif in the N-terminal part of the second intracellular loop (Sawzdargo *et al.,* 1999). It has been categorised into the Class A or Rhodopsin-like family of seven-transmembrane spanning GPCRs (Henstridge *et al.,* 2011; Müller *et al.,* 2012). The *GPR55* gene is located on chromosome 2 in mice and chromosome 6 in humans and its open reading frame was found to encode a short protein comprised of 319 amino acids (Sawzdargo *et al.,* 1999). GPR55 shares sequence homology with purinergic receptor P2Y5 (29%), the purinergic receptor-like orphan receptors GPR23 (30%) and GPR35 (27%), the chemokine receptor CCR4 (23%) and with the lysophosphatidic acid (LPA) receptor GPR92/$LPA_5$ (Ryberg *et al.,* 2007; Sawzdargo *et al.,* 1999; Yin *et al.,* 2009). Interestingly, GPR55 has much less homology with the classical cannabinoid receptors, $CB_1$ (13.5%) and $CB_2$ (14.4%) (Henstridge *et al.,* 2011; Sharir & Abood, 2010). This discrepancy has led to speculation over whether it is a good candidate for being a putative novel cannabinoid receptor.

### *1.3. Ligand-biased signalling*

The activation of GPCRs by ligands leads to alterations in receptor conformation. The signal transduced from these ligand-receptor interactions can in turn lead to the activation of G-proteins. G-proteins consist of Gα and Gβγ subunits. Several types of Gα subunits exist, including $G\alpha_s$, $G\alpha_i$, $G\alpha_{q/11}$ and $G\alpha_{12/13}$ (Hurowitz *et al.,* 2000). G-proteins function as molecular switches. Their activation on the inner surface of the cell membrane by a transmembrane-spanning GPCR causes the Gα subunit to dissociate from the Gβγ subunit and to exchange guanine diphosphate (GDP) for guanine triphosphate (GTP). The activated G-protein then induces a signalling cascade downstream (Hurowitz *et al.,* 2000). Ligands are capable of inducing GPCRs to selectively transduce their signals via distinct G-proteins to a certain mediator/second messenger over another, leading to specific cellular responses and effects depending on the efficacy of the ligand for the receptor (Khoury *et al.,* 2014). GPCRs can adopt multiple conformations e.g. active and inactive states, and ligands can stabilise these receptor conformations by inducing the "on" conformation with respect to one signalling pathway and the "off" conformation for another pathway. This differential-signalling concept is known as biased agonism or ligand-biased signalling (Onaran, Rajagopal, & Costa, 2014) and the ability of a ligand to induce certain signalling effects has led to the classification of ligands into agonists, antagonists and inverse agonists (Khoury *et al.,* 2014). GPR55 stimulation leads to signal transduction involving the activation of various effectors, and therefore has the potential for agonist-biased signalling.

### *1.4. Ligand-induced GPR55 signalling*

Ligand binding to GPR55 induces a signalling cascade that leads to various cellular effects (Sharir & Abood, 2010). Although it is now widely accepted that GPR55 transduces signals via a G-protein coupled mechanism, there is still speculation over which type of heterotrimeric G-protein this receptor couples to. Initial experiments using specific peptides to block $G\alpha_s$ and $G\alpha_i$ proteins, as well as inhibitors of each G-protein subtype, were conducted in order to determine which G-protein coupled to GPR55. This led to the characterisation of $G\alpha_{13}$ as a potential mediator of GPR55 signalling (Ryberg *et al.,* 2007). Other studies such as the one conducted by Lauckner *et al.* (2008) suggested that GPR55 coupled to $G\alpha_{12}$ and $G\alpha_q$ proteins. Some reports even suggest that different signalling arms could be activated by the same GPR55 ligand, with stimulation of both

$G\alpha_{13}$ and $G\alpha_q$ signalling pathways occurring after ligand-induced GPR55 activation in sensory neurons (Gangadharan *et al.,* 2013).

In support of the findings reported by Ryberg *et al.* (2007) though, an extensive study performed by Henstridge *et al.* (2009a) using the human embryonic kidney cell line, hGPR55-HEK293, implicated a $G\alpha_{13}$-RhoA-Rho-associated protein kinase (ROCK) signalling cascade to be associated with GPR55. This cascade induces phospholipase-C-ε (PLCε) activation, which leads to inositol 1,4,5-triphosphate ($IP_3$) formation followed by the release of $Ca^{2+}$ from internal endoplasmic reticulum (ER) stores (Figure 1). This $Ca^{2+}$ increase was shown to trigger the activation of nuclear factor of activated T-cells (NFAT) proteins. Once activated, NFAT translocates to the nucleus and causes gene transcription. It has also been suggested that there are other downstream effectors of GPR55 activated by the $G\alpha_{13}$-RhoA-ROCK cascade, including ERK, protein kinase B/Akt, p38 MAPK and activating transcription factor-2 (ATF-2) (Oka *et al.,* 2010; Piñeiro *et al.,* 2011). The functionality of these effectors appears to differ from cell type to cell type (Gasperi *et al.,* 2013). It has previously been found that $G\alpha_q$ is required for LPI-induced $Ca^{2+}$release from intracellular stores in DU145 prostate cancer cells (Penman, 2013) via PLCβ-mediated hydrolysis of $PIP_2$ into $IP_3$ and DAG (Hubbard & Hepler, 2006). $IP_3$ then goes on to induce the release of $Ca^{2+}$ from intracellular ER stores (Clapham, 2007). In Figure 1, $G\alpha_{13}$-coupled signalling as determined in HEK293 cells stably overexpressing hGPR55 (Fig 1. (A)), and $G\alpha_q$-coupled signalling in the DU145 prostate cancer cell line (Fig 1. (B)) is illustrated.

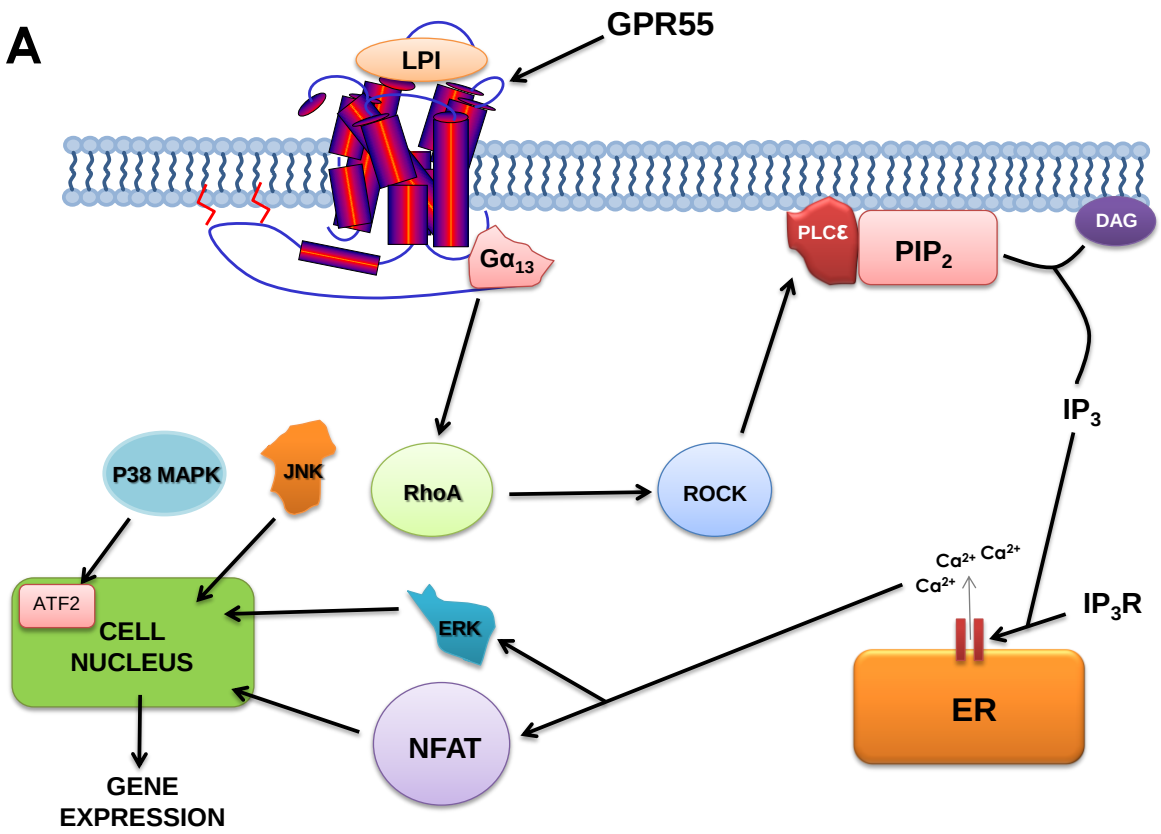
A
GPR55
LPI
Gα13
PLCε
PIP2
DAG
IP3
P38 MAPK
JNK
RhoA
ROCK
Ca2+ Ca2+
Ca2+
IP3R
ATF2
CELL NUCLEUS
ERK
NFAT
ER
GENE EXPRESSION

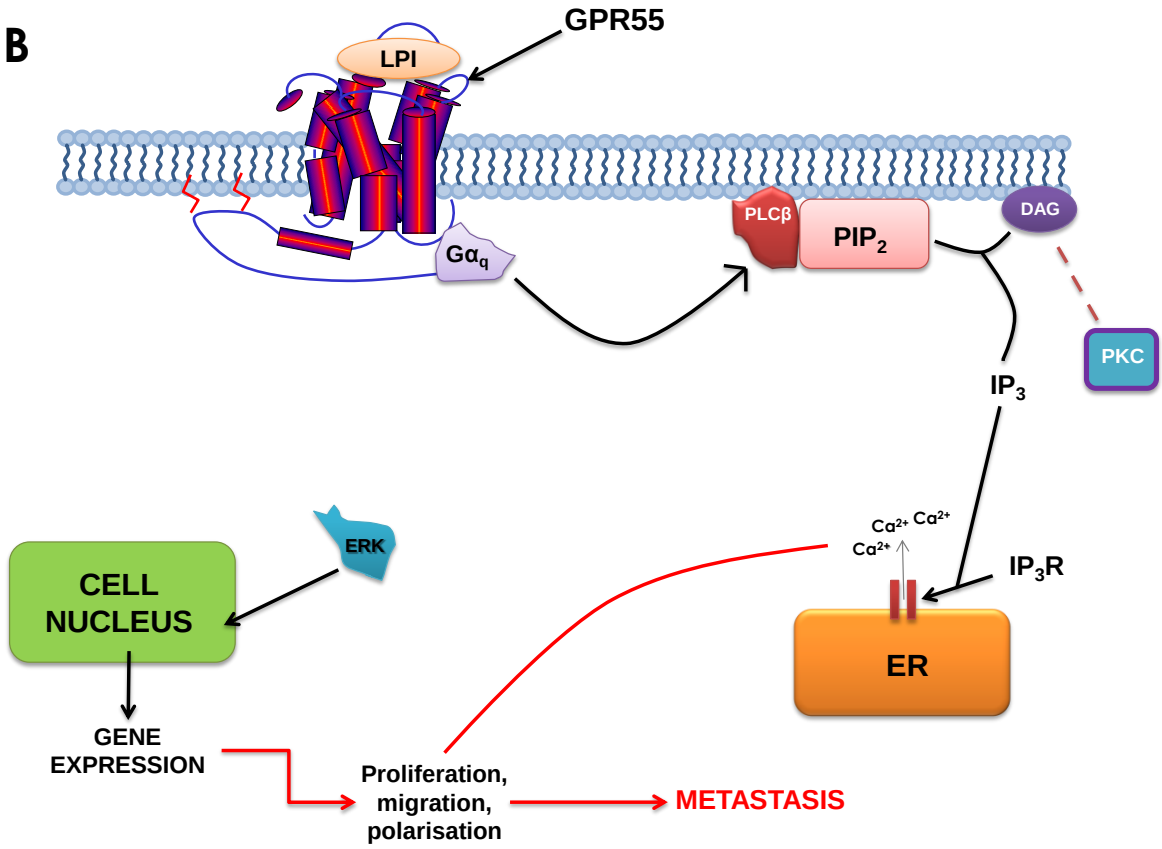
B
GPR55
LPI
Gαq
PLCβ
PIP2
DAG
PKC
IP3
Ca2+ Ca2+
Ca2+
IP3R
ERK
CELL NUCLEUS
ER
GENE EXPRESSION
Proliferation, migration, polarisation
METASTASIS

**Figure 1. GPR55 signalling cascade following agonist stimulation and coupling to $G\alpha_{13}$ protein in hGPR55-HEK293 cells and $G\alpha_q$ in DU145 prostate cancer cells.** (A) Upon activation of GPR55, $G\alpha_{13}$ protein couples to GPR55 and stimulates RhoA GTPase activity. RhoA then activates Rho kinase (ROCK) which in turn induces PLCε to hydrolyse $PIP_2$ to $IP_3$ and DAG. $IP_3$ causes the release of $Ca^{2+}$ from intracellular stores. This increase in cytoplasmic $Ca^{2+}$ levels leads to the activation and translocation of NFAT to the cell nucleus. Once in the cell nucleus, NFAT induces transcription of DNA and gene expression. Cytoplasmic calcium has also been reported to lead to the stimulation of ERK. ERK and other kinases such as JNK and p38 MAPK all go on to induce gene transcription by activating transcription factors within the cell nucleus. (B) Upon activation of GPR55, $G\alpha_q$ protein couples to GPR55 and stimulates PLCβ which hydrolyses $PIP_2$ to $IP_3$ and DAG. DAG activates PKC. $IP_3$ causes the release of $Ca^{2+}$ from intracellular stores. Effectors such as ERK stimulate transcription factors in the nucleus to induce gene expression. This gene expression leads to metastasis of cancer cells. $Ca^{2+}$ is suggested to induce cell metastasis as well. DAG: diacylglycerol; GTP: guanosine triphosphate; $PIP_2$: phosphatidylinositol 4,5-bisphosphate; JNK: c-Jun N-terminal kinases; PKC: Protein Kinase C.

Agonist stimulation of GPR55 and subsequent signalling also induces receptor trafficking. GPR55 normally resides on the cell membrane but agonist stimulation leads to its internalisation. Methods used to observe this internalisation include the use of haemagglutinin (HA) antibodies, which bind to GPR55 tagged with the HA epitope, and β-arrestin assays (Henstridge *et al.*, 2009a, 2010; Sharir *et al.*, 2012). β-arrestins can be recruited to activated GPCRs to form stable receptor-arrestin complexes that can be monitored following agonist stimulation using β-arrestin detector assays (Kapur *et al.,* 2009; Yin *et al.,* 2009).

### *1.5. Phosphorylation of cyclic AMP (cAMP)-response element binding protein (CREB)*

cAMP-response element binding protein (CREB) is a transcription factor that is widely expressed in the body, with particularly high levels of expression found in the brain (Carlezon Jr *et al.,* 2005). It was initially found that cAMP induced the transcription of somatostatin gene via the phosphorylation of CREB at Serine 133 (Gonzalez & Montminy, 1989). CREB phosphorylation occurs via different effectors depending on cell type, with some mediators including protein kinase A (PKA), $Ca^{2+}$-calmodulin-dependent protein kinases (CaM kinases), MAPKs (Carlezon Jr *et al.,* 2005; Gonzalez & Montminy, 1989; Sheng *et al.,* 1991), PKC (Johannessen *et al.,* 2004) and more. Phosphorylation of CREB leads to the translocation of phospho-CREB (pCREB) to the cell

nucleus and the activation of CREB-mediated gene transcription (Stevenson *et al.,* 2001). Some examples of expressed genes include *c-Fos*, cAMP response element modulator (*CREM*) and brain-derived neurotrophic factor (*BDNF*) (Carlezon Jr *et al.,* 2005). Due to its high levels of expression within the brain, CREB is believed to play an important role in synaptic plasticity, memory consolidation and learning (Carlezon Jr *et al.,* 2005; Josselyn & Nguyen, 2005). CREB is also suggested to function in glucose homeostasis, growth-factor-dependent survival (Mayr & Montminy, 2001), in the control of uterine activity during pregnancy (Bailey, 2000) and in spermatogenesis (Walker & Habener, 1996).

Numerous receptors on the cell membrane are suggested to mediate intracellular signalling pathways that ultimately lead to CREB activation within the cell nucleus. Some examples of these receptors include neurotrophin receptors e.g. TrkB, N-methyl-D-aspartate (NMDA) receptors and GPCRs (Carlezon Jr *et al.,* 2005). Upon ligand stimulation, GPR55 mediates the downstream activation of various transcription factors, including CREB phosphorylation (Henstridge *et al.,* 2010).

### *1.6. GPR55 pharmacology: agonism*

Despite the vast amount of research carried out surrounding the pharmacology of GPR55, the issue of whether or not it is a true cannabinoid receptor has not been resolved. Numerous reports have provided evidence that GPR55 is sensitive to cannabinoid ligands, thus supporting this notion. Indeed, Ryberg *et al.* (2007) reported that HEK293 cells stably transfected with hGPR55 were activated by nanomolar (nM) concentrations of various endocannabinoids, including AEA, 2-AG. This study also reported that the phytocannabinoid $\Delta^9$-THC and synthetic cannabinoids e.g. O-1602, the inverse $CB_1$ agonist AM251, activated downstream signalling mechanisms via GPR55. These signalling mechanisms led to GTPγS binding. However, other studies only reproduced some of the results shown by Ryberg *et al.* (2007) in the hGPR55-HEK293 cell line (Johns *et al.,* 2007), while another research group could not reproduce any of the findings (Oka *et al.,* 2007).

In contrast, there are reports suggesting that endocannabinoids are not the most potent class of endogenous agonists of GPR55. Various studies have found that a different class of endogenous lyso-phospholipid interacts more effectively with GPR55. L-α-lysophosphatidylinositol (LPI) has previously been suggested to be the endogenous ligand for GPR55 (Nevalainen & Irving, 2010;

Piñeiro & Falasca, 2012), with the 2-arachidonyl species of LPI being the most potent based on structure-activity relationships (Oka *et al.,* 2009). LPI has been reported to activate other orphan GPCRs. For instance, it was found that LPI significantly induced intracellular cAMP accumulation via the orphan GPCR, GPR119, in a dose-dependent manner in rat hepatoma cells stably expressing human GPR119 (Soga *et al.,* 2005). However, Piñeiro *et al.* (2011) found that knockdown of GPR119 had no effect on LPI-induced ERK activation and the release of $Ca^{2+}$ from stores in prostate and ovarian cancer cell lines, which indicates that GPR55 was mediating those effects. Other suggested lipid agonists at GPR55 include N-arachidonoyl-serine (ARA-S) (Zhang *et al.,* 2010) and palmitoylethanolamide (PEA) (Mackie & Stella, 2006).

Studies conducted in order to produce next-generation agonists for GPR55 have attempted to model those agonists on LPI because LPI has been found to possess a conformation and binding mode that is suitable for interaction with GPR55 (Kotsikorou *et al.,* 2011a, 2011b). LPI-mediated stimulation of GPR55 leads to the activation of downstream signalling cascades that are consistent with what is already known about the pharmacological effects associated with GPR55 activation. Some examples of these effects include GPR55 receptor internalisation, $Ca^{2+}$ release, NFAT activation, ERK phosphorylation and p38 MAPK activation (Henstridge *et al.,* 2009a; Oka *et al.,* 2007, 2010).

Although LPI is currently the most potent endogenous GPR55 agonist, ligand selectivity for GPR55 has recently come under scrutiny. For instance, the synthetic GPR55 agonist O-1602 also activates the orphan receptor GPR18 (Ashton, 2012). Recent findings suggest that N-arachidonyl-glycine (NAGly), the endogenous agonist for GPR18 (Kohno *et al.,* 2006), also activates GPR55 (Penman, 2013). Findings such as these have led to the suggestion that GPR55 communicates with GPR18, thereby altering ligand selectivity under certain physiological circumstances. This is why it is ever more pertinent to identify other potent and specific agonists for GPR55. Heynen-Genel *et al.* (2011) identified several potent and selective agonists for GPR55 – ML184 (2440433) with 263 nM potency for GPR55; ML185 (CID1374043) with 658 nM potency for GPR55; and ML186 (CID15945391) with 305 nM potency for GPR55. The agonists were all found to cause downstream ERK phosphorylation and PKC β II translocation. Brown *et al.* (2011) identified the benzoylpiperazines, GSK494581A and GSK575594A, as GPR55 agonists, which were originally patented as inhibitors of glycine transporter subtype 1 (GlyT1). GSK575594A was 60-fold selective for GPR55 ($pEC_{50}$ = 6.8) over GlyT1 ($pIC_{50}$ = 5.0). However, these agonists only showed activity at human GPR55, whereas endogenous agonists such as LPI show specificity for both human and rodent GPR55. It could be disadvantageous to use these agonists in studies that utilise

tissue and *in vivo* models if one wished to compare human and rodent orthologs of GPR55. Nevertheless, with the discrepancies surrounding the selectivity of cannabinoid ligands and LPI for GPR55, it is therefore important to continue identifying selective GPR55 agonists in order to truly characterise the physiological role of GPR55.

### *1.7. GPR55 pharmacology: antagonism*

Although there appears to be no shortage of potential agonist ligands for GPR55, only a small number of putative antagonists have been identified. Some research groups have suggested that certain cannabinoid ligands act as GPR55 antagonists. The cannabinoid ligand CP55,940 was found to antagonise LPI-induced release of $Ca^{2+}$ from ER stores in hGPR55-HEK293 cells (Henstridge *et al.,* 2009a). Lauckner *et al.* (2008) reported that low micromolar ($\mu$M) concentrations of $CB_1$ antagonist SR141716A (rimonabant) caused antagonism of GPR55 and a decline in $Ca^{2+}$ when co-perfused with various agonists ($\Delta^9$-THC, methanandamide (MEA) and JWH015) in hGPR55-HEK293 cells and dorsal root ganglion (DRG) neurons. JWH015 and $\Delta^9$-THC did antagonise GPR55 and cause a reduction in $Ca^{2+}$ release in DRG neurons when co-perfused with SR141716A but MEA did not. In contrast, Kapur *et al.* (2009) and Henstridge *et al.* (2009b, 2010) demonstrated that varying concentrations of SR141716A caused agonist-induced effects to occur via GPR55 stimulation in human osteosarcoma and hGPR55-HEK293 cells respectively. The differing effects of SR141716A previously reported may have been related to the doses used, efficacy and even cell type (Sharir & Abood, 2010). However, it is also worth noting that SR141716A is structurally similar to the $CB_1$ inverse agonist AM251, which has previously been reported to have agonistic effects at GPR55 (Henstridge *et al.,* 2009b, 2010; Ryberg *et al.,* 2007).

Cannabidiol was suggested to act as a GPR55 antagonist in a GTPγS-binding assay (Ryberg *et al.,* 2007). Similarly, the cannabidiol analogue O-1918 has been identified to act as a GPR55 antagonist in several studies. Schmuhl *et al.* (2014) recently demonstrated that GPR55 antagonism with O-1918 or CBD induced mesenchymal stem cell migration. This pro-migratory effect was associated with concentration-dependent activation of p42/44 MAPK, and was inhibited by pre-treating cells with the GPR55 agonist O-1602 (Schmuhl *et al.*, 2014). O-1918 inhibited the firing of nociceptive C fibres induced by O-1602 in a rat model of acute joint inflammation (Schuelert & McDougall, 2011). Interestingly, O-1918 is a recognised antagonist of GPR18. O-1918 inhibited the effects on intraocular pressure (IOP) induced by the GPR18 agonists Abnormal-CBD (Abn-CBD) and NAGly in a murine model (Caldwell *et al.,* 2013). O-1918 inhibited the NAGly-, Abn-CBD-, and

O-1602-induced cellular migration of both BV-2 microglia and GPR18-HEK293 transfected cells (McHugh *et al.,* 2010). O-1918 was suggested to equivalently antagonise the vasodilator effects of Abn-CBD in WT and GPR55-KO murine models (Johns *et al.,* 2007), which could lead one to speculate that the observed antagonistic effects on vasodilation could instead have been GPR18-mediated. O-1602 and NAGly have been identified as both GPR55 (Romero-Zerbo *et al.,* 2011; Schuelert & McDougall, 2011; Penman, 2013) and GPR18 (Ashton, 2012; Kohno *et al.,* 2006) agonists. Given that O-1918 is theorised to act as an antagonist at both GPR55 and GPR18, it seems more likely than ever that these receptors are capable of communicating with one another.

Rempel *et al.* (2013) used β-arrestin assays to identify 3-substituted coumarins as GPR55 antagonists. Structure-activity relationships were performed and compared to $CB_1$, $CB_2$ and GPR18 receptors. The study showed that when there was no lipophilic residue in position 7 of the coumarin scaffold, this resulted in the antagonism of LPI-induced β-arrestin translocation. In contrast, these compounds had little or no affinity for CB receptors or GPR18. Coumarin derivatives with an enhanced alkyl moiety possessed the greatest antagonistic potency in the series of compounds tested. 7-(1,1-Dimethyloctyl)-5-hydroxy-3-(2-hydroxybenzyl)-2H-chromen-2-one (PSB-SB-487, $IC_{50}$ = 0.113 $\mu$M, $K_B$ = 0.561 $\mu$M) and 7-(1,1-dimethylheptyl)-5-hydroxy-3-(2-hydroxybenzyl)-2H-chromen-2-one (PSB-SB-1203, $IC_{50}$ = 0.261 $\mu$M) were the two most potent GPR55 antagonists tested. Interestingly, these two compounds also acted as potent $CB_2$ receptor agonists in this study. The compounds could therefore be useful therapeutic tools for the study of cross-talk mechanisms and dual functionality between $CB_2$ and GPR55 in the future (Rempel *et al.,* 2013).

Previous studies such as the ones described in this section have identified putative GPR55 antagonists. However, these antagonists are not completely selective for GPR55 and this lack of selectivity considerably limits their suitability as pharmacological tools. This makes the need for pharmacologically specific or selective GPR55 antagonists all the more essential so that the (patho)physiological roles of GPR55 can be properly elucidated. A study conducted by Heynen-genel *et al.* (2011) screened for selective GPR55 antagonists. Three potent antagonists were reported on in that study, one of which being the piperadinyloxadiazolone ML191 (3-[1-[1-(4-methylphenyl)cyclopropanecarbonyl]piperidin-4-yl]-5-phenyl-1,3,4-oxadiazol-2-one), which is also referred to as D327-0013. D327-0013 was reported to have 160nM potency for GPR55 in a β-arrestin high-content screen (HCS) assay and was capable of inhibiting the downstream signalling responses of ERK phosphorylation and PKC translocation. Another antagonist was also

screened for during that study but the data was not published at the time. The antagonist in question, known as CID16020046 ((4-[4-(3-hydroxyphenyl)-3-(4-methylphenyl)-6-oxo-1H,4H,5H,6H-pyrrolo[3,4-c]pyrazol-5-yl] benzoic acid) or C390-0219, was originally reported to antagonise GPR55-mediated β-arrestin internalisation (Abood, 2010). Kargl *et al.* (2013) recently performed a study and reported that C390-0219 antagonised agonist-induced receptor trafficking in yeast cells expressing hGPR55 and LPI-mediated effects in the hGPR55-HEK293 cell line e.g. LPI-induced $Ca^{2+}$ release, stimulation of ERK, NFAT and Nuclear factor κ of activated B cells (NF-κB). Kargl *et al.* (2013) also showed that C390-0219 prevented LPI-induced stimulation of wound healing in human lung microvascular endothelial cells (HMVEC-L) (Kargl *et al.,* 2013). The potency of C390-0219 at GPR55 and the inhibition of LPI-mediated effects was estimated to be between 0.1–1 $\mu$M in that study.

The structures of both D327-0013 and C390-0219 are illustrated in Figure 2. Both antagonists were used in a study conducted by Kotsikorou *et al.* (2013) to characterise their structures and conformations. The antagonists possess a head region that occupies a horizontal binding pocket extending into the extracellular loop region of GPR55; they possess a central ligand segment that occupies a vertical binding region of GPR55; and they possess aromatic rings that extend out from their central regions and are located deepest in the horizontal binding pocket of GPR55. The study was carried out in order determine their functionality as GPR55 antagonists and also to facilitate the creation of more potent and effective next-generation antagonist ligands that are selective for GPR55. This will prove beneficial in future because the most effective GPR55 antagonist can be used to evaluate the therapeutic potential of GPR55.

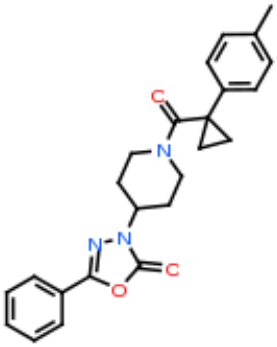


**D327-0013 [ML191]**
**(3-[1-[1-(4-methylphenyl)cyclopropanecarbonyl]piperidin-4-yl]-5-phenyl-1,3,4-oxadiazol-2-one)**

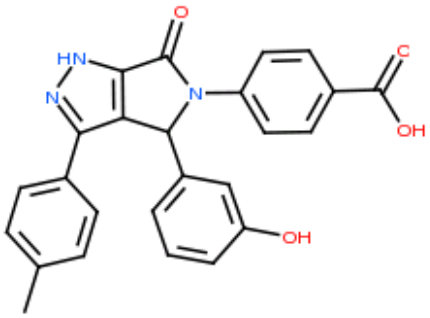


**C390-0219**
**(4-[4-(3-hydroxyphenyl)-3-(4-methylphenyl)-6-oxo-1H,4H,5H,6H-pyrrolo[3,4-c]pyrazol-5-yl] benzoic acid)**

**Figure 2. Chemical structures of GPR55 antagonists.** Adapted from Heynen-Genel *et al.* (2011) and Kotsikorou *et al.* (2013).

### *1.8. The expression and (patho)physiological function of GPR55*

The GPR55 receptor is expressed in many different tissues and cell types. Numerous studies have provided evidence supporting GPR55 expression in the blood, cardiovasculature, bone metabolism (Henstridge *et al.,* 2011), the brain (Sawzdargo *et al.,* 1999), the gastrointestinal tract (Ryberg *et al.,* 2007) and pancreatic tissue (Bondarenko *et al.,* 2010, 2011), to name but a few.

Due to its fairly ubiquitous expression, GPR55 has been implicated in numerous pathophysiological conditions e.g. neurological diseases, inflammatory and neuropathic pain, osteoporosis and diabetes (Henstridge *et al.,* 2011). GPR55 has also been increasingly linked to having a regulatory role in cancer. Cannabinoid signalling via cannabinoid receptors has previously been shown to elicit anti-cancer effects and to regulate cancer cell proliferation in different *in vitro* and *in vivo* models of cancer (Alexander *et al.*, 2009; Guzmán, 2003). Similarly, certain cannabinoids such as AM251, SR141716A and others, act as ligands at GPR55 (Henstridge *et al.,* 2009b, 2010; Kapur *et al.,* 2009; Ryberg *et al.,* 2007), thus implicating GPR55 in having a potential role in the regulation of cancer cell activity. Indeed, studies have provided evidence that links GPR55 stimulation to the promotion of cancer cell proliferation in various models of cancer. For instance, levels of the established GPR55 agonist LPI were found to be augmented in the plasma of female patients with ovarian cancer compared to healthy patients (Oka *et al.,* 2007). LPI was shown to be

secreted by fibroblasts, epithelial cancer cells and transformed thyroid cells. This led to mitogenic effects and it was suggested that LPI was a mitogen that could play a role in Ras-dependent cell proliferation (Falasca & Corda, 1994; Falasca *et al.,* 1995, 1998). Overexpression of GPR55 and LPI caused an increase in cell migration, cell viability and ERK activation in breast and glioma cancer cells (Andradas *et al.,* 2011; Ford *et al.,* 2010). ERK is an important mediator of cell proliferation because it regulates the activity of transcription factors e.g. c-Fos, c-Jun. These genes are well-known oncogenes and upon their dysregulation they aid in modulating the rates of cell proliferation in carcinogenesis (Formosa & Vassallo, 2014). Studies such as these suggest that GPR55 is a regulator of pro-cancer activity. However, the modulation of GPR55-mediated signalling pathways may have a therapeutic impact. Blockade of GPR55 using small interfering RNA (siRNA) decreased cellular proliferation in prostate and ovarian cancer cells (Andradas *et al.,* 2011; Piñeiro *et al.,* 2011). The formation of GPR55-$CB_2$ heteromers in human breast adenocarcinoma cells and in human glioblastoma cells was shown to have a major impact on cannabinoid signalling and pharmacology in these cells and it was suggested that the modulation of these receptors could potentiate anti-tumoural activity *in vivo* (Moreno *et al.,* 2014). In consideration of this evidence, the use of GPR55 antagonists to inhibit GPR55 signalling could have therapeutic effects in models of cancer.

### *1.9. GPR55 and apoptosis*

In contrast to the potential role GPR55 has in promoting cell proliferation, GPR55 has recently been linked to promoting programmed cell death in certain cell types and in different physiological conditions. Apoptosis is vital for the removal of unwanted and potentially harmful cells during developmental processes, homeostasis and disease (Jacobson *et al.,* 1997; Thompson, 1995). Although there are various mediators that function in the apoptotic pathway, the cysteine-aspartic proteases or caspases are particularly essential. Caspases are an evolutionarily conserved family of proteases and 14 types have been identified in mammals to date (Zhang *et al.,* 2003). Although largely linked with apoptosis and inflammation in the past, newer evidence now links caspases to having major roles in promoting cell survival, proliferation and differentiation (Lamkanfi *et al.*, 2007).

There are two types of apoptotic pathway: extrinsic and intrinsic. In the intrinsic apoptotic pathway, various signals directly or indirectly alter mitochondrial membrane permeability which leads to the release of intermembrane proteins from the mitochondria e.g. cytochrome *c*, into the

cytoplasm. In the cytoplasm, cytochrome *c* assembles with procaspase-9 and apoptotic protease activating factor 1 (apaf-1) to form an apoptosome. Procaspase-9 is cleaved and activated in the apoptosome. Activated caspase-9 then goes on to cleave and activate other downstream caspases e.g. caspase-3 (Zhang *et al.,* 2003).

Caspase-3 is a frequently activated death protease, also known as an executioner caspase. It functions in apoptotic processes in a cell- and tissue-specific manner (Porter & Jänicke, 1999). In pathological conditions such as cancer, caspase-3 and apoptosis are downregulated. GPR55 can play a role in mediating this downregulation. Piñeiro *et al.* (2011) measured caspase-3 activity in cancer cells transfected with GPR55 siRNA which led to an absence of apoptosis induction. From these findings they suggested that GPR55 was critical for the regulation of cell proliferation.

Caspases such as caspase-3 also have a major role in normal brain development and in the progression of neurological disorders. In chronic neurodegenerative disorders such as Alzheimer's disease for instance, caspase-dependent apoptotic mechanisms promote cell dysfunction, synaptic failure and cognitive dysfunction (D'Amelio *et al.,* 2011; Friedlander, 2003). In the brains of Alzheimer's patients, a four-fold increase in caspase-cleaved amyloid precursor protein (APP) fragments was discovered in comparison to age-matched controls (Banwait *et al.*, 2008; Bredesen, 2009). Cannabinoids have a regulatory effect on processes such as these. $\Delta^9$-THC has previously been shown to induce apoptosis in cortical neurons via a caspase-3 dependent mechanism (Campbell, 2001; Downer *et al.,* 2007; Gowran *et al.*, 2011). Interestingly, GPR55 mRNA expression has been identified in different regions of the brain e.g. frontal cortex, hypothalamus, striatum, amygdala and cerebellar granule cells (Chiba *et al.,* 2011; Kerr *et al.,* 2013; Ryberg *et al.,* 2007; Sawzdargo *et al.,* 1999) and in microglia (Pietr *et al.,* 2009). It would now be of particular interest to examine whether GPR55 also has a regulatory role over caspase-3 and apoptotic mechanisms in primary neuronal cell models.

GPR55 is a putative cannabinoid receptor which responds to certain cannabinoid ligands along with other endogenous lipids. Its most potent endogenous ligand to date is believed to be LPI. However, an absence of selective GPR55 ligands up until recently has made it difficult to elucidate the physiological and pathological processes mediated by this receptor. This is particularly true of cells that express GPR55 endogenously, whereby there is greater potential for non-specific binding of ligands. Thus, the development of new GPR55-selective pharmacological tools will allow for a much greater understanding of the physiological and pathological roles of GPR55.

## OBJECTIVES

The objectives of this research project were as follows:

1. To compare GPR55-mediated responses in a stable cell line that stably expresses recombinant human GPR55 (hGPR55-HEK293 cells) with a prostate cancer cell line that expresses GPR55 endogenously at high levels (DU145).
2. To determine the effectiveness of two novel GPR55-selective antagonists on agonist-mediated GPR55 responses using these *in vitro* models.
3. To compare the effects of the endogenous GPR55 agonist (LPI) with synthetic GPR55-selective agonists.
4. To determine if LPI mediates neuroprotective effects in degenerating primary cortical neurons and if these actions involve GPR55.

# Chapter Two

## Materials and Methods

## 2.1. Materials

### *2.1.1. Cell culture: Plasticware and general reagents*

EZBiolab, Carmel, Indiana, USA:

- $A\beta_{1-40}$ peptide
- Reverse $A\beta_{40-1}$ peptide

Fisher-Scientific, Loughboriugh, UK:

- Falcon™ Bacteriological Petri Dishes with Lid (30 mm)

Greiner bio-one, Stonehouse,UK:

- $25cm^2$ TC-treated flask with filter cap ($T_{25}$ TC flask)
- Cryo.s™, 2 ml, polypropylene, round bottom, internal thread, sterile
- Pipette tips; 10 µl, 200 µl, 1000 µl
- Sample container 25x90mm, 30ml, Conical skirted bottom
- 15ml polypropylene centrifuge tube with conical base

Life Technologies, Paisley, UK:

- Dulbecco Modified Eagle Medium/F-12
- Trypsin-Ethylenediaminetetraacetic acid (EDTA) (0.05%), phenol red
- Phosphate Buffered Solution

  **Trinity College Dublin**

  - Neurobasal Medium
  - Heat-inactivated horse serum; New Zealand origin
  - Penicillin
  - Streptomycin
  - B27 Supplement

Merck Millipore Darmstadt, Germany:

- Millex-GP, 0.22 µm, polyethersulfone, 33 mm, gamma sterilised

Roche Diagnostics Limited, West Sussex, UK:

- G418 Solution

Sera labs International, West Sussex, UK:

- Heat inactivated foetal bovine serum; New Zealand origin

Sigma-Aldrich, Dorset, UK:

- L-glutamine
- Poly-D-lysine
- Sodium Hydroxide
- HEPES
- Glucose
- Paraformaldehyde
- Dimethyl Sulphoxide
- Phorbol 12-myristate 13-acetate/12-O-Tetradecanoylphorbol-13-acetate (TPA)

  **Trinity College Dublin**

  - Poly-L-lysine
  - Saponin
  - Trypsin
  - Trypsin Inhibitor
  - Deoxyribonuclease (DNase)
  - Magnesium Sulphate
  - GlutaMAX
  - Cytosine-arabinofuranoside

Thermo Fisher Scientific, Waltham, MA, USA:

- Nalgene™ Cryo 1°C freezing container

Tocris Bioscience, Bristol, UK:

- Fura 2-acetoxymethyl (AM) ester

Vector Laboratories, Peterborough, UK:

**Trinity College Dublin**

- Normal goat serum

VWR International, Leicestershire, UK:

- Dow Corning® high-vacuum silicone grease
- Sodium Chloride
- Potassium Chloride
- Calcium Chloride
- Magnesium Chloride
- Coverglasses, round, 9 mm
- Ethanol

### *2.1.2. Cell lines*

- Human Embryonic Kidney 293 (HEK293)-AD cells; Life Technologies, Paisley, UK.
- DU145 prostate cancer cell line;
    - Division of Cancer Research, University of Dundee, Dundee, UK

      **and**
    - Centre for Diabetes, Blizard Institute, Queen Mary University of London, London, UK.

### *2.1.3. Antibodies, probes and dyes*

| ANTIBODY/DYE | COMPANY | DILUTION |
|---|---|---|
| **University of Dundee** | | |
| Mouse anti-phosphoCREB (serine 133) clone 10E9 | Millipore, Watford, Hertfordshire, UK | 1:250 |
| Alexa Fluor® 488 donkey anti-mouse | Molecular Probes®, Life Technologies, Paisley, UK | 1:500 |
| **Trinity College Dublin** | | |
| Anti-active caspase-3 primary rabbit antibody | Promega Corporation, Madison, WI, USA | 1:250 |
| Biotinylated Goat Anti-Rabbit IgG Antibody | Vector Laboratories, Peterborough, UK | 1:500 |
| Alexa Fluor® 633 goat anti-rabbit | Bio-Sciences Ltd., Dublin, Ireland | 1:500 |
| Anti-NeuN Antibody, clone A60 | Millipore, Watford, Hertfordshire, UK | 1:500 |

| | | |
|---|---|---|
| Biotinylated Horse Anti-Mouse IgG Antibody | Vector Laboratories, Peterborough, UK | 1:1000 |
| Alexa Fluor® 488 goat anti-mouse | Bio-Sciences Ltd., Dublin, Ireland | 1:500 |
| Hoechst 33342, Trihydrochloride, Trihydrate | Life Technologies, Paisley, UK: | 1:500 |

### *2.1.4. Ligands*

| LIGAND NAME | COMPOUND STRUCTURE | COMPANY |
|---|---|---|
| **L-α-lysophosphatidylinositol** sodium salt from *Glycine max* (soybean)<br><br>1-Acyl-sn-glycero-3-phospho-(1-D-myo-inositol) | 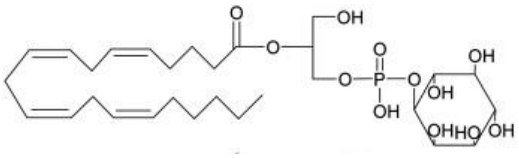 | Sigma-Aldrich, Dorset, UK |
| **SY-020** | 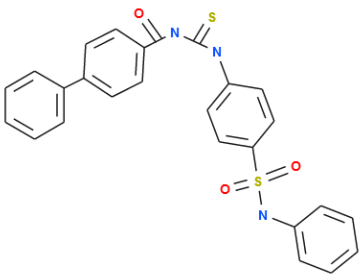 | Gift from Prof. Tapio Nevalainen, The University of Eastern Finland, Kuopio, Finland |
| **12-O-Tetradecanoylphorbol-13-acetate**<br><br>Phorbol 12-myristate 13-acetate; 4β,9α,12β,13α,20-Pentahydroxytiglia-1,6-dien-3-one 12-tetradecanoate 13-acetate | 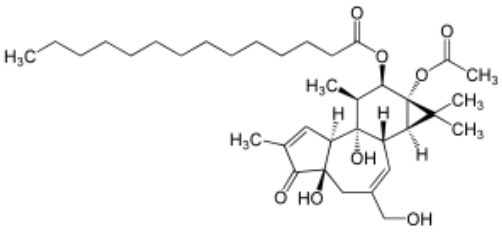 | Sigma-Aldrich, Dorset, UK |

| LIGAND NAME | COMPOUND STRUCTURE | COMPANY |
|---|---|---|
| **D327-0013**<br>ML191 (CID23612552)<br><br>3-[1-[1-(4-methylphenyl)cyclopropanecarbonyl]piperidin-4-yl]-5-phenyl-1,3,4-oxadiazol-2-one | 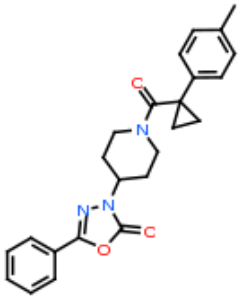 | ChemDiv, San Diego, CA, USA |
| **C390-0219**<br>(CID16020046)<br><br>4-[4-(3-hydroxyphenyl)-3-(4-methylphenyl)-6-oxo-1H,4H,5H,6H-pyrrolo[3,4-c]pyrazol-5-yl] benzoic acid | 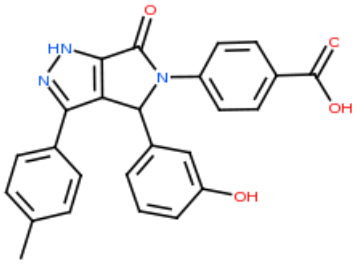 | ChemDiv, San Diego, CA, USA |

## 2.2. Methods

### *2.2.1. Cell line maintenance*

hGPR55-HEK293 cells were cultured in Dulbecco's Modified Eagle Medium: Nutrient Mixture F-12 media (DMEM/F-12) supplemented with 10% heat-inactivated fetal bovine serum (FBS), 2mM L-glutamine and 400μg/ml G418 antibiotic and maintained at 37°C with 5% $CO_2$ in a Jouan IGO150 CELLlife $CO_2$ Incubator (Thermo Fisher Scientific Inc., MA, USA).

HEK293 cells were cultured in DMEM/F-12 media supplemented with 10% heat-inactivated fetal bovine serum and 2mM L-glutamine and maintained at 37°C with 5% $CO_2$.

DU145 prostate cancer cells were cultured in DMEM/F-12 media supplemented with 10% heat-inactivated fetal bovine serum and 2mM L-glutamine and maintained at 37°C with 5%.

### *2.2.2. Subculturing cell lines*

Cells were grown in 25$cm^2$/$T_{25}$ flasks and subcultured once they had reached 80-90% confluency. To subculture cells, 0.5-1ml of pre-warmed 0.05% trypsin-EDTA solution was added to the confluent flask. The flask was gently tapped or rocked side to side in a north-east-south-west motion to dislodge adherent cells. To aid the cells in lifting off, the flask could be placed in an incubator set at 37°C for 1-2 minutes. Cells were checked under the microscope to examine rate of detachment. Once the cells had properly lifted and were not clumped together, ~2ml of pre-warmed culture medium was added to the flask to cease trypsinisation; the serum in the media aids in ceasing the trypsinisation reaction. A pre-calculated amount of cell suspension was then pipetted into ~4ml of warm media in sterile flasks and/or petri dishes (Falcon) to create an appropriate dilution of cells for experimentation. The newly passaged cells were then incubated at 37°C with 5% $CO_2$ to allow them time to adhere to their container(s).

### *2.2.3. Freezing cell lines*

Freezing medium was made up using normal culture medium (with 10% FBS) and 5% dimethyl sulphoxide (DMSO). The medium was then stored at 4°C until needed for use. Cells were subcultured as described above. The cells were re-suspended in warm culture media and transferred to a sterile 15 ml conical tube. The tube was centrifuged at 1000rpm for 3-5 minutes. The supernatant was aspirated off using a sterile Pasteur pipette. The pellet was re-suspended in 1ml of freezing media per vial to be frozen. 1 ml aliquots of the cell-freezing media solution were decanted into cryogenic vials and placed into an isopropanol chamber. The chamber was placed

into a -80°C freezer so that the temperature of the chamber would drop -1°C per minute overnight. The following day the cryovials were removed from the chamber and stored indefinitely at -80°C.

### *2.2.4. Thawing cell lines*

Warm culture medium (~5ml) was decanted into a $T_{25}$ flask. The flask was then kept warm in an incubator until needed. A cryovial was removed from the -80°C freezer and placed into an incubator set at 37°C until almost all of the solution inside had thawed. The outside of the vial was gently sprayed with ethanol and the vial was placed in the fumehood. The $T_{25}$ flask was retrieved from the incubator. The cap of the cryovial was opened and, using a P1000 (Gilson, Inc., Bedfordshire, UK), its contents were gently pipetted into the pre-warmed media in the $T_{25}$ flask. The flask was gently rocked to allow for even cell coverage. The flask was placed into a 37°C incubator with 5% $CO_2$.

After about an hour (or until the cells had adhered), the flask was removed from the incubator. Around three-quarters of the medium was aspirated away using a P1000 and decanted into a new $T_{25}$ flask which already contained 4-5 ml of warm culture medium. About 4-5 ml of fresh, warm culture medium was then added to the first flask. The new flask acted as a recovery and was diluted with more media because it contained more DMSO (DMSO is toxic to cells). The old flask now contained an attached cell line and little to no DMSO.

### *2.2.5. Preparation of cells for experimentation*

To prepare cell lines for experimentation, petri dishes were lined with coverslips that were pre-coated in poly-D-lysine. To achieve this, 9mm coverslips were placed into a sterile 50 ml Falcon tube and washed twice with 70% ethanol followed by washing x2 with distilled $H_2O$ ($dH_2O$). The water was aspirated away and poly-D-lysine (20μg/ml) was made up (diluted in $dH_2O$) and poured over the coverslips. The Falcon tube was then placed on a rocker and the coverslips were incubated for 1 hour or longer. The coverslips were then stored at 4°C until required and used within a maximum of two weeks.

To plate out cells, confluent flasks were subcultured as described before. The cell suspension was diluted appropriately by pipetting a pre-determined amount of the suspension into warm culture medium in coverslip-lined petri dishes. This took place 24-72 hours in advance of experimentation. The cells were then maintained at 37°C with 5% $CO_2$ in a cell culture incubator to facilitate their adherence.

The night before an experiment was due to take place, cells were incubated in serum-free medium supplemented with 2mM L-glutamine. Serum-free medium was used because serum-derived lipoproteins and other bioactive components such as sphingosine 1-phosphate (S1P) are capable of activating membrane surface proteins and proteases (Benaud *et al.,* 2002) as well as Rho GTPases (Dupont *et al.*, 2011). It was therefore crucial to attempt to eliminate the possibility of receptor activation and internalisation before experimentation.

### *2.2.6. Preparation of primary neuronal cultures*

Cortical neuronal cultures were prepared from 1-day-old male Wistar rats (BioResources Unit, Trinity College, Dublin 2, Ireland). The rats were decapitated and the cortices dissected. The meninges were removed from the cortices using a curved forceps. The cortical tissue was chopped into smaller pieces of tissue using a sterile razor blade. Using a sterile Pasteur pipette, the tissue was aspirated and transferred into a sterile 15 ml conical tube and incubated with trypsin diluted in PBS (0.3% (w/v)) for 25 minutes at 37°C with 5% $CO_2$ in a cell incubator (AutoFlow NU-4750 Water-Jacket $CO_2$ Incubator, NuAire). The tube was removed from the incubator and a solution of trypsin inhibitor diluted in PBS (0.1%) was added to the tissue. The tube was inverted repeatedly. The tissue was allowed to settle and the supernatant was aspirated away using a Pasteur pipette. A solution of trypsin inhibitor (0.1%(w/v)), deoxyribonuclease (DNase; 0.2mg/ml) and magnesium sulphate (0.1 M) was added to the tissue and the tube was inverted repeatedly. The tissue was triturated repeatedly using a sterile pipette and passed through a sterile mesh filter (0.2 μm). The tissue was centrifuged at 2000 rpm (Sigma 2-16K model, Sigma-Aldrich, Dorset, UK) for 3 minutes at 20°C. The supernatant was aspirated off and the pellet was re-suspended in warm neurobasal medium (NBM) supplemented with heat-inactivated horse serum, penicillin (100 units/ml), streptomycin (100 units/ml), GlutaMAX (2 mM), and B27 (1%(v/v)). The cell-medium suspension was pipetted out onto coverslips pre-coated in poly-L-lysine (40 μg/ml). These coverslips lined 24-well plates. The plate(s) were maintained at 37°C with 5% $CO_2$ in a cell culture incubator for 3 hours. After 3 hours, the cells were flooded with 300 μl of warm culture medium.

After 3-4 days, the media was removed from the plates and replaced with warm NBM containing cytosine-arabinofuranoside (5 $\mu$g/ml) in order to prevent proliferation of non-neuronal cells. The plates were incubated in this medium at 37°C with 5% $CO_2$ overnight. The next day, the media was removed and replaced with normal NBM supplemented with B27. The culture medium was replaced every 24-48 hours prior to treatment.

### *2.2.7. Treatment of neuronal cells*

$A\beta_{1-40}$ peptide was diluted in 84% PBS and 16% double $dH_2O$ and allowed to aggregate for 48 hours at 37°C. The peptide was made up as a 200 $\mu$M stock and stored at -20°C. For treatment of cortical neurons, Aβ was diluted to a working concentration of 1 $\mu$M in pre-warmed NBM. Control treatment groups were incubated in normal NBM only. Drug treatments were diluted to a working concentration using NBM. For treatment groups that were exposed to Aβ, cells were initially exposed to ligands for 30 minutes without Aβ. Following this, the ligand treatment-media was removed and replaced with warm NBM containing the same drug treatments and Aβ (1 $\mu$M). Cells were maintained at 37°C with 5% $CO_2$ in a cell culture incubator for a further 72 hours.

## 2.3. Experimental Protocols

### *2.3.1. $Ca^{2+}$ imaging*

Cells that were attached to coverslips coated in poly-D-lysine and incubated in serum-free medium were washed once with 1x HEPES-buffered saline (HBS in mM: NaCl 135; KCl 5; $MgCl_2$ 1; $CaCl_2$ 1; HEPES 10; Glucose 10; pH 7.4). The cells were loaded with *bis*-fura 2-acetoxymethyl (AM) ester at 6 $\mu$M for 45 minutes-1 hour and were left to incubate in darkness at room temperature. The cells were washed x2 in HBS and left for 15-30 minutes to allow for the de-esterification of the AM groups.

Prior to imaging, the tubes required for perfusion were washed for 10 minutes with 70% ethanol, followed by a 10 minute wash with distilled water. The tubes were then perfused with 1x HBS for 10-15 minutes at 30°C. A single coverslip containing cells loaded with fura-2 was adhered to the bottom surface of a Falcon™ petri dish (30mm) using high vacuum grease. The open petri dish was then mounted on a microscopic stage. A digital epifluorescence imaging system mounted on an Olympus BX50WI microscope (Olympus, Tokyo, Japan) was used to measure changes in intracellular $Ca^{2+}$ signal. Cells were excited at 350 and 380 nm, with emission detected above 500 nm. Changes in the fura-2 fluorescence ratio were visualised using MetaFluor® offline imaging software (Molecular Devices Corporation, CA, USA). Cells were perfused with ligand solution typically for ~5 minutes at a rate of 2 ml/min. Recordings were made at 5 second intervals.

Experiments were conducted as follows: firstly, cells were continuously perfused with HBS for 10-15 minutes to obtain a baseline. Then (1) if only agonist responses were being examined, a pre-determined amount of agonist solution was applied and allowed to perfuse over the cells to allow

for an increase in $Ca^{2+}$, as visualised by a change in fluorescence ratio. Cells were then washed for 30 minutes with HBS to completely rid the tubing of stimulant solution before beginning another experiment with another coverslip; (2) if antagonist effectiveness was being examined, a pre-determined amount of antagonist solution was applied and allowed to perfuse over the cells. Immediately after this, a solution was applied which contained both agonist and antagonist. After this, a solution of antagonist alone was again applied to inhibit any possible change in $[Ca^{2+}]_i$ that may have occurred during the prior period. The cells were washed for 30 minutes or more in HBS to rid the tubing of stimulant/antagonist. If there were no responses during ligand application or during the washout period, agonist solution was allowed to perfuse over the cells in order to visualise cellular responses and recovery from antagonist perfusion.

### *2.3.2. Immunocytochemistry*

*Phospho-CREB* – Cultured cell lines were attached to coverslips coated in poly-D-lysine (20 μg/ml) and incubated in serum-free media overnight at 37°C with 5% $CO_2$. The next day, the cells were washed three times in 1x HBS. Agonist ligands were applied for 25 min at 37°C and 0% CO2. Antagonists were applied for 30 min prior to co-application with agonist ligands for a further 25 min. The cells were then fixed in ice cold methanol for 5 minutes at -20°C. The cells were washed x3 in HBS and blocked for 30 minutes in 5% Marvel® milk powder (diluted in HBS; Premier Foods, Hertfordshire, UK) at room temperature. After washing x3 in HBS, the cells were incubated with primary Mouse anti-phospho-CREB monoclonal antibody at 1:250 dilution for 1 hour at room temperature. The cells were washed x3 in HBS. A Donkey anti-mouse secondary antibody conjugated with AlexaFluor® 488 dye at 1:500 dilution was applied to the coverslips and they were left to incubate at room temperature in darkness for 30 minutes. Cells were washed x3 with HBS. The coverslips were affixed to glass slides (VWR international, Leicestershire, UK) using Fluoromount-G mounting media (Southern Biotech, Birmingham, AL, USA) and allowed to set for <1 hour in darkness. An Axiovert 200M inverted confocal microscope (Zeiss, LSM-510-META, Carl Zeiss, Cambridge, UK) was used to examine the incorporated fluorophores.

In CREB experiments, 12-O-tetradecanoylphorbol-13-acetate (TPA) was used as a control stimulus. TPA is a specific activator of PKC and has previously been found to induce the transcription of CREB in mouse embryonic fibroblast cells (Johannessen *et al.,* 2004).

*Caspase-3* – Cultured primary cortical neurons attached to poly-L-lysine coated coverslips (40 μg/ml) were permeabilised using 1% saponin (diluted in $dH_2O$) for 5 minutes at room temperature. The cells were washed twice with PBS. The neurons were incubated in normal goat

serum (10%) for 2 hours at room temperature. The cells were washed x2 in PBS. The cells were incubated overnight at 4°C with anti-active caspase-3 primary rabbit antibody that also contained 10% normal goat serum (1:250 dilution). The next day, the neurons were washed x3 with PBS. They were incubated with secondary biotinylated goat anti-rabbit antibody (1:500; 20% normal goat serum included) for 90 minutes at room temperature. The cells were washed x3 with PBS. The cells were incubated with an Alexa Fluor® 633 goat anti-rabbit fluorescent probe (1:500; 10% normal goat serum included) for 40 minutes at room temperature. Following this they were washed x3 with PBS. The cells were blocked again using 5% normal goat serum and incubated at room temperature for 2 hours. They were washed x2 with PBS. The neurons were double-stained for NeuN at a 1:500 dilution (10% normal goat serum included) and incubated at 4°C overnight. The following day, the cells were incubated in secondary horse anti-mouse antibody (1:1000 dilution; 20% normal goat serum included) for 90 minutes at room temperature. They were washed x3 with PBS. The neurons were incubated with an Alexa Fluor® 488 goat anti-mouse fluorescent probe (1:500 dilution; 10% normal goat serum included) for 40 minutes at room temperature. They were then washed x3 with PBS. The neurons were incubated with Hoechst fluorescent dye (1:500 dilution; Invitrogen, CA, USA) for 15 minutes at room temperature. The Hoescht dye was removed from the coverslips and they were washed once with PBS. Excess PBS was removed and the coverslips were affixed to glass slides (Ramboldi, Limassol, Cyprus) using Vectashield mounting media (Vector Laboratories, Peterborough, UK). The mounting media protected against photobleaching. The edges of the coverslips were sealed using clear nail polish and the slides were stored in darkness at 4°C until needed for analysis. An Axiovert 200M inverted confocal microscope (Zeiss, LSM-510-META, Carl Zeiss, Cambridge, UK) was used to examine the incorporated fluorophores.

## 2.4. Sample Analysis and Quantification

### *2.4.1. Peak $Ca^{2+}$ response height*

To analyse the extent of $Ca^{2+}$ mobilisation during an experiment, raw data was extracted from cellular recordings using MetaFluor® offline software (Molecular Devices Corporation, CA, USA). The background was subtracted from these recordings. The raw data was then transferred to Origin 7 software (OriginLab Corporation, Stoke Mandeville, UK) where cell traces were created. The response height was obtained by measuring the raw data from the timepoint where the ligand was first applied up until 10 minutes after the ligand was removed during the washout. A baseline

height reading was also obtained by measuring the raw data from 5 minutes before the ligand was first applied. The following calculation was then used:

Peak response height = Response height – Baseline height

An average peak response height was calculated from the cells (in this case 9 cells per experiment). An example trace of a typical $Ca^{2+}$ imaging experiment can be observed in Figure 2.4.1. One trace represents one cell. Therefore, if there are multiple traces that are differentially coloured in one figure, each trace represents one cell recorded during one experiment. In this study, the release of $Ca^{2+}$ from intracellular stores measured with $Ca^{2+}$ imaging shall be referred to as an increase in $Ca^{2+}$ signal.

The peak response height data of $Ca^{2+}$ imaging experiments were transferred to GraphPad Prism 4 software (GraphPad Software, Inc., CA, USA) in order to construct histograms.

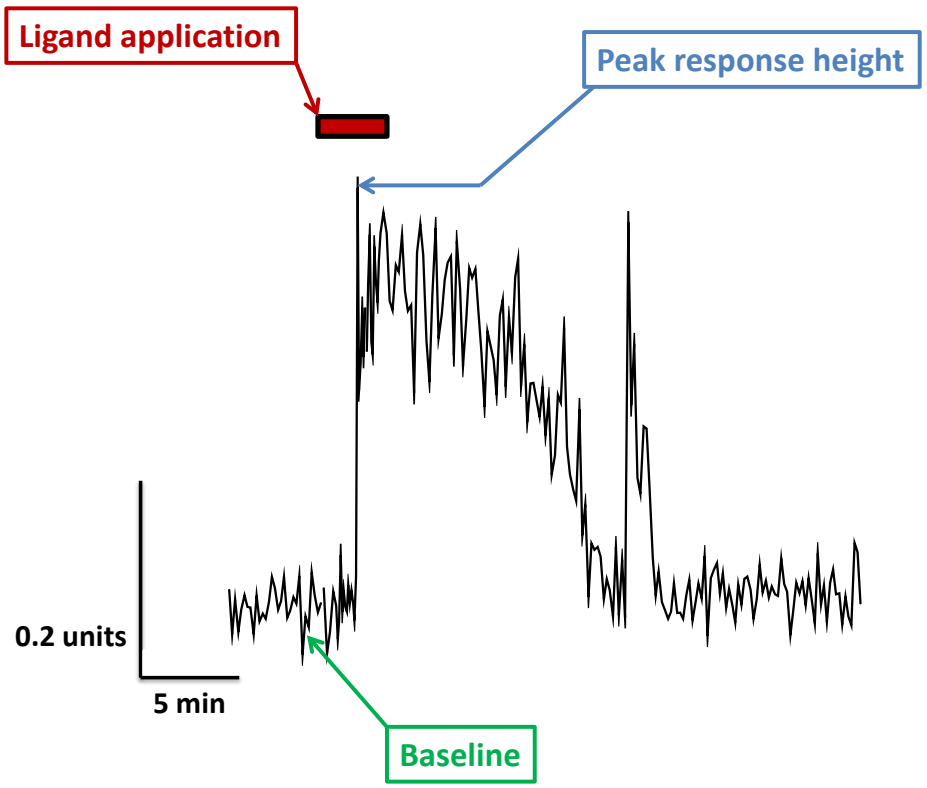


**Figure 2.4.1: An example trace of one cell recorded during a $Ca^{2+}$ imaging experiment.**

### *2.4.2. Phospho-CREB nuclear fluorescence*

As previously stated, cells on coverslips that underwent immunocytochemical staining were affixed to glass slides and images were taken using a confocal microscope. Nuclear fluorescence measurements of phospho-CREB were taken from these images using ImageJ free software (http://imagej.nih.gov/ij/; National Institutes of Health) in order to provide quantifiable data. To measure nuclear fluorescence, the following settings were applied in ImageJ: the 'Set Measurements' option was selected from the drop-down 'Analyse' menu on the toolbar. In the 'Set Measurements' tab, the boxes next to 'Area', 'Min and max gray value' 'Integrated density', 'Mean gray value' and 'Add to overlay' were ticked. 'Redirect to' was set to 'None' and 'Decimal places' were set to '3'. Once this was completed, 'OK' was clicked (See Figure. 2.3.1).

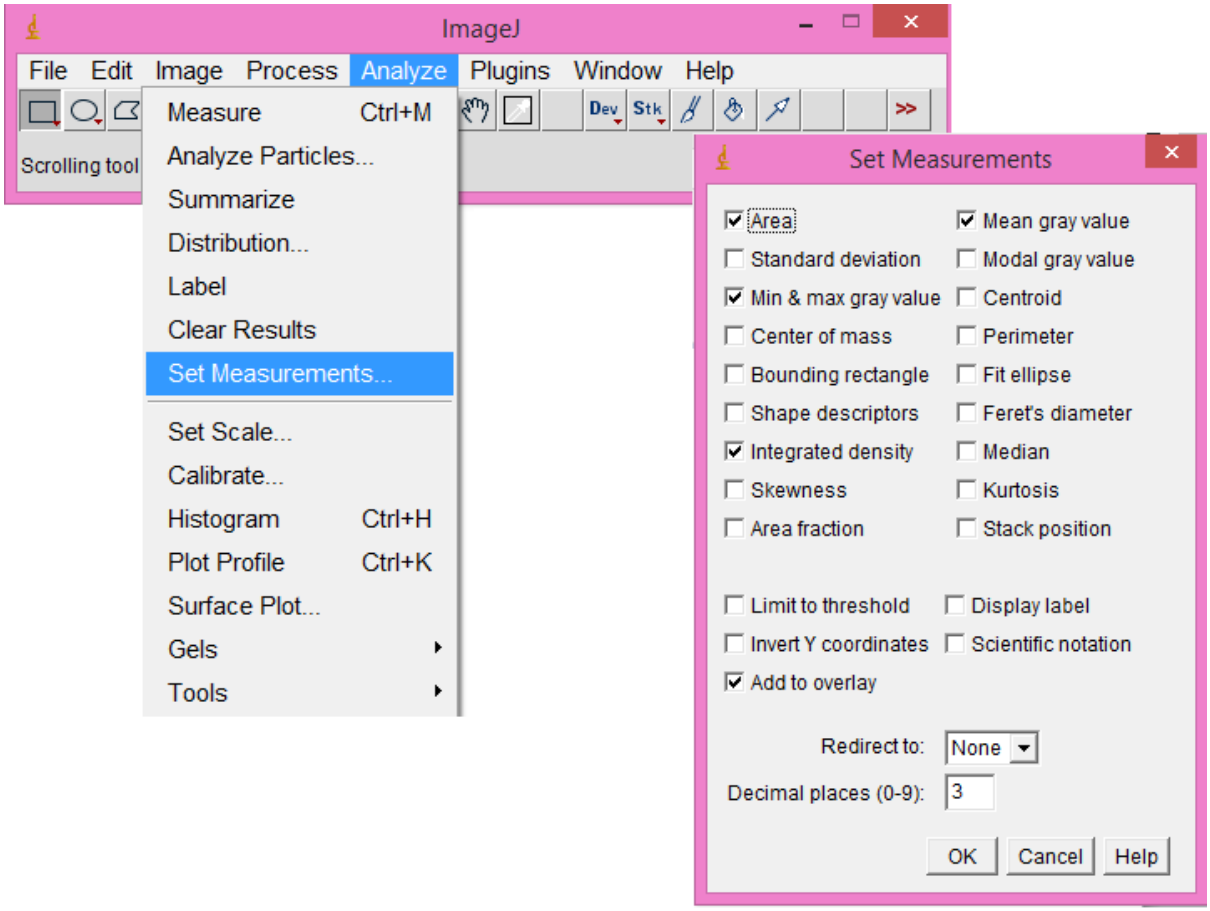

**Figure 2.4.2: Settings required in order to measure nuclear fluorescence in ImageJ software.**

An image of pCREB-stained cells, originally obtained using Zeiss LSM 510 software, was opened on ImageJ. On the main toolbar, the 'Polygon' option was selected. The author manually traced shapes on the background of the fluorescent image. By clicking 'm' on the keyboard, this brought up a 'Results' tab which detailed various parameters of the area just measured. The author then clicked '>' to switch to the brightfield view. In this view, lines were traced around the nuclei of cells using the 'polygon' tool because the nuclei were more distinct from the cytoplasm in this view. It also aided in keeping the recordings unbiased because the author did not know if the nuclei positively expressed pCREB in the brightfield view. The nuclear measurements were recorded by switching back to the fluorescent view of the image and clicking 'm' again (See Figure 2.3.2).

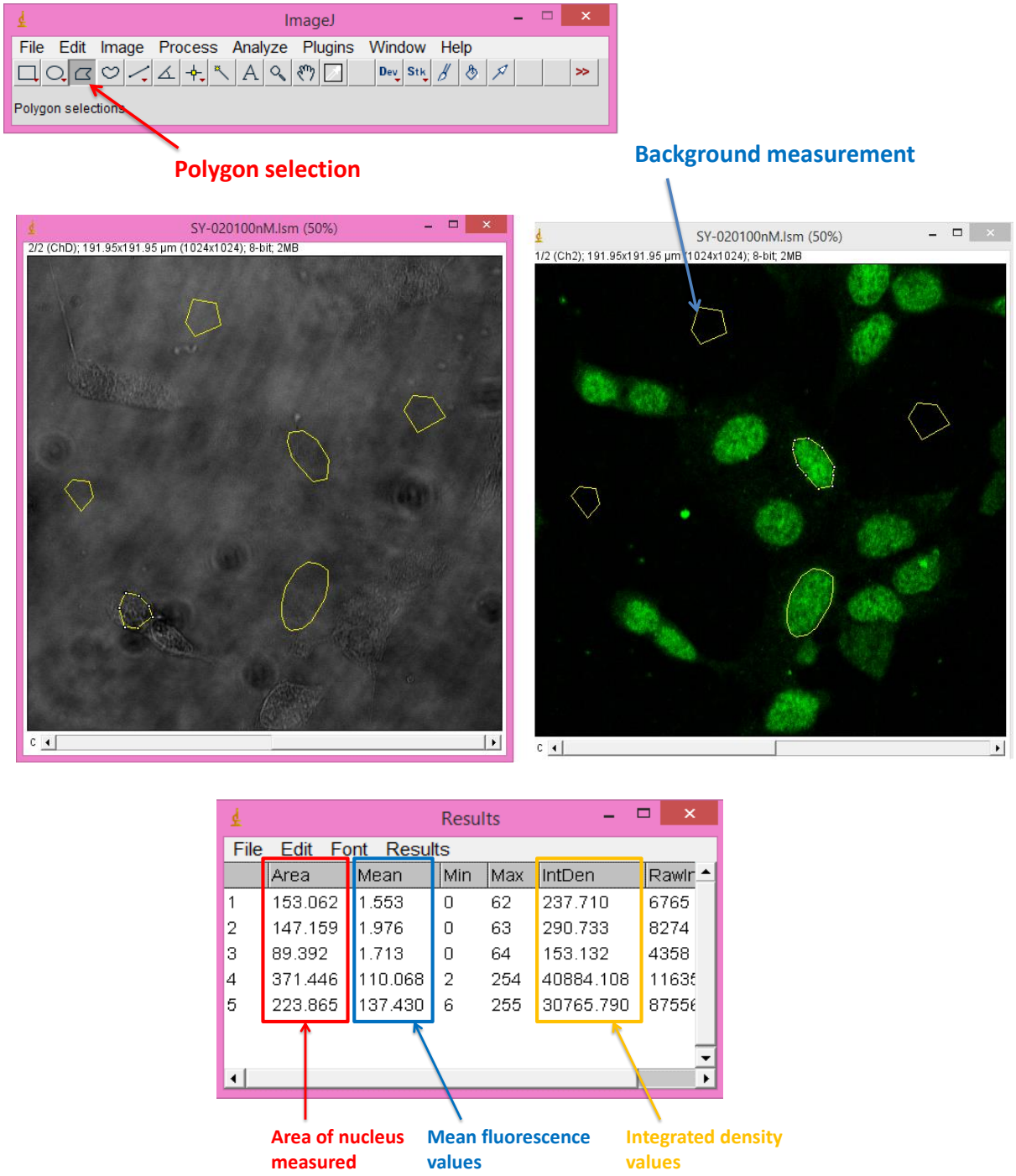


**Figure 2.4.3: Settings required in order to obtain raw data for analysis.**

The nuclear measurements were transferred to an excel file. An average fluorescence value was obtained from the three background areas measured by averaging the 'mean' values of each area.

The corrected total nuclear fluorescence (CTNF) was then obtained from the cells using the following formula:

CTNF = Integrated Density – (Area of nucleus x Mean of background)

This formula ensured that the size of the nuclear area in number of pixels, the integrated intensity of all pixels within the nuclear area and the average intensity per pixel were all corrected for background. Essentially, CTNF is a measurement of fluorescence intensity within a cell nucleus minus the background fluorescent intensity (Bülow *et al.,* 2014; Nederlof *et al.,* 1992; Potapova *et al.,* 2011). Data displayed on histograms was created by normalising CTNF values for an experiment against the mean 1 $\mu$M TPA value of that experiment. Histograms were then created using GraphPad Prism 4 software (GraphPad Software, Inc., CA, USA). Twelve nuclei were selected from each pCREB experiment in order to visualise the quantified data on graphs.

### *2.4.3. Caspase-3 fluorescence intensity*

Coverslips fixed with cortical neurons that were stained for caspase-3 and affixed to glass slides were analysed and images taken using a confocal microscope (Zeiss, LSM-510-META, Carl Zeiss, Cambridge, UK). Multiple images were taken for each treatment group at both a low magnification (40x) and a high magnification (63x). Different wavelengths were used that corresponded to the antibodies and stain materials used on the neurons during prior immunocytochemical staining. Images were taken at 633 nm for capase-3 detection, at 488 nm for NeuN detection and UV light was used to detect the Hoechst stain.

Caspase-3 fluorescence values were obtained using LSM-510 image examiner software (Zeiss, Carl Zeiss, Cambridge, UK). An image taken at 63x magnification was opened on-screen. Images at 63x magnification were chosen for measurement because there was greater detail and the fluorescence was more consistent than in images taken at 40x magnification. Once an image was open, the 'Histogram' tab was clicked on the right-hand panel. Using a line tool, lines were drawn around the cellular bodies of the neurons (not the processes). Once a complete shape was drawn around the cellular body, a fluorescence value for that measured area was given on-screen by clicking the 'Statistics' tab on the right hand panel. This process was repeated for other neurons in the image and again for other images taken of neurons in each treatment group. Background measurements were not taken.

Fluorescence values were transferred to an excel file and the average fluorescence intensity value was obtained for each treatment group in each experiment. In this study, 7 neuronal cellular bodies were measured per treatment group and per experiment. Histograms of the data were then created using GraphPad Prism 4 software (GraphPad Software, Inc., CA, USA).

## 2.5. Statistical Analyses

### *2.5.1. $Ca^{2+}$ imaging data analysis*

Statistical analyses were performed using a paired and two-tailed Student's *t* test in order to compare differences in the effects of ligands treatments on the same population of cells in the same experiment. If experiments were conducted in different cell populations, then a Mann-Whitney *U* test or One-Way Analysis of Variance (ANOVA) with Bonferroni's post hoc test were applied. $P < 0.05$ was considered a significant result. Data was obtained from 9 cells in a field per experiment.

### *2.5.2. Phospho-CREB nuclear fluorescence data analysis*

Statistical analyses were performed using One-Way ANOVA. If the results were significant, Bonferroni's Post hoc test was applied to determine which groups were significantly different from one another. A Mann-Whitney *U* test was applied if only two treatment groups were being compared. $P < 0.05$ was considered a significant result. Fluorescence data was obtained from 12 cellular nuclei in a field per experiment.

### *2.5.3. Caspase-3 fluorescence data analysis*

Statistical analyses were performed using One-Way ANOVA. Fluorescence data was obtained from the cellular bodies of 7 cells in a field per experiment.

# Chapter Three

## Results

### 3.1.1. LPI stimulation leads to an increase in intracellular $Ca^{2+}$ release in the hGPR55-HEK293 cell line.

GPR55 stimulation has previously been shown to lead to the release of $Ca^{2+}$ from intracellular ER stores in hGPR55-HEK293 cells via a $G\alpha_{13}$-RhoA-ROCK signalling pathway (Henstridge *et al.,* 2009a). In the hGPR55-HEK293 cell line, perfusion with a supramaximal concentration of LPI led to an increase in $Ca^{2+}$ signal (1 $\mu$M LPI = 0.171 ± 0.035 ratio units; Figure 3.1.1A). Recombinant HEK293 cells were compared to HEK293 control cells. Upon stimulation with 1 $\mu$M LPI, these cells did not produce an increase in $Ca^{2+}$ signal (1 $\mu$M LPI = 0.059 ± 0.003 ratio units; Figure 3.1.1Bi). This corroborates with previous data (Henstridge *et al.,* 2009a). However, stimulation with 10 $\mu$M LPI resulted in an increase in $Ca^{2+}$ signal (10 $\mu$M LPI = 0.103 ± 0.016 ratio units; Figure 3.1.1Bii). This is in contrast to findings previously reported (Henstridge *et al.,* 2009a), but it is worth noting that 10 $\mu$M LPI is a very high dose of ligand and could therefore be inducing an increase in intracellular $Ca^{2+}$ independently of GPR55. Due to time constraints, GPR55 antagonists were not tested against LPI (10 $\mu$M) in control HEK293 cells. This should be investigated in future. Sphingosine-1-phosphate (S1P) was applied to control HEK293 cells (1 $\mu$M S1P = 0.366 ± 0.109 ratio units; Figure 3.1.1Biii) and acted as a positive control ligand in order to show an increase in $Ca^{2+}$ signal (Gupta *et al.,* 2012).

## hGPR55-HEK293

**A**

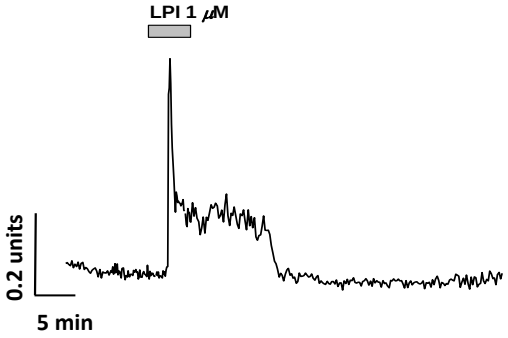


## HEK293

**Bi**

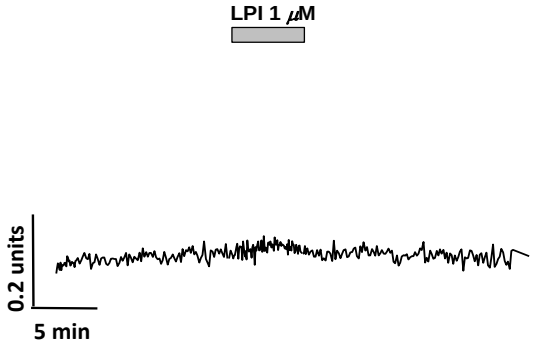


**Bii**

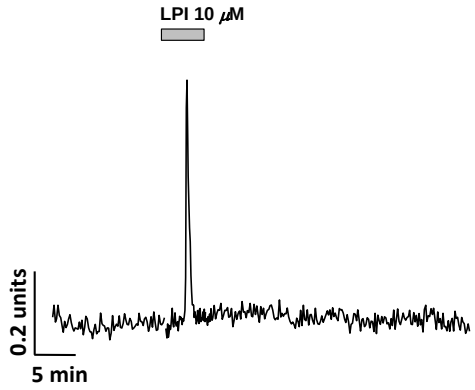


**Biii**

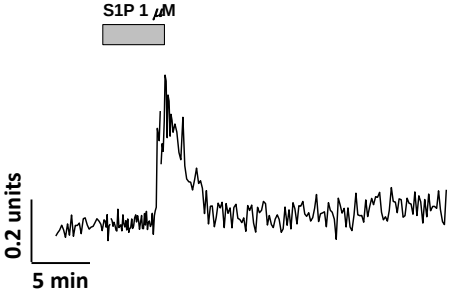

**Figure 3.1.1: LPI induces an increase in $Ca^{2+}$ signal in hGPR55-HEK293 cells.** (A-B**)** Representative traces of cell recordings from individual hGPR55-HEK293 cells and control HEK293 cells treated with various ligands. Each trace from each part of the figure represents one cell exposed to one ligand in one experiment. hGPR55-HEK293 cells were treated with (A) 1 $\mu$M LPI. HEK293 cells were treated with (Bi) 1 $\mu$M LPI, (Bii) 10 $\mu$M LPI, (Biii) 1 $\mu$M S1P. Data is represented as mean ± standard error of the mean (SEM). n = 3. Mean peak response measured from 9 cells per experiment.

### 3.1.2. CREB phosphorylation is induced by LPI in hGPR55-HEK293 cells but not in control HEK293 cells.

CREB is a member of a family of proteins that act as transcription factors. Phosphorylation of CREB causes it to translocate from the cell cytoplasm into the nucleus. In the nucleus, phospho-CREB activates CREB-mediated gene transcription e.g. *c-Fos*, which can lead to downstream effects such as cell proliferation (Carlezon Jr *et al.,* 2005; Shaywitz & Greenberg, 1999; Stevenson *et al.,* 2001).

In order to delineate if LPI mediates its effects via GPR55, CREB phosphorylation was compared in both stably transfected HEK293-AD cells (hGPR55-HEK293) and in control HEK293-AD cells. Cells treated with LPI (1 $\mu$M) for 25 minutes exhibited evidence of substantial CREB phosphorylation, which is indicated by a bright green nucleus (1 $\mu$M LPI = 0.698 ± 0.173 units; Figure 3.1.2C). A 25 minute application was chosen because it has been previously shown that this time point induces maximal pCREB activation in hGPR55-HEK293 cells (Henstridge, 2009). The cells also became rounder in morphology. In comparison, cells treated with DMSO (1:1000) for 25 minutes failed to show signs of CREB phosphorylation and the cells remained flat in morphology (DMSO = 0.329 ± 0.038 units; Figure 3.1.2A). In Figure 3.1.2B, it can be seen that treatment of cells with 1 $\mu$M 12-O-tetradecanoylphorbol-13-acetate (TPA) for 25 minutes resulted in robust CREB phosphorylation (1 $\mu$M TPA = 1.000 units).

Treatment with 1 $\mu$M LPI for 25 minutes did not cause CREB phosphorylation to occur in control HEK293 cells (HEK293, 1 $\mu$M LPI = 0.324 ± 0.033 units; Figure 3.1.2F). The cells were comparable to cells exposed to DMSO (HEK293, DMSO = 0.365 ± 0.212 units; Figure 3.1.2D). To test if control HEK293 cells were responsive, cells were treated with 1 $\mu$M TPA, which induced robust CREB phosphorylation (HEK293, 1 $\mu$M TPA = 1.000 units; Figure 3.1.2E).

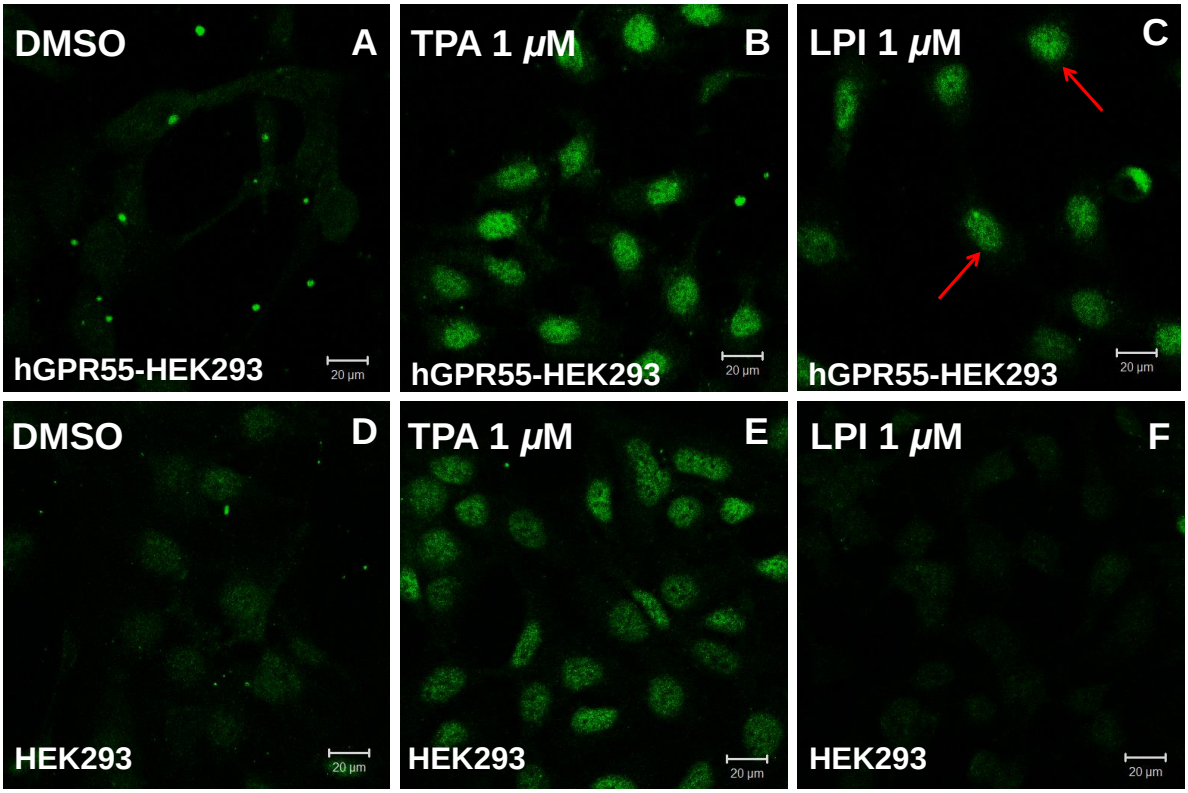


**Figure 3.1.2: CREB phosphorylation is induced by LPI in hGPR55-HEK293 cells.** Phosphorylated cAMP response element-binding protein (CREB) labelling in hGPR55-HEK293 cells treated with (A) DMSO; (B) 1 $\mu$M TPA and (C) 1 $\mu$M LPI, and labelling in HEK293 cells treated with (D) DMSO; (E) 1 $\mu$M TPA and (F) 1 $\mu$M LPI. Rounded-up cells are denoted by red arrows. A-E, n= 3, F, n =2. Fluorescence intensities measured from 12 cellular nuclei per experiment. Scale bar = 20 µm.

### 3.1.3. The GPR55 antagonist D327-0013 inhibits LPI-induced increases in $Ca^{2+}$ signal in the hGPR55-HEK293 cell line.

At 10 $\mu$M D327-0013 did not cause an increase in $Ca^{2+}$ signal when applied alone (10 $\mu$M D327-0013 = 0.057 ± 0.006 ratio units; Figure 3.1.3Aii). D327-0013 markedly inhibited $Ca^{2+}$ responses to LPI (1 $\mu$M) by 90.4 ± 0% (3 $\mu$M D327-0013 + 1 $\mu$M LPI = 0.029 ± 0.010 ratio units; later 1 $\mu$M LPI treatment = 0.303 ± 0.041 ratio units). This contrasts to cells exposed to 1 $\mu$M LPI in separate populations of cells, where there was a potent increase in $Ca^{2+}$ signal (1 $\mu$M LPI = 0.192 ± 0.020 ratio units; Figure 3.1.3Ai) A paired Student's *t* test was performed and indicated that 3 $\mu$M D327-0013 significantly inhibited 1 $\mu$M LPI compared to when the same cells were exposed

to only 1 $\mu$M LPI later on in the experiment (*P < 0.0131; Figure 3.1.3Aiii, Biii).. A lower concentration of 1 $\mu$M D327-0013 inhibited LPI-induced increase in $Ca^{2+}$ signal by 75.4 ± 0% (1 $\mu$M D327-0013 + 1 $\mu$M LPI = 0.048 ± 0.002 ratio units; later 1 $\mu$M LPI treatment = 0.194 ± 0.061 ratio units). A paired Student's *t* test was performed and indicated that 1 $\mu$M D327-0013 did not significantly inhibit 1 $\mu$M LPI compared to when the same cells were exposed to only 1 $\mu$M LPI later on in the experiment (P < 0.2477; Figure 3.1.4Bii).

When cells were exposed to 1-3 $\mu$M D327-0013 and 1 $\mu$M LPI and were compared to cells exposed to 1 $\mu$M LPI in separate populations, there was a marked inhibition in $Ca^{2+}$ signal (3 $\mu$M D327-0013 + 1 $\mu$M LPI = 0.019 ± 0.010 ratio units; 1 $\mu$M D327-0013 + 1 $\mu$M LPI = 0.048 ± 0.002 ratio units; 1 $\mu$M LPI, separate experiment = 0.192 ± 0.020 ratio units; Figure 3.1.3Ai). A One-Way ANOVA and Bonferroni's post hoc test were performed on this data and determined that 1-3 $\mu$M D327-0013 significantly inhibited LPI-induced increases in $Ca^{2+}$ signal compared to when cells were exposed to 1 $\mu$M LPI only in separate cell populations [$F_{(2,3)}$ = 650.9, ***P < 0.001] (Figure 3.1.3Biv).

No antagonism of LPI-induced responses were observed when nanomolar concentrations of D327-0013 were applied (300 nM D327-0013 + 1 $\mu$M LPI = 0.519 ± 0.287 ratio units; later 1 $\mu$M LPI treatment = 0.494 ± 0.368 ratio units; Figure 3.1.3Aii). A paired Student's *t* test was performed and indicated that 300nM D327-0013 did not significantly inhibit 1 $\mu$M LPI compared to when the same cells were exposed to just 1 $\mu$M LPI later on in the experiment (P < 0.807206). A One-Way ANOVA and a Bonferroni post hoc test were performed on this data and determined that 300 nM D327-0013 did not inhibit LPI-induced increases in $Ca^{2+}$ signal compared to when cells were exposed to 1 $\mu$M LPI only in separate populations of cells (Figure 3.1.4Biv).

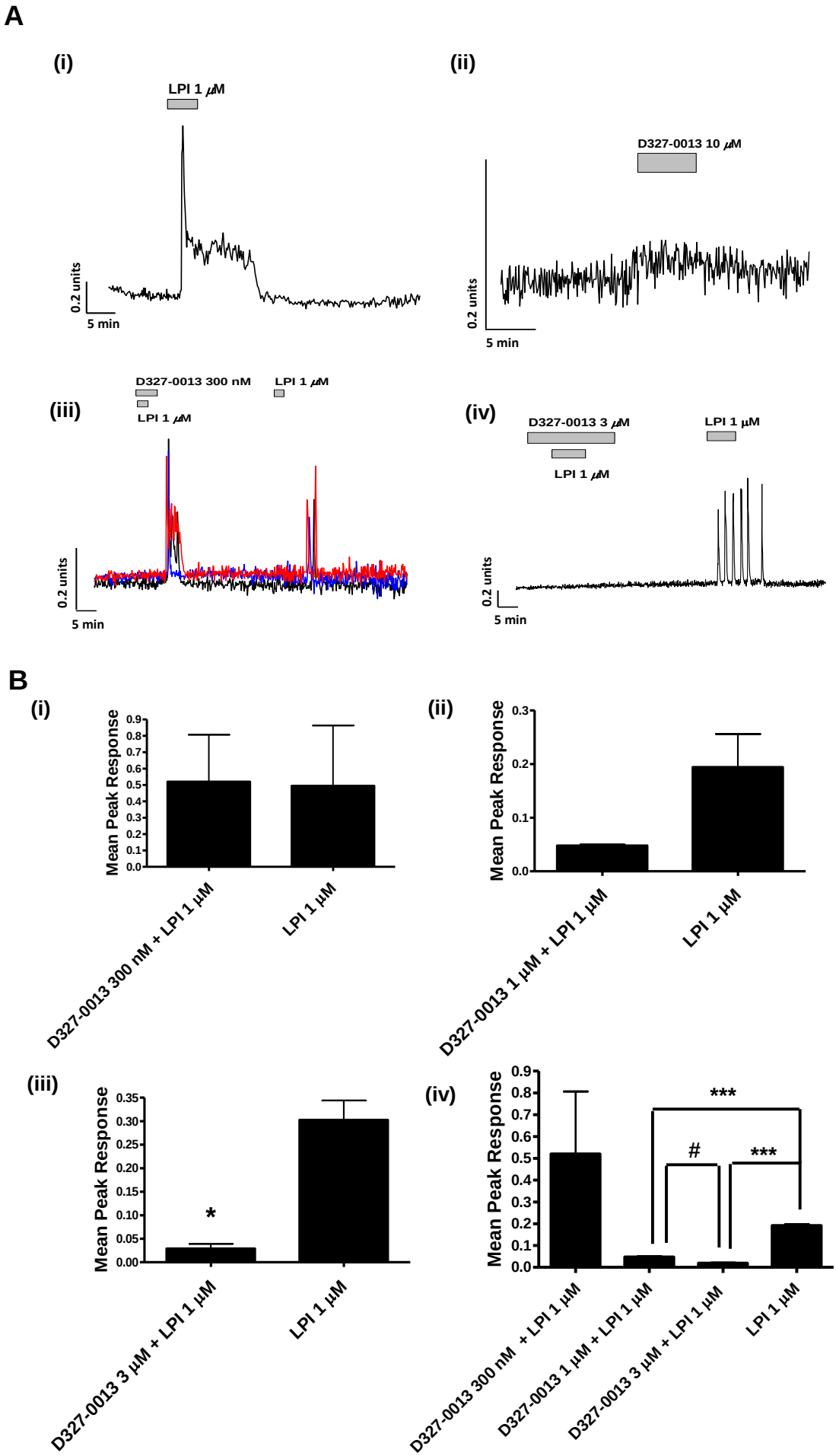
A
(i)
LPI 1 μM
0.2 units
5 min
(ii)
D327-0013 10 μM
0.2 units
5 min
(iii)
D327-0013 300 nM
LPI 1 μM
LPI 1 μM
0.2 units
5 min
(iv)
D327-0013 3 μM
LPI 1 μM
LPI 1 μM
0.2 units
5 min
B
(i)
Mean Peak Response
D327-0013 300 nM + LPI 1 μM
LPI 1 μM
(ii)
Mean Peak Response
D327-0013 1 μM + LPI 1 μM
LPI 1 μM
(iii)
Mean Peak Response
*
D327-0013 3 μM + LPI 1 μM
LPI 1 μM
(iv)
Mean Peak Response
***
#
***
D327-0013 300 nM + LPI 1 μM
D327-0013 1 μM + LPI 1 μM
D327-0013 3 μM + LPI 1 μM
LPI 1 μM

**Figure 3.1.3: The GPR55 antagonist D327-0013 inhibits LPI-induced increases in $Ca^{2+}$ signal in hGPR55-HEK293 cells.** (Ai-iv) Representative traces of hGPR55-HEK293 cells treated with ligands. (Ai) A trace representing the response of one cell to 1 $\mu$M LPI treatment alone. (Aii) 10 $\mu$M D327-0013 did not induce $Ca^{2+}$ release alone. (Aiii-iv) Cells were treated with D327-0013 at differing concentrations. LPI was co-perfused over the cells during antagonist exposure. In (iii), each differently coloured trace represents one cell. (Bi-iv) Histograms representing changes in $Ca^{2+}$ signal in cells exposed to 300nM-3 $\mu$M of D327-0013. A paired Student's *t* test was performed to compare cell treatment with D327-0013 and 1 $\mu$M LPI, with later LPI (1 $\mu$M)-only treatment in the same population of cells. * = D327-0013 significantly inhibited LPI-induced increases in cellular $Ca^{2+}$ signal compared to LPI application alone later on in the experiment ($P < 0.0131$). A One-Way ANOVA followed by a Bonferroni post hoc test was performed to compare cell treatment with D327-0013 and 1 $\mu$M LPI, with cell exposure to 1 $\mu$M LPI only in separate populations of cells. *** = D327-0013 significantly inhibited LPI-induced increases in cellular $Ca^{2+}$ signal compared to LPI application alone in separate populations ($P < 0.001$) . # = 3 $\mu$M D327-0013 inhibition of 1 $\mu$M LPI-induced changes in $Ca^{2+}$ signal is significantly different to 1 $\mu$M D327-0013-mediated inhibition of LPI-induced changes in $Ca^{2+}$ signal in different populations of cells ($P < 0.05$). Data is represented as mean ± SEM. Ai-ii, iv, Biii, n =3; Aiii, Bi-ii, iv, n =2. Mean peak response measured from 9 cells per experiment.

### 3.1.4. The GPR55 antagonist D327-0013 attenuates LPI-induced CREB phosphorylation levels in the hGPR55-HEK293 cell line.

The antagonistic effects of 3-10 $\mu$M D327-0013 against 1 $\mu$M LPI were analysed in relation to levels of pCREB fluorescence. D327-0013 (10 $\mu$M) inhibited 1 $\mu$M LPI by 59.9 ± 0% (10 $\mu$M D327-0013 alone = 0.310 ± 0.020 units; 10 $\mu$M D327-0013 + 1 $\mu$M LPI = 0.276 ± 0.004 units; Figure 3.1.4Aiv and Av). A concentration of 3 $\mu$M D327-0013 inhibited 1 $\mu$M LPI by 37.3 ± 0% (3 $\mu$M D327-0013 alone = 0.298 ± 0.041 units; 3 $\mu$M D327-0013 + 1 $\mu$M LPI = 0.431 ± 0.041 units). D327-0013 (1 $\mu$M) failed to inhibit LPI-induced CREB phosphorylation (1 $\mu$M D327-0013 alone = 0.261 units; 1 $\mu$M D327-0013 + 1 $\mu$M LPI = 0.850 units; Figure 3.1.4Avi and Avii). A histogram of fluorescence intensity data can be observed in Figure 3.1.4B. A One-Way ANOVA was applied with Bonferroni's post hoc test to determine if D327-0013 had a significant inhibitory

effect on LPI-induced CREB phosphorylation. The post hoc indicated that there was no significant difference in nuclear pCREB fluorescence between each treatment group. In comparison, cells treated with 1 $\mu$M LPI underwent robust CREB phosphorylation (1 $\mu$M LPI = 0.698 $\pm$ 0.173 units; Figure 3.1.4Aiii). DMSO-treated cells did not exhibit increased pCREB fluorescence (DMSO = 0.329 $\pm$ 0.038 units; Figure 3.1.4Ai). Cells stimulated with TPA showed evidence of robust CREB phosphorylation (1 $\mu$M TPA = 1.000 units; Figure 3.1.4Aii).

**A**

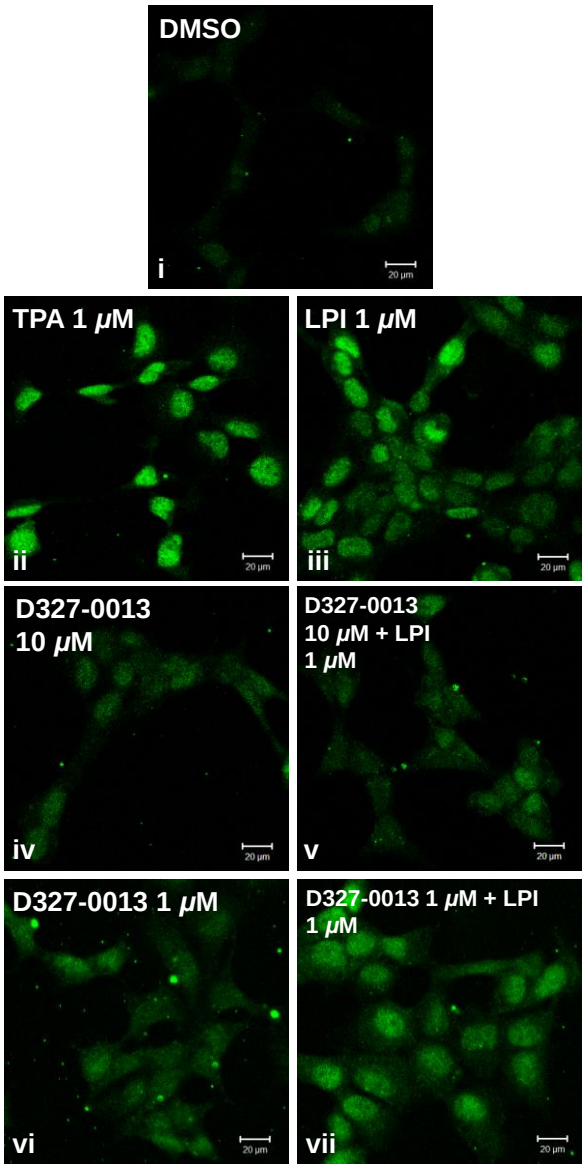
DMSO
i
TPA 1 μM
ii
LPI 1 μM
iii
D327-0013
10 μM
iv
D327-0013
10 μM + LPI
1 μM
v
D327-0013 1 μM
vi
D327-0013 1 μM + LPI
1 μM
vii
20 μm

**B**

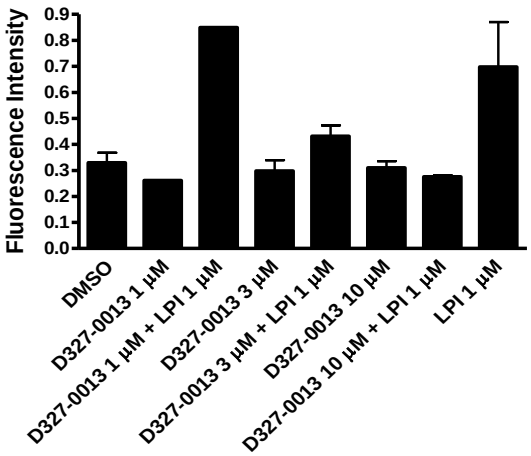
Fluorescence Intensity
0.0
0.1
0.2
0.3
0.4
0.5
0.6
0.7
0.8
0.9
DMSO
D327-0013 1 μM
D327-0013 1 μM + LPI 1 μM
D327-0013 3 μM
D327-0013 3 μM + LPI 1 μM
D327-0013 10 μM
D327-0013 10 μM + LPI 1 μM
LPI 1 μM

**Figure 3.1.4: The GPR55 antagonist D327-0013 GPR55 attenuates LPI-induced CREB phosphorylation levels in hGPR55-HEK293 cells.** (A) Phosphorylated CREB labelling in hGPR55-HEK 293 cells treated with (i) DMSO; (ii) 1 $\mu$M TPA; (iii) 1 $\mu$M LPI; (iv) 10 $\mu$M D327-0013; (v) 10 $\mu$M D327-0013 + 1 $\mu$M LPI; (vi) 1 $\mu$M D327-0013 and (vii) 1 $\mu$M D327-0013 + 1 $\mu$M LPI. (B) Histogram representing the effects of D327-0013 and LPI on phospho-CREB fluorescence. A One-Way ANOVA and Bonferroni's post hoc were performed to determine if there was a significant difference in pCREB fluorescence between each treatment group. The differences in fluorescence were not significant. Data is represented as mean ± SEM. Aiv-v, n = 2; Avi-vii, n =1; all other treatment groups, n = 3. Fluorescence intensities measured from 12 cellular nuclei per experiment. Scale bar = 20 μm.

### 3.1.5. The GPR55 antagonist C390-0219 inhibits LPI-induced increases in $Ca^{2+}$ signal in the hGPR55-HEK293 cell line.

Kargl *et al.* (2013) observed that the GPR55 antagonist C390-0219 inhibited LPI-mediated $Ca^{2+}$ release in a concentration-dependent manner in hGPR55-HEK293 cells. Similar experiments were performed in the current study. At 10 $\mu$M C390-0219 did not cause an increase in $Ca^{2+}$ signal when applied alone (10 $\mu$M C390-0219 = 0.053 ± 0.004 ratio units; Figure 3.1.5Aii). C390-0219 (3 $\mu$M) markedly inhibited responses to LPI (1 $\mu$M) by 75.8 ± 0% (3 $\mu$M C390-0219 + 1 $\mu$M LPI = 0.059 ± 0.013 ratio units; Figure 3.1.5Aiv). The effects of the antagonist were reversed following a 30 minute washout period. This contrasts to cells exposed to 1 $\mu$M LPI in separate populations of cells, where there was a potent increase in $Ca^{2+}$ signal (1 $\mu$M LPI = 0.192 ± 0.020 ratio units; Figure 3.1.3Ai). A paired Student's *t* test was performed and the *t* test indicated that 3 $\mu$M C390-0219 significantly inhibited 1 $\mu$M LPI in comparison to when the same cells were exposed 1 $\mu$M LPI later on in the same experiment (*P < 0.0157) (Figure 3.1.5Bi). C390-0219 (1 $\mu$M and 100 nM) did not antagonise LPI signalling (1 $\mu$M C390-0219 + 1 $\mu$M LPI = 0.090 ratio units, n =1; 100 nM C390-0219 + 1 $\mu$M LPI, n = 1 = 0.288 ± 0.218 ratio units; Figure 3.1.5Aiii).

A One-Way ANOVA and a Bonferroni post hoc test were performed on this data and determined that 100 nM and 3 $\mu$M C390-0219 did not significantly inhibit LPI-induced increases in $Ca^{2+}$ signal compared to when cells were exposed to 1 $\mu$M LPI only in separate populations of cells (Figure 3.1.5Bii). Statistical tests could not be performed on cells exposed to 1 $\mu$M C390-0219 because only an n = 1 was obtained (Figure 3.1.5Bii).

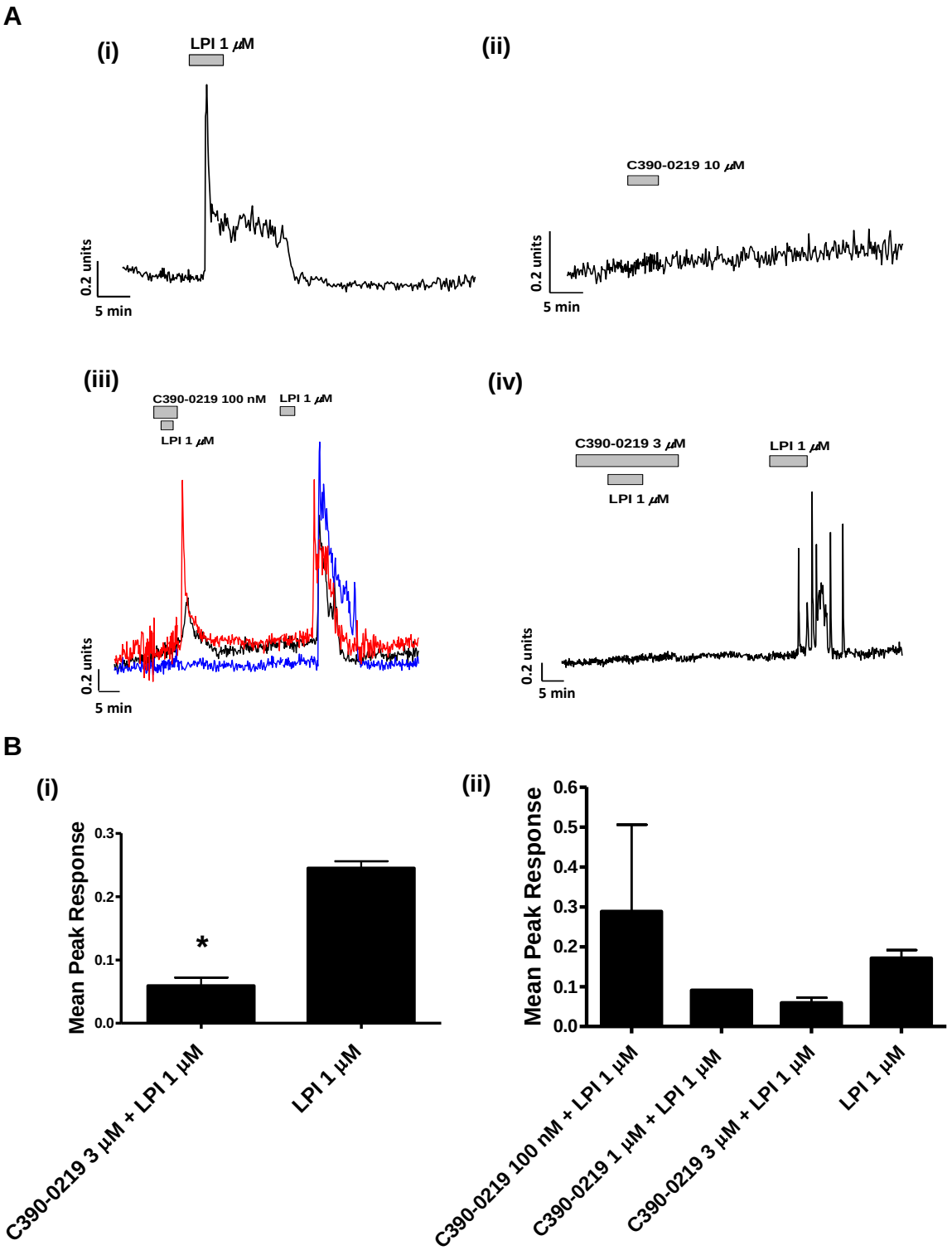
A
(i)
LPI 1 μM
0.2 units
5 min
(ii)
C390-0219 10 μM
0.2 units
5 min
(iii)
C390-0219 100 nM
LPI 1 μM
LPI 1 μM
0.2 units
5 min
(iv)
C390-0219 3 μM
LPI 1 μM
LPI 1 μM
0.2 units
5 min
B
(i)
Mean Peak Response
0.0
0.1
0.2
0.3
*
C390-0219 3 μM + LPI 1 μM
LPI 1 μM
(ii)
Mean Peak Response
0.0
0.1
0.2
0.3
0.4
0.5
0.6
C390-0219 100 nM + LPI 1 μM
C390-0219 1 μM + LPI 1 μM
C390-0219 3 μM + LPI 1 μM
LPI 1 μM

**Figure 3.1.5: The GPR55 antagonist C390-0219 inhibits LPI-induced increases in $Ca^{2+}$ signal in hGPR55-HEK293 cells.** (Ai-iv) Representative traces of hGPR55-HEK293 cells treated with ligands. (Ai) A trace representing the response of one cell to 1 $\mu$M LPI treatment alone. (Aii) 10 $\mu$M C390-0219 did not induce $Ca^{2+}$ release alone. (Aiii-iv) Cells were treated with C390-0219 at differing concentrations. LPI was co-perfused over the cells during antagonist exposure. In (iii), each differently coloured trace represents one cell. (Bi-ii) Histograms representing changes in $Ca^{2+}$ signal in cells exposed to 100nM-3 $\mu$M of C390-0219. A paired Student's *t* test was performed to compare cell treatment with C390-0219 and 1 $\mu$M LPI, with later LPI (1 $\mu$M)-only treatment in the same population of cells. * = C390-0219 significantly inhibited LPI-induced increases in cellular $Ca^{2+}$ signal compared to LPI application alone later on in the experiment (*$P < 0.0157$). Data is represented as mean ± SEM. Ai-ii, iv, Bi, n =3; Aiii, n = 2; 10 $\mu$M C390-0219 (+/- LPI), n = 1. Mean peak response measured from 9 cells per experiment.

### 3.1.6. The GPR55 antagonist C390-0219 attenuates LPI-induced CREB phosphorylation levels in the hGPR55-HEK293 cell line.

The putative GPR55 antagonist C390-0219 was not capable of antagonising $CB_1$-mediated CREB activation in $CB_1$-HEK293 cells. It also did not induce CREB phosphorylation when applied alone in the $CB_1$-HEK293 and control HEK293 cell lines (Kargl *et al.,* 2013). This suggests that C390-0219 does not mediate antagonistic effects via $CB_1$ receptor. It was therefore of interest to investigate if C390-0219 could inhibit agonist-induced CREB phosphorylation via GPR55.

Concentrations of 1 $\mu$M-10 $\mu$M C390-0219 and 1 $\mu$M LPI were tested in a CREB phosphorylation assay (10 $\mu$M C390-0219 alone = 0.202 ± 0.035 units; 10 $\mu$M C390-0219 + 1 $\mu$M LPI = 0.262 ± 0.017 units; 61.9 ± 0% inhibition; Figure 3.1.6Avi-v; 3 $\mu$M C390-0219 alone = 0.260 ± 0.038 units; 3 $\mu$M C390-0219 + 1 $\mu$M LPI = 0.348 ± 0.120 units; 49.4 ± 0.1% inhibition; Figure 3.1.5B; 1 $\mu$M C390-0219 alone = 0.229 ± 0.05 units; 1 $\mu$M C390-0219 + 1 $\mu$M LPI = 0.650 ± 0.125 units; Figure 3.1.6Avi-vii). A histogram of pCREB fluorescence intensities can be observed in Figure 3.1.6B. A One-Way ANOVA deduced that there was a significant difference in fluorescence intensities between the groups analysed [$F_{(3,8)} = 6.405$, *$P < 0.0161$]. A Bonferroni's Post hoc test was applied and the test indicated that C390-0219 (1-10 $\mu$M) did not significantly inhibit 1 $\mu$M LPI compared to 1 $\mu$M LPI treatment alone. LPI (1 $\mu$M) application by itself induced robust CREB phosphorylation (1 $\mu$M LPI = 0.698 ± 0.173 units; Figure 3.1.6Aiii). When DMSO vehicle (1:1000) was applied to hGPR55-HEK293 cells, it failed to induce CREB phosphorylation (DMSO = 0.329

± 0.038 units; Figure 3.1.6Ai). TPA (1 $\mu$M) induced robust CREB phosphorylation (1 $\mu$M TPA = 1.000 units; Figure 3.1.6Aii).

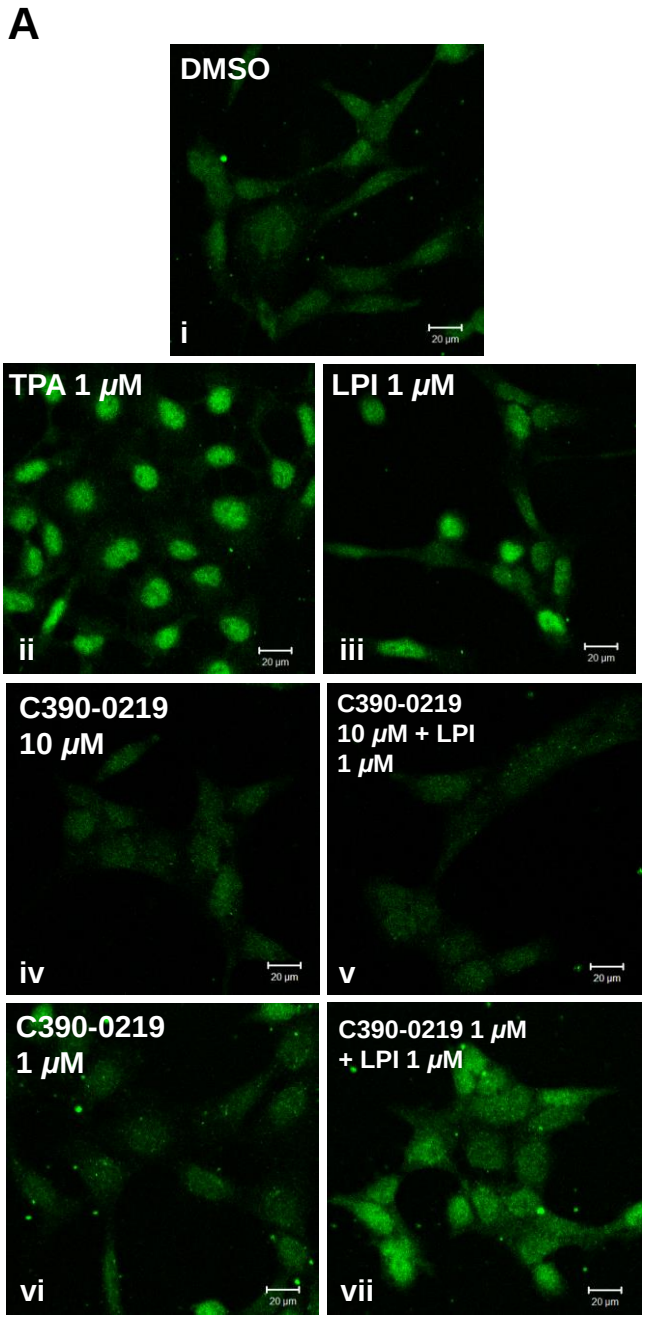
A
DMSO
i
20 µm
TPA 1 µM
ii
20 µm
LPI 1 µM
iii
20 µm
C390-0219
10 µM
iv
20 µm
C390-0219
10 µM + LPI
1 µM
v
20 µm
C390-0219
1 µM
vi
20 µm
C390-0219 1 µM
+ LPI 1 µM
vii
20 µm
B
*
Fluorescence Intensity
0.0
0.1
0.2
0.3
0.4
0.5
0.6
0.7
0.8
0.9
DMSO
C390-0219 1 µM
C390-0219 1 µM + LPI 1 µM
C390-0219 3 µM
C390-0219 3 µM + LPI 1 µM
C390-0219 10 µM
C390-0219 10 µM + LPI 1 µM
LPI 1 µM

**Figure 3.1.6: The GPR55 antagonist C390-0219 attenuates LPI-induced CREB phosphorylation in hGPR55-HEK293 cells.** (A) Phosphorylated CREB labelling in hGPR55-HEK 293 cells treated with (i) DMSO; (ii) 1 $\mu$M TPA (iii) 1 $\mu$M LPI; (iv) 10 $\mu$M C390-0219; (v) 10 $\mu$M C390-0219 + 1 $\mu$M LPI; (vi) 1 $\mu$M C390-0219 and (vii) 1 $\mu$M C390-0219 + 1 $\mu$M LPI. (B) Histogram representing the effects of C390-0219 and LPI on phospho-CREB fluorescence. ***** = LPI-induced CREB phosphorylation application is statistically significant compared to application of 10 $\mu$M C390-0219 treatment alone ($P < 0.05$). Data is represented as mean ± SEM. Ai-v, n = 3; Avi-vii, n = 2. Fluorescence intensity measured from 12 cellular nuclei per experiment. Scale bar = 20 μm.

### 3.2.1. GPR55 stimulation with the synthetic agonist SY-020 leads to an increase in $Ca^{2+}$ signal in the hGPR55-HEK293 cell line.

To date, it has been extremely difficult to delineate the physiological function of GPR55 due to an absence of selective pharmacological tools. The development of novel GPR55 antagonists such as the ones used throughout this study (Heynen-genel *et al.,* 2011; Kargl *et al.,* 2013; Kotsikorou *et al.,* 2013) will help researchers to better understand the true physiological and pathological role of this orphan receptor. However, the selectivity of GPR55 agonists is worth scrutinising. There has been much debate over the classification of GPR55 as a true cannabinoid receptor or as an orphan receptor due to its differential responsiveness to cannabinoid and non-cannabinoid ligands in different cell types (Gasperi *et al.,* 2013; Henstridge *et al.,* 2011; Nevalainen & Irving, 2010; Sharir & Abood, 2010). Although LPI has been established as a potent and direct agonist of GPR55 (Oka *et al.,* 2007), the selectivity of LPI for GPR55 could be contentious. For instance, LPI has previously been reported to signal via GPR119 in rat hepatoma cells overexpressing GPR119 (Soga *et al.,* 2005), and ligands previously believed to be GPR18 agonists also signal via GPR55 (Ashton, 2012; Ryberg *et al.,* 2007). It is therefore important to utilise both GPR55 antagonists and GPR55-selective agonists to determine if an experimental effect is truly GPR55-mediated.

The effects of the synthetic GPR55 agonist SY-020 were compared with those of the endogenous GPR55 agonist LPI during this study. SY-020 was created by the Nevalainen research group (experimental work in progress). The chemical structure of SY-020 is illustrated in Figure 3.2.1A. Previous data has shown that hGPR55-HEK293 cells can respond to concentrations of SY-020 in the picomolar range. The $EC_{50}$ of SY-020 in a $Ca^{2+}$ mobilisation assay was found to be 6 nM (Penman, experimental work in progress).

In this study, it was found that the application of supramaximal concentrations of SY-020 (30 nM-100 nM) to hGPR55-HEK293 cells induced robust mobilisation of $Ca^{2+}$ (hGPR55-HEK293 cells, 30 nM SY-020 = 0.143 ± 0.014 ratio units; 100 nM SY-020 = 0.281 ratio units, n = 1; Figure 3.2.1B). Cells produced oscillatory increases in $Ca^{2+}$ signal that appeared different to the changes induced by LPI – the duration of the $Ca^{2+}$ responses lasted substantially longer than that seen with LPI stimulation. Control HEK293 cells were also stimulated with SY-020 in order to determine if any changes in $Ca^{2+}$ signal were GPR55-mediated. In Figure 3.2.1Cii, it can be observed that stimulation with SY-020 at concentrations below 10 $\mu$M had little or no effect on $Ca^{2+}$ signal levels in control cells (HEK293 cells, 100 nM SY-020 = 0.058 ± 0.022 ratio units; 300 nM SY-020 = 0.046 ± 0.002 ratio units; 1 $\mu$M SY-020 = 0.054 ± 0.015 ratio units; 3 μM SY-020 = 0.049 ± 0.015 ratio units). However, some variable responses were observed in cells exposed to 10 $\mu$M SY-020 (10 $\mu$M SY-020 = 0.126 ± 0.067 ratio units). An $EC_{50}$ was not calculated because the response did not reach maximal level. It will be crucial to investigate in future if this high SY-020 concentration is inhibited in control HEK293 cells by the selective GPR55 antagonists utilised in this study. This will help to determine whether HEK293 cells may express low levels of GPR55.

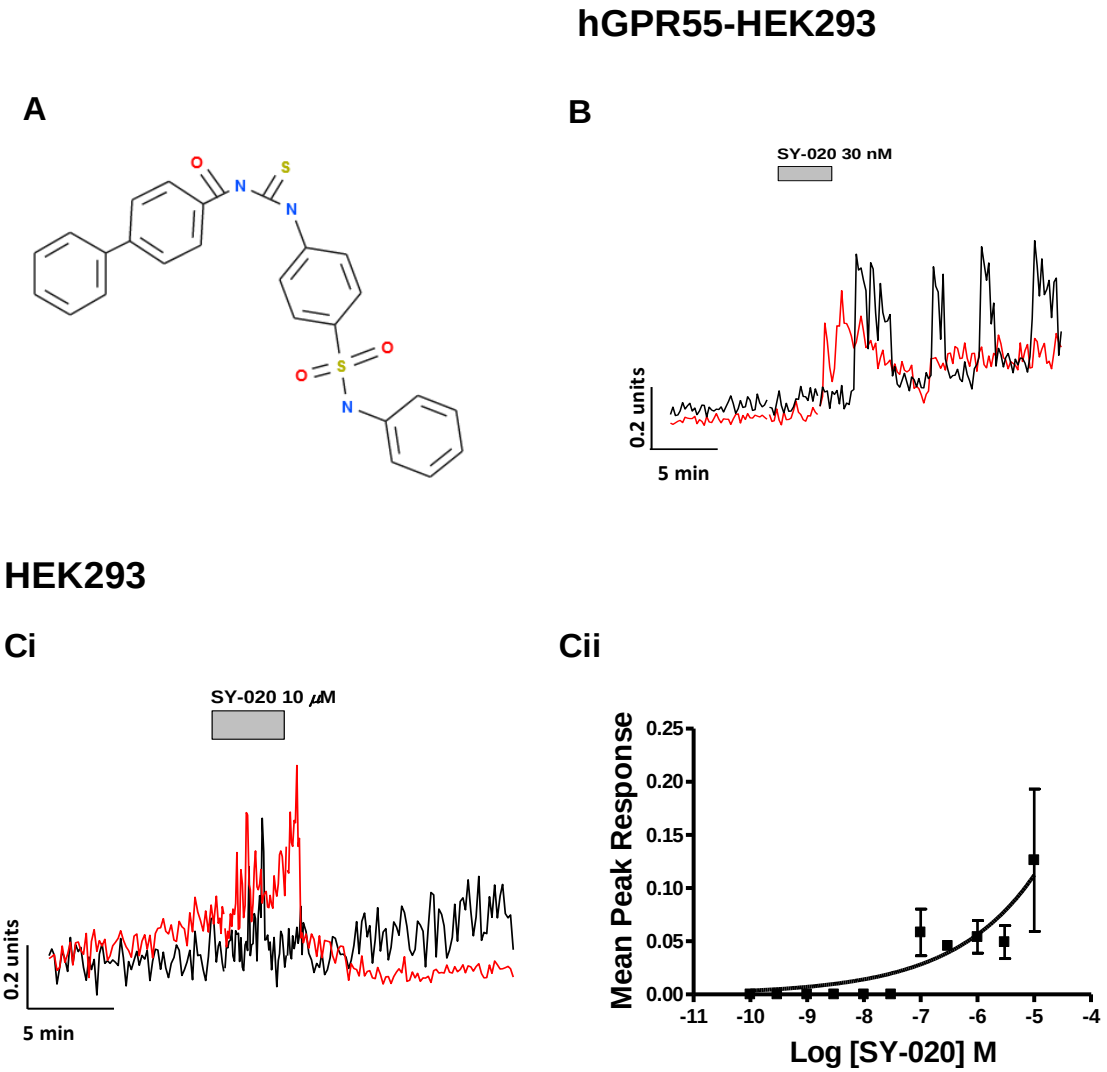


**Figure 3.2.1: The synthetic GPR55 agonist SY-020 induces increases in $Ca^{2+}$ signal in hGPR55-HEK293 cells.** (A) Chemical structure of the synthetic GPR55 agonist SY-020. (B-Ci) Representative traces from hGPR55-HEK293 cells and control HEK293 cells exposed to SY-020. hGPR55-HEK293 cells were treated with (B) 30 nM SY-020. HEK293 cells were treated with (Ci) 10 $\mu$M SY-020. (Cii) Concentration-response curve representing $Ca^{2+}$ release induced by SY-020 (100 nM-10 $\mu$M) in HEK293 cells. Data is represented as mean ± SEM. n = 3. Mean peak response measured from 9 cells per experiment.

### 3.2.2. The synthetic GPR55 agonist SY-020 induces CREB phosphorylation in hGPR55-HEK293 cells but not in control HEK293 cells.

To determine if SY-020 mediates its effects via GPR55, CREB phosphorylation was compared in both stably transfected HEK293 cells (hGPR55-HEK293) and in control HEK293 cells. Although an $EC_{50}$ value has not yet been determined for SY-020 in the phospho-CREB assay in hGPR55-HEK293 cells, preliminary findings indicated that nanomolar and micromolar (30 nM-10 $\mu$M) concentrations of SY-020 were capable of activating CREB. SY-020 (100 nM) seemed to effectively induce CREB phosphorylation so this concentration of ligand was used for the duration of this study (100 nM SY-020 = 1.012 ± 0.147 units; Figure 3.2.2Aii). Cells treated with DMSO (1:1000) did not induce pCREB activation in comparison (DMSO = 0.263 ± 0.046 units; Figure 3.2.2Ai). Treatment with 1 $\mu$M TPA led to CREB phosphorylation (1 $\mu$M TPA = 1.000 units; data not shown).

HEK293 cells were treated with 100 nM SY-020 for different lengths of time to determine whether time exposed to the ligand caused any variation in effect. In control HEK293 cells, 100 nM SY-020 failed to induce CREB phosphorylation at any of the time points tested (100 nM SY-020 5 min = 0.236 ± 0.066 units; 10 min = 0.290 ± 0.073 units; 15 min = 0.234 ± 0.122 units; 20 min = 0.265 ± 0.092 units; 25 min = 0.186 ± 0.061 units; 30 min = 0.138 ± 0.100 units; Figure 3.2.2Av-x). Treatment with DMSO (1:1000) did not cause CREB phosphorylation (DMSO-treated HEK293 cells = 0.365 ± 0.212 unit; Figure 3.2.2Aiii). CREB phosphorylation was induced in response to 1 $\mu$M TPA (1 $\mu$M TPA-treated HEK293 cells = 1.000 units; Figure 3.2.2Aiv). A One-Way ANOVA was performed and determined that there was no significant difference in pCREB nuclear fluorescence intensities between cells exposed to SY-020 (100 nM) for different lengths of time of SY-020 and cells exposed to DMSO (Figure 3.2.2B).

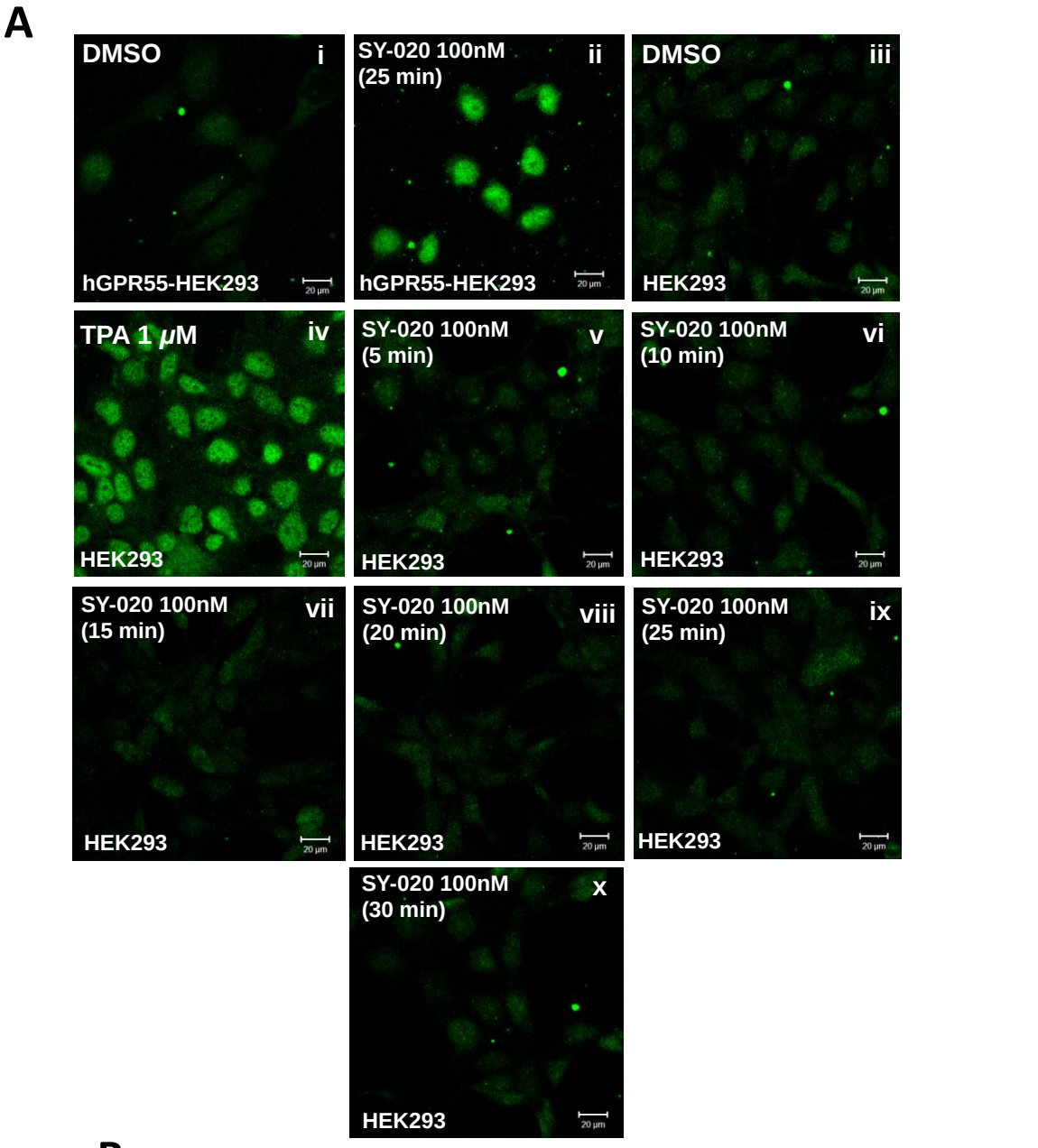
A
DMSO
i
hGPR55-HEK293
SY-020 100nM
(25 min)
ii
hGPR55-HEK293
DMSO
iii
HEK293
TPA 1 μM
iv
HEK293
SY-020 100nM
(5 min)
v
HEK293
SY-020 100nM
(10 min)
vi
HEK293
SY-020 100nM
(15 min)
vii
HEK293
SY-020 100nM
(20 min)
viii
HEK293
SY-020 100nM
(25 min)
ix
HEK293
SY-020 100nM
(30 min)
x
HEK293
B
Control (DMSO)
SY-020 100 nM
Fluorescence intensity
0.0
0.1
0.2
0.3
0.4
0.5
0.6
Control
5 min
10 min
15 min
20 min
25 min
30 min

**Figure 3.2.2: SY-020 induces CREB phosphorylation in hGPR55-HEK293 cells but not in control HEK293 cells.** (A) Phosphorylated CREB labelling in hGPR55-HEK293 cells treated with (i) DMSO and (ii) 100 nM SY-020; and in control HEK293 cells treated with (iii) DMSO; (iv) 1 $\mu$M TPA and (v-x) 100 nM SY-020 for 5-30 minutes. (B) Histogram representing HEK293 cell pCREB fluorescence intensity levels when the cells were treated with SY-020 for different lengths of time. n = 3. Fluorescence intensities measured from 12 cellular nuclei per experiment. Scale bar = 20 μm.

### 3.2.3. The GPR55 antagonist D327-0013 inhibits SY-020-induced increases in $Ca^{2+}$ signal in the hGPR55-HEK293 cell line.

Overexpressing cells were exposed to co-applications of D327-0013 (1-10 $\mu$M) and 30 nM SY-020 to determine if D327-0013 was capable of inhibiting SY-020-induced increases in $Ca^{2+}$ signal. This data was compared to later application of SY-020 (30 nM) to the same populations of cells (10 $\mu$M D327-0013 + SY-020 30 nM = 0.039 ± 0.000 ratio units; post-washout 30 nM SY-020 = 0.081 ± 0.006 ratio units; 52.6 ± 0% inhibition; Figure 3.2.3Aiii-iv; 3 $\mu$M D327-0013 + 30 nM SY-020 = 0.096 ± 0.004 ratio units; post-washout 30 nM SY-020 = 0.081 ± 0.000 ratio units; 42 ± 0% inhibition; 1 $\mu$M D327-0013 + 30 nM SY-020 = 0.153 ± 0.060 ratio units; 37.3 ± 0.1% inhibition; Figure 3.2.3Aii). These experiments contrast to 30 nM SY-020 application alone in a separate experiment, whereby robust increases in $Ca^{2+}$ signal can be observed (30 nM SY-020 alone = 0.143 ± 0.014 ratio units; Figure 3.2.3Ai). For clarity, data of cellular traces from one $Ca^{2+}$ imaging recording has been separated into two figures; initial co-treatment with 10 $\mu$M D327-0013 and SY-020 (Figure 3.2.3Aiii), and later treatment with SY-020 (Figure 3.2.3Aiv). This was to reduce the amount of visual noise present that would have been observed in one whole graph. A paired Student's *t* test was performed to compare treatments of 1-10 $\mu$M D327-0013 and 30 nM SY-020 with later treatment of SY-020 (30 nM)-only. The *t* test indicated that only 3 $\mu$M D327-0013 significantly inhibited 30nM SY-020 compared to when 30 nM of SY-020 was applied after HBS washout in the same populations of cells (*$P < 0.0451$).

Cells exposed to co-applications of 1-10 $\mu$M D327-0013 and 30 nM SY-020 were also compared to cells exposed to 30 nM SY-020 in separate populations of cells (30 nM SY-020 only = 0.143 ± 0.014 ratio units; Figure 3.2.3Ai). A histogram of this data can be observed in Figure 3.2.3Biv. A One-Way ANOVA determined that there was no significant difference in mean peak response between the different treatment groups.

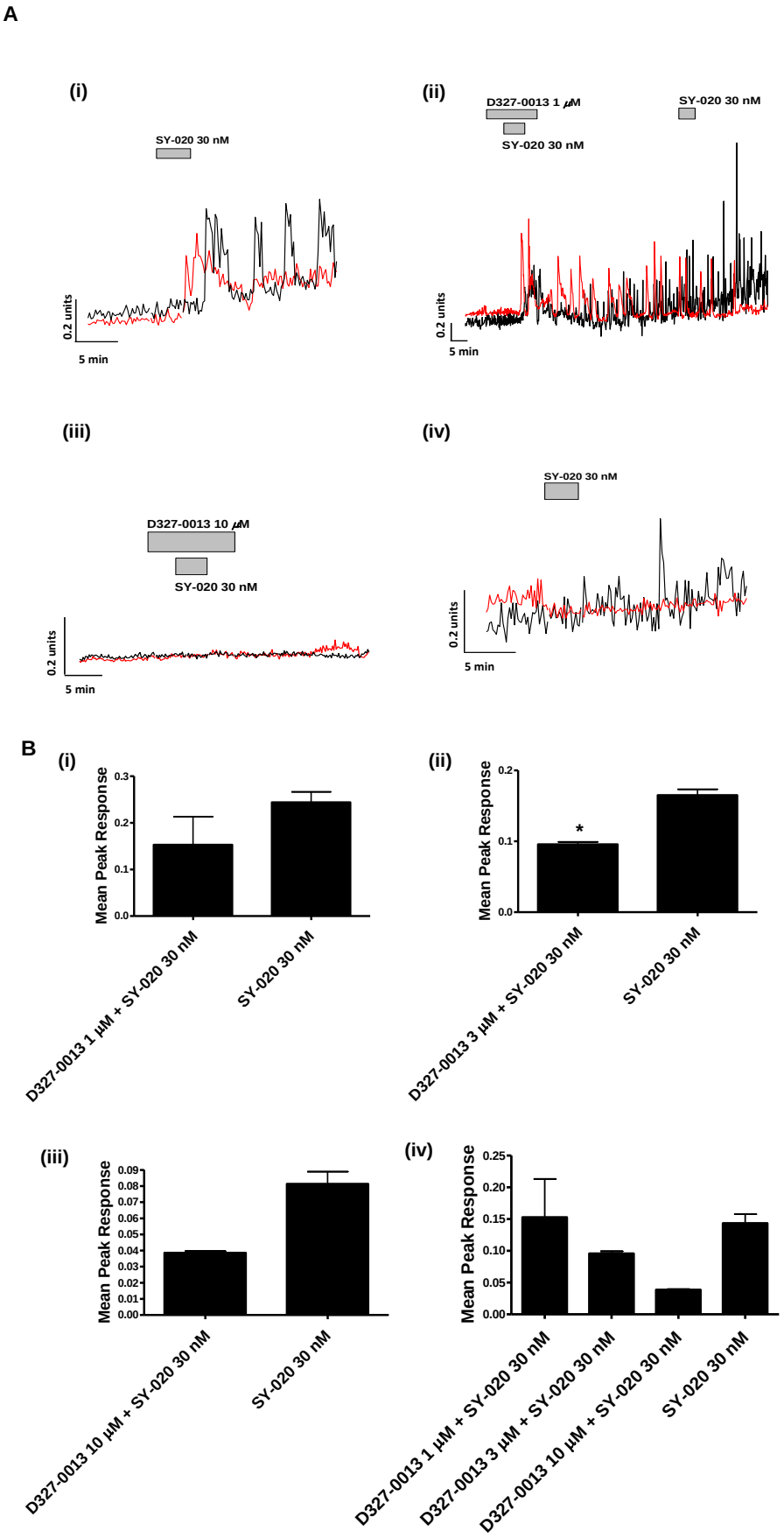
A
(i)
SY-020 30 nM
0.2 units
5 min
(ii)
D327-0013 1 μM
SY-020 30 nM
SY-020 30 nM
0.2 units
5 min
(iii)
D327-0013 10 μM
SY-020 30 nM
0.2 units
5 min
(iv)
SY-020 30 nM
0.2 units
5 min
B
(i)
Mean Peak Response
0.0
0.1
0.2
0.3
D327-0013 1 μM + SY-020 30 nM
SY-020 30 nM
(ii)
Mean Peak Response
0.0
0.1
0.2
*
D327-0013 3 μM + SY-020 30 nM
SY-020 30 nM
(iii)
Mean Peak Response
0.00
0.01
0.02
0.03
0.04
0.05
0.06
0.07
0.08
0.09
D327-0013 10 μM + SY-020 30 nM
SY-020 30 nM
(iv)
Mean Peak Response
0.00
0.05
0.10
0.15
0.20
0.25
D327-0013 1 μM + SY-020 30 nM
D327-0013 3 μM + SY-020 30 nM
D327-0013 10 μM + SY-020 30 nM
SY-020 30 nM

**Figure 3.2.3: D327-0013 GPR55 antagonist inhibits SY-020-induced increases in $Ca^{2+}$ signal in hGPR55-HEK293 cells.** (Ai-iv) Representative traces recorded from hGPR55-HEK293 cells treated with ligands. (Ai) Traces of recorded cell data showing increases in $Ca^{2+}$ signal induced by 30 nM of SY-020 alone. (Aii) Traces of recorded cell data exposed to 1 $\mu$M D327-0013 and 30 nM SY-020. (Aiii) Traces of recorded cell data exposed to 10 $\mu$M D327-0013 and SY-020, and (Aiv) later SY-020 (30 nM) treatment following HBS washout. (Bi-iv) Histograms representing the effects on $Ca^{2+}$ signal when cells were exposed to 1-10 $\mu$M of D327-0013. Paired *t* tests were performed to compare the effects of 1-10 $\mu$M D327-0013 and 30 nM SY-020, with 30 nM SY-020 when it was applied later on to the same populations of cells. * = 3 $\mu$M D327-0013 significantly inhibits SY-020-induced increases in $Ca^{2+}$ signal compared to later 30 nM SY-020 treatment alone (*P < 0.0451). Data is represented as mean ± SEM. Ai-Aii, n = 3; Aiii-iv, n =2. Mean peak response measured from 9 cells per experiment.

### 3.2.4. CREB phosphorylation induced by SY-020 is attenuated by a micromolar concentration of the GPR55 antagonist D327-0013 in hGPR55-HEK293 cells.

Application of D327-0013 alone did not induce CREB phosphorylation (10 $\mu$M D327-0013 = 0.567 ± 0.208 units; Figure 3.2.4Aiv; 3 $\mu$M D327-0013 = 0.301 ± 0.066 units; 1 $\mu$M D327-0013 = 0.379 ± 0.223; Figure 3.2.4Avi). A concentration of 10 $\mu$M D327-0013 inhibited 100 nM SY-020-induced CREB phosphorylation by 71.2 ± 0.1% (10 $\mu$M D327-0013 + 100 nM SY-020 = 0.259 ± 0.056 units; Figure 3.2.4Av). No antagonism of CREB phosphorylation was observed when 1-3 $\mu$M concentrations of D327-0013 and 100 nM SY-020 co-treatments were applied (3 $\mu$M D327-0013 + 100 nM SY-020= 0.647 ± 0.2120 units; 28.1 ± 0.1% inhibition; 1 $\mu$M D327-0013 + 100 nM SY-020= 0.873 ± 0.047 units; Figure 3.2.4Avii). A histogram of fluorescence intensity data can be observed in Figure 3.2.4B. A One-Way ANOVA was performed and determined that was no significant difference in fluorescence intensities between the treatment groups. Cells solely treated solely with 100 nM SY-020 underwent robust CREB phosphorylation (100 nM SY-020 = 0.900 ± 0.167 units; Figure 3.2.4Aiii). DMSO (1:1000) application did not induce CREB phosphorylation (DMSO = 0.228 ± 0.052 units; Figure 3.2.4Ai). Stimulation with 1 $\mu$M TPA induced robust CREB phosphorylation (1 $\mu$M TPA = 1.000 units; Figure 3.2.4Aii).

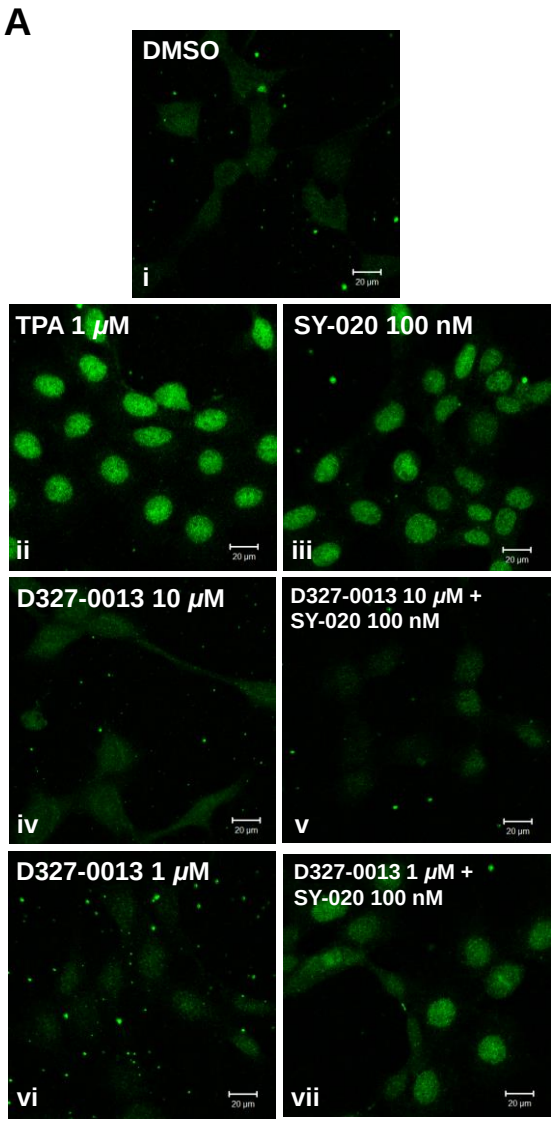
A
DMSO
i
TPA 1 μM
ii
SY-020 100 nM
iii
D327-0013 10 μM
iv
D327-0013 10 μM +
SY-020 100 nM
v
D327-0013 1 μM
vi
D327-0013 1 μM +
SY-020 100 nM
vii
B
Fluorescence Intensity
1.25
1.00
0.75
0.50
0.25
0.00
DMSO
D327-0013 1 μM
D327-0013 1 μM + SY-020
D327-0013 3 μM
D327-0013 3 μM + SY-020 100 nM
D327-0013 10 μM
D327-0013 10 μM + SY-020 100nM
SY-020 100 nM

**Figure 3.2.4: The GPR55 antagonist D327-0013 attenuates SY-020-induced CREB phosphorylation in hGPR55-HEK293 cells.** (A) Phosphorylated CREB labelling in hGPR55-HEK 293 cells treated with (i) DMSO; (ii) 1 $\mu$M TPA (iii) 100 nM SY-020; (iv) 10 $\mu$M D327-0013; (v) 10 $\mu$M D327-0013 + 100 nM SY-020; (vi) 1 $\mu$M D327-0013 and (vii) 1 $\mu$M D327-0013 + 100 nM SY-020. (B) Histogram representing the effects of D327-0013 and SY-020 on phospho-CREB fluorescence. Data is represented as mean ± SEM. n =2. Fluorescence intensity measured from 12 cellular nuclei per experiment. Scale bar = 20 μm.

### 3.2.5. The GPR55 antagonist C390-0219 attenuates SY-020-induced increases in $Ca^{2+}$ signal in the hGPR55-HEK293 cell line.

Overexpressing cells were exposed to co-applications of C390-0219 (1 and 10 $\mu$M) and 30 nM SY-020 to determine if C390-0219 was capable of inhibiting SY-020-induced increases in $Ca^{2+}$ signal (Figure 3.2.5Aii-iv). This data was compared to later application of SY-020 (30 nM) alone later on in the same populations of cells (10 $\mu$M C390-0219 + SY-020 30 nM = 0.124 ± 0.001 ratio units; post-washout 30 nM SY-020 = 0.496 ± 0.186 ratio units; 75.0 ± 0% inhibition; Figure 3.2.5Aiii-iv; 1 $\mu$M C390-0219 + 30 nM SY-020 = 0.070 ± 0.261 ratio units; Figure 3.2.3Aii). These experiments contrast to 30 nM SY-020 application alone in a separate experiment, whereby robust increases in $Ca^{2+}$ signal can be observed (30 nM SY-020 alone = 0.143 ± 0.014 ratio units; Figure 3.2.5Ai). For clarity, data of cellular traces from one $Ca^{2+}$ imaging recording has been separated into two figures; initial co-treatment with 10 $\mu$M C390-0219 and SY-020 (Figure 3.2.5Aiii), and later treatment with SY-020 (Figure 3.2.5Aiv). This was to reduce the amount of visual noise present that would have been observed in one whole graph. A paired Student's *t* test was performed to compare treatments of 10 $\mu$M C390-0219 and 30 nM SY-020 with later treatment of SY-020 (30 nM)-only (Figure 3.2.5Bii). The *t* test that determined that 10 $\mu$M C390-0219 did not significantly inhibit 30 nM SY-020 ($P < 0.2240$). A paired *t* test could not be performed on cellular data obtained from cells exposed to 1 $\mu$M C390-0219 and 30 nM SY-020 because only an n =1 was obtained (Figure 3.2.5Aii, Bi). However, one can see from Figure 3.2.5Aii-iv and Bi-ii that there appears to be attenuative effects of C390-0219 (1 $\mu$M and 10 $\mu$M) on SY-020-induced increases in $Ca^{2+}$ signal.

Cells exposed to co-applications of 10 $\mu$M C390-0219 and 30 nM SY-020 were also compared to cells exposed to just 30 nM SY-020 in separate populations of cells (30 nM SY-020 only = 0.143

± 0.014 ratio units; Figure 3.2.3Ai). A histogram of this data can be observed in Figure 3.2.3Biii. A Mann-Whitney *U* test determined that 10 $\mu$M C390-0219 did not have a significant inhibitory effect on SY-020 (30nM)-induced increases in $Ca^{2+}$ signal.

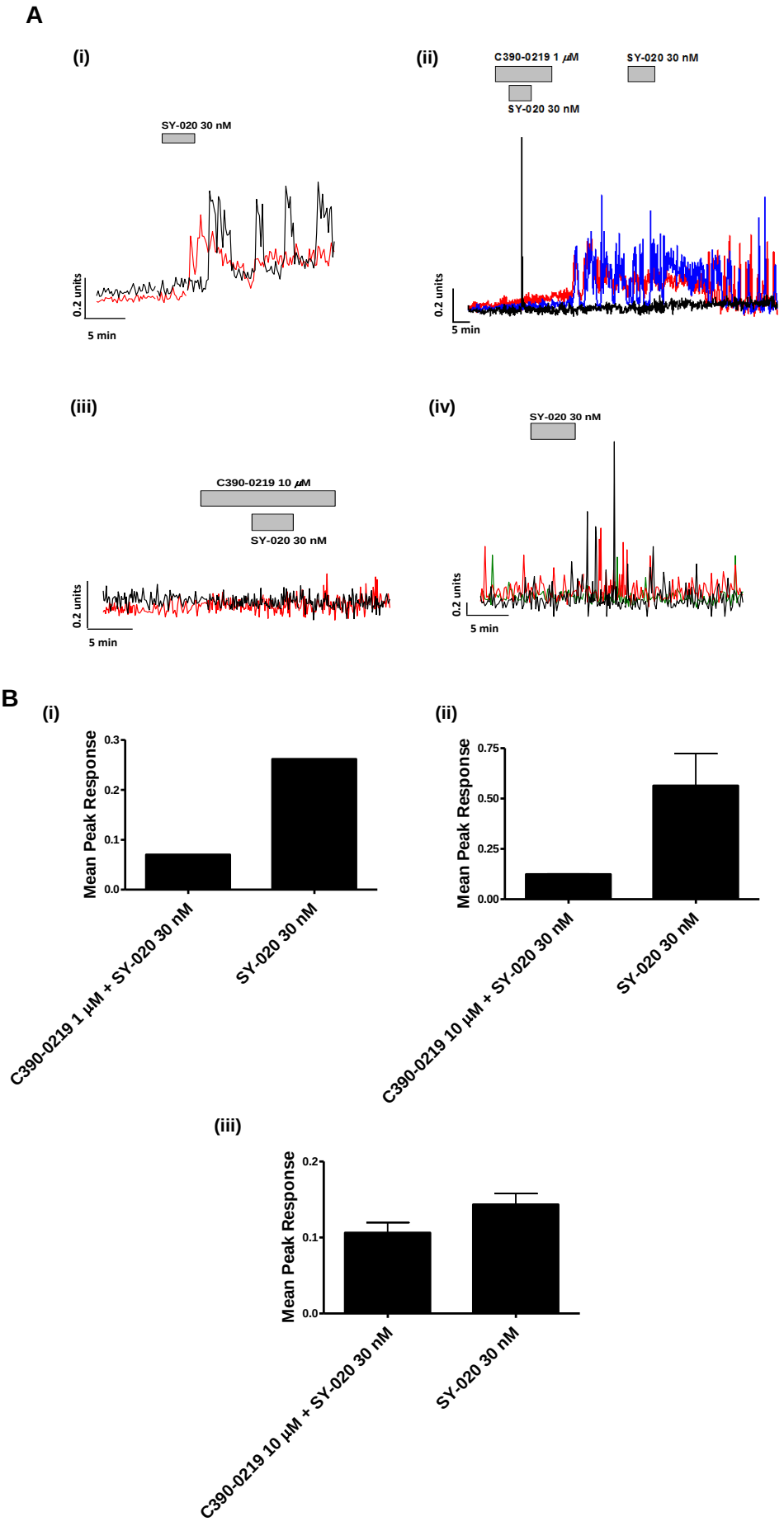
A
(i)
SY-020 30 nM
0.2 units
5 min
(ii)
C390-0219 1 μM
SY-020 30 nM
SY-020 30 nM
0.2 units
5 min
(iii)
C390-0219 10 μM
SY-020 30 nM
0.2 units
5 min
(iv)
SY-020 30 nM
0.2 units
5 min
B
(i)
Mean Peak Response
0.3
0.2
0.1
0.0
C390-0219 1 μM + SY-020 30 nM
SY-020 30 nM
(ii)
Mean Peak Response
0.75
0.50
0.25
0.00
C390-0219 10 μM + SY-020 30 nM
SY-020 30 nM
(iii)
Mean Peak Response
0.2
0.1
0.0
C390-0219 10 μM + SY-020 30 nM
SY-020 30 nM

**Figure 3.2.5: The GPR55 antagonist C390-0219 attenuates SY-020-induced increases in $Ca^{2+}$ signal in hGPR55-HEK293 cells.** (Ai-iv) Representative traces recorded from hGPR55-HEK293 cells treated with ligands. (Ai) Traces of recorded data showing cellular increases in $Ca^{2+}$ signal induced by 30 nM of SY-020 alone. (Aii) Traces of recorded data when cells were exposed to 1 $\mu$M C390-0219 and 30 nM SY-020. (Aiii) Traces of recorded data when cells were exposed to 10 $\mu$M C390-0219 and 30 nM SY-020, and (Aiv) later SY-020 (30 nM) treatment following HBS washout. (Bi-iv) Histograms representing the effects on $Ca^{2+}$ signal when cells were exposed to 1 and 10 $\mu$M of C390-0219. Paired *t* tests were performed to compare the effects induced by 10 $\mu$M C390-0219 and 30 nM SY-020, with the effects induced by 30 nM SY-020 when it was applied later on to the same populations of cells. Data is represented as mean ± SEM. Ai, Aiii-iv n = 3; Aii, n = 1. Mean peak response measured from 9 cells per experiment.

### 3.2.6. CREB phosphorylation induced by SY-020 is attenuated by the GPR55 antagonist C390-0219 in hGPR55-HEK293 cells.

Application of C390-0219 alone did not induce CREB phosphorylation (10 $\mu$M C390-0219 = 0.302 ± 0.037 units; 3 $\mu$M C390-0219 = 0.321 ± 0.060 units; 1 $\mu$M C390-0219 = 0.377 ± 0.099 units; Figure 3.2.6Aiv, vi). Treatment with 10 $\mu$M C390-0219 and 100 nM SY-020 led to inhibition of pCREB by 49.8 ± 0.3% (10 $\mu$M C390-0219 + 100 nM SY-020 = 0.507 ± 0.295 units; Figure 3.2.6Av). A concentration of 3 $\mu$M C390-0219 + 100 nM SY-020 did not antagonise SY-020-induced CREB phosphorylation (3 $\mu$M C390-0219 + 100 nM SY-020 = 1.112 ± 0.831 units). However, a concentration of 1 $\mu$M C390-0219 appeared to antagonise 100 nM SY-020 more-so than 10 $\mu$M C390-0219 (1 $\mu$M C390-0219 + 100 nM SY-020 = 0.343 ± 0.084 units; 66 ± 0.1% inhibition; n = 2; Figure 3.2.6 Avii). There was variability in the data obtained for 10 $\mu$M C390-0219 and 100 nM SY-020 treatment however, so this may be why 10 $\mu$M of C390-0219 appeared to be less effective at inhibiting 100 nM of SY-020.

A histogram of fluorescence intensity data can be observed in Figure 3.2.6B. A One-Way ANOVA was performed to determine if there was a significant difference in fluorescence intensities when cells were treated with 1-10 $\mu$M C390-0219 and 100 nM SY-020. The One-Way ANOVA confirmed that there was a significant difference in fluorescence intensities between the groups but Bonferroni's Post hoc test did not detect a significant effect of C390-0219-mediated inhibition on SY-020-induced CREB phosphorylation. SY-020 (100 nM) treatment alone induced robust CREB phosphorylation (100 nM SY-020 = 1.012 ± 0.147 units; Figure 3.2.6Aiii). DMSO (1:1000)

application did not induce CREB phosphorylation (DMSO = 0.433 ± 0.207 units; Figure 3.2.6Ai). Stimulation with 1 $\mu$M TPA induced robust CREB phosphorylation (1 $\mu$M TPA = 1.000 units; Figure 3.2.6Aii).

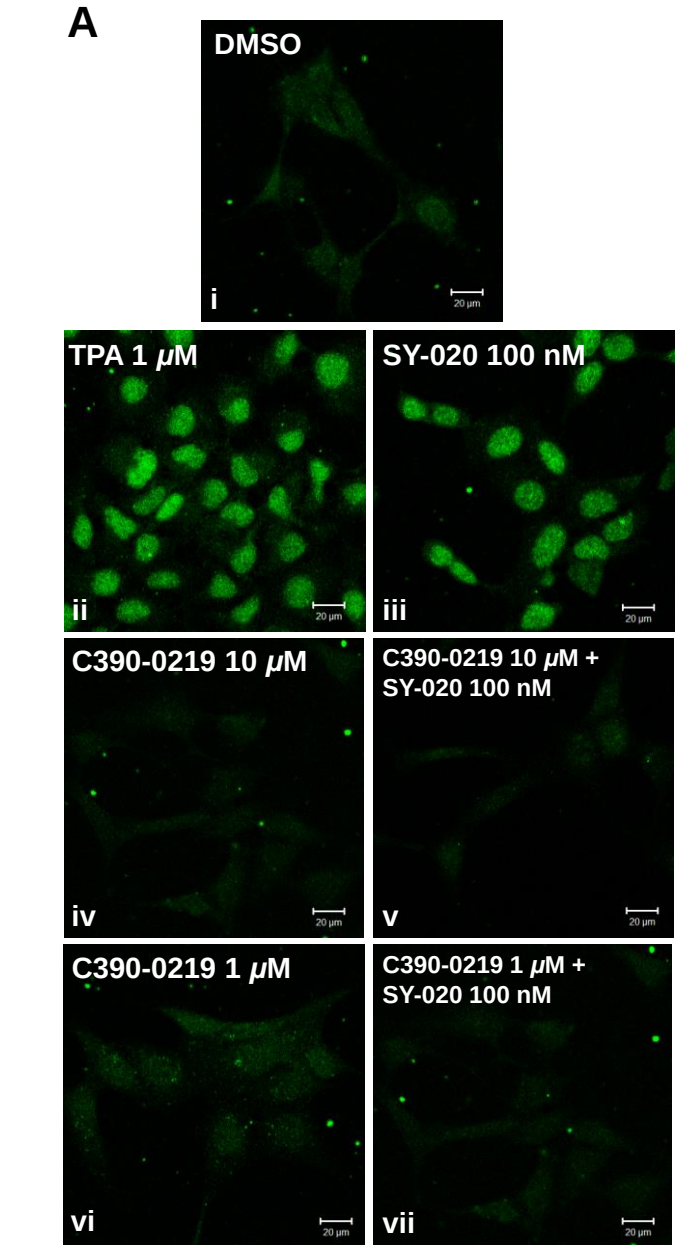
A
DMSO
i
20 µm
TPA 1 µM
ii
SY-020 100 nM
iii
C390-0219 10 µM
iv
C390-0219 10 µM +
SY-020 100 nM
v
C390-0219 1 µM
vi
C390-0219 1 µM +
SY-020 100 nM
vii
B
Fluorescence intensity
2
1
0
DMSO
C390-0219 1 µM
C390-0219 1 µM + SY-020 100nM
C390-0219 3 µM
C390-0219 3 µM + SY-020 100 nM
C390-0219 10 µM
C390-0219 10 µM + SY-020 100nM
DMSO
SY-020 100 nM

**Figure 3.2.6: C390-0219 GPR55 antagonist attenuate SY-020-induced CREB phosphorylation in hGPR55-HEK293 cells.** (A) Phosphorylated CREB labelling in hGPR55-HEK293 cells treated with (i) DMSO; (ii) 1 $\mu$M TPA (iii) 100 nM SY-020; (iv) 10 $\mu$M C390-0219; (v) 10 $\mu$M C390-0219 + 100 nM SY-020; (vi) 1 $\mu$M C390-0219 and (vii) 1 $\mu$M C390-0219 + 100 nM SY-020. (Bi-ii) Histograms representing the effects of C390-0219 and SY-020 on phospho-CREB fluorescence. A One-Way ANOVA was performed to analyse the significance of C390-0219 effectiveness in inhibiting SY-020-induced CREB phosphorylation. Data is represented as mean ± SEM. Ai-v, Bi, n =3; Avi-ii, Bii, n = 2. Fluorescence intensity measured from 12 cellular nuclei per experiment. Scale bar = 20 μm.

### 3.3.1. LPI stimulation leads to an increase $Ca^{2+}$ signal in the DU145 prostate cancer cell line.

In the DU145 prostate cancer cell line, perfusion with a supramaximal concentration of LPI (3 $\mu$M) induced an increase in $Ca^{2+}$ signal (3 $\mu$M LPI = 0.326 ± 0.157 ratio units; Figure 3.3.1A). This corroborates with previous data, whereby 3 $\mu$M LPI was sufficient to induce increases in $Ca^{2+}$ signal in DU145 cells (Penman, 2013). *In vitro* models that express GPR55 endogenously e.g. DU145 prostate cancer cells, need higher concentrations of agonist to stimulate the receptor because GPR55 is not expressed as highly in native cells as it is in recombinant systems (Piñeiro *et al.,* 2011).

Please note that at the beginning of this research project, DU145 cells originally obtained from the Division of Cancer Research at the University of Dundee were used for experiments. However, further into the project this batch of cells became unresponsive to LPI. A new batch of DU145 cells obtained from the Centre for Diabetes at the Queen Mary University of London was used for the remainder of the project.

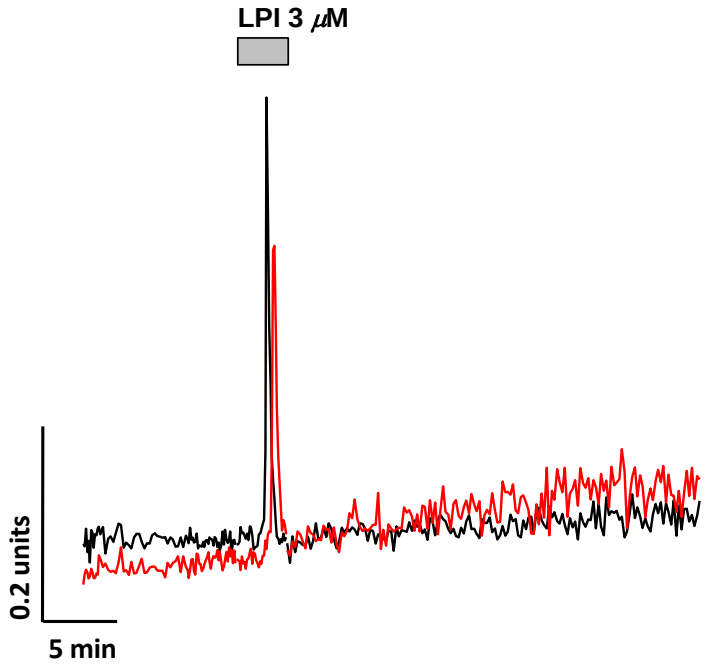


**Figure 3.3.1: LPI induces increases in $Ca^{2+}$ signal in DU145 prostate cancer cells.** Traces from two DU145 cells representing an increase in fluorescence ratio signal when the cells were exposed to 3 $\mu$M LPI. n = 3.

### 3.3.2. LPI stimulation leads to the phosphorylation of CREB in the DU145 prostate cancer cell line.

CREB phosphorylation was investigated in DU145 prostate cancer cells because receptor stimulation and protein kinase-dependent signalling mechanisms induce the activation of CREB in these cells. Interestingly, CREB phosphorylation has been linked to tumorigenicity and prostate cancer cell progression (Park *et al.,* 2013). It was therefore of interest to see if GPR55 stimulation with LPI could induce CREB phosphorylation.

Cells treated with 1 $\mu$M LPI exhibited evidence of substantial CREB phosphorylation which was localised to the cell nucleus (1 $\mu$M LPI = 0.614 ± 0.081 units; Figure 3.3.2Aiii). This corroborates with previous data, whereby 1 $\mu$M LPI was sufficient to induce CREB phosphorylation in DU145 cells (Penman, 2013). A Mann-Whitney *U* test determined that there was no significant difference in pCREB fluorescence between cells treated with 1 $\mu$M LPI and those treated with DMSO ($P < 0.1000$; Figure 3.3.2B). Cells treated with DMSO (1:1000) for 25 minutes failed to show signs of CREB phosphorylation (DMSO = 0.241 ± 0.028 units; Figure 3.3.2Ai). In Figure 3.3.2Aii,

treatment of the cells with 1 $\mu$M TPA for 25 minutes resulted in a substantial increase in the phosphorylation of CREB (1 $\mu$M TPA = 1.000 units).

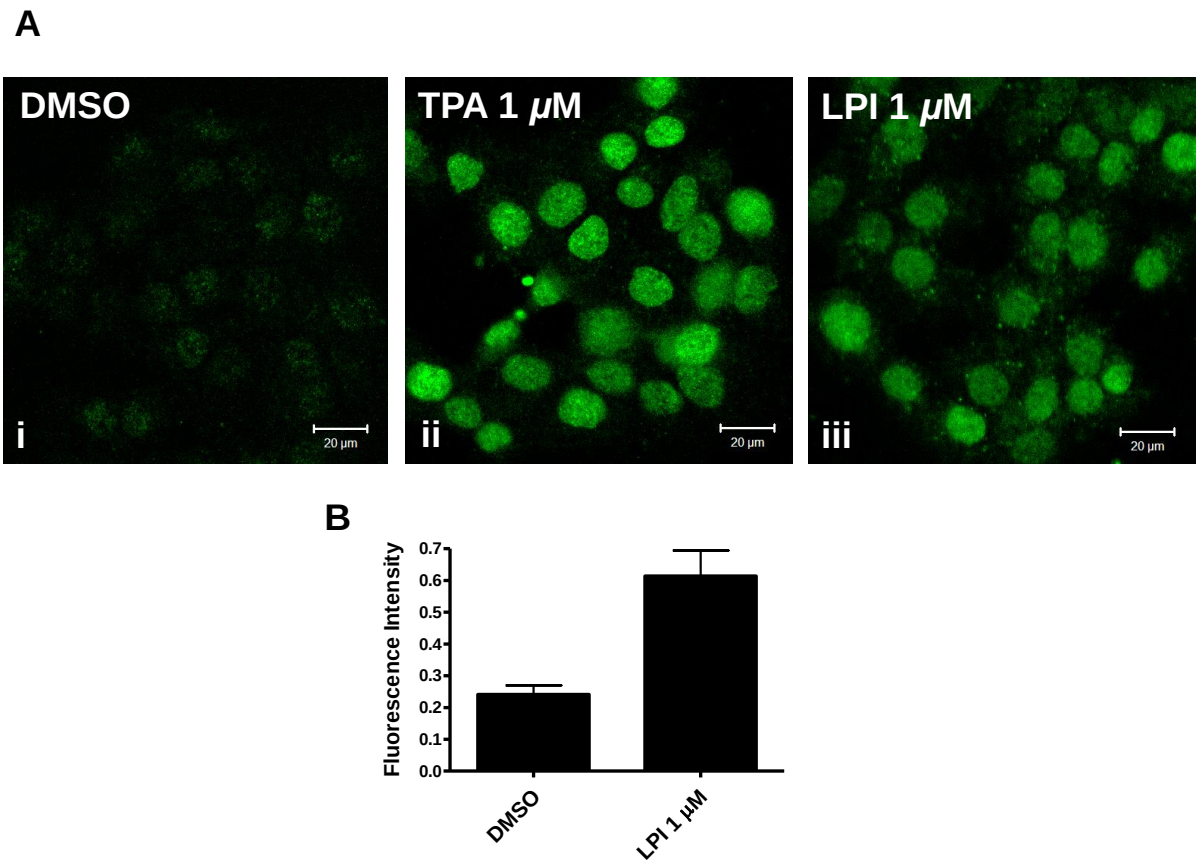


**Figure 3.3.2: LPI induces CREB phosphorylation in DU145 cells.** (A) Phosphorylated CREB labelling in DU145 cells treated with (i) DMSO; (ii) 1 $\mu$M TPA and (iii) 1 $\mu$M LPI. (B) A histrogram representing the effects of ligand treatments on pCREB fluorescence levels. Ai-iii, B, n = 3. Fluorescence intensities measured from 12 cellular nuclei per experiment. Scale bar = 20 μm.

### 3.3.3. The GPR55 antagonist D327-0013 fails to inhibit LPI-induced increases in $Ca^{2+}$ signal in the DU145 prostate cancer cell line.

Not all of the experimental groups obtained for treatment with 10 $\mu$M D327-0013 and 3 $\mu$M LPI were exposed to later application with 3 $\mu$M of LPI following a washout with HBS. For this reason, an unpaired and two-tailed Mann-Whitney *U* test was performed to compare groups treated with

10 $\mu$M D327-0013 and 3 $\mu$M LPI with treatment groups exposed to 3 $\mu$M of LPI in separate populations of cells. The *U* test showed that 10 $\mu$M D327-0013 did not inhibit LPI (3 $\mu$M)-induced increases in $Ca^{2+}$ signal (10 $\mu$M D327-0013 + 3 $\mu$M LPI = 0.322 ± 0.038 ratio units; $P < 0.7000$; Figure 3.3.3A-B) compared to LPI (3 $\mu$M) application alone (0.326 ± 0.157 ratio units; Figure 3.3.3B).

Due to time constraints, cells were not treated with D327-0013 alone. In future it will be pertinent to treat cells with D327-0013 to observe if the ligand itself induces increases in fluorescence ratio signal, which would indicate the release of $Ca^{2+}$ from intracellular stores.

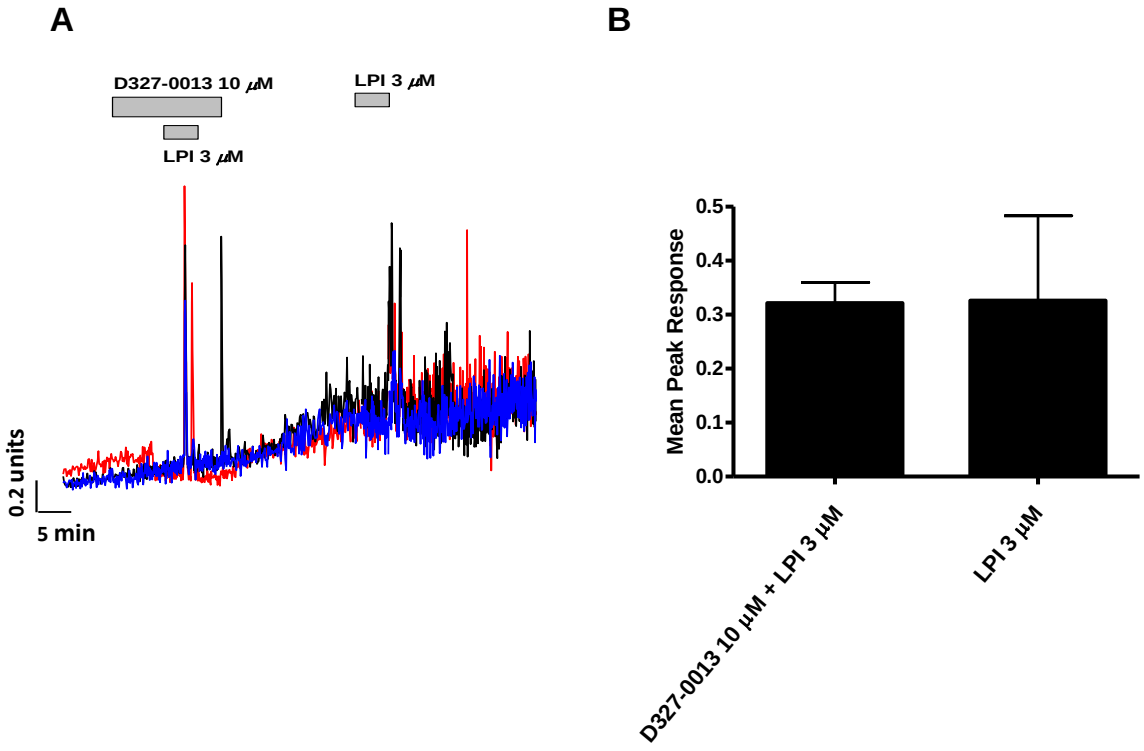


**Figure 3.3.3: The GPR55 antagonist D327-0013 fails to inhibit LPI-induced increases in $Ca^{2+}$ signal in DU145 cells.** (A) Representative traces from DU145 cells treated with ligands. Cells were exposed to 10 $\mu$M D327-0013 and LPI (3 $\mu$M) was co-perfused over the cells during antagonist exposure. (B) Histogram representing differences in mean peak response between treatment groups. Data is represented as mean ± SEM. n = 3. Mean peak response measured from 9 cells per experiment. Some data produced by June Penman.

### 3.3.4. The GPR55 antagonist C390-0219 fails to inhibit LPI-induced increases in $Ca^{2+}$ signal in the DU145 prostate cancer cell line.

Not all of the experimental groups obtained for treatment with 10 $\mu$M C390-0219 and 3 $\mu$M LPI were exposed to later application with 3 $\mu$M of LPI following a washout with HBS. For this reason, an unpaired and two-tailed Mann-Whitney *U* test was performed to compare groups treated with 10 $\mu$M C390-0219 and 3 $\mu$M LPI with treatment groups exposed to 3 $\mu$M of LPI in separate populations of cells. The *U* test showed that 10 $\mu$M C390-0219 did not significantly attenuate increases in $Ca^{2+}$ signal induced by LPI (3 $\mu$M), with a percentage of inhibition of 22.5 ± 0.1% (10 $\mu$M C390-0219 + 3 $\mu$M LPI = 0.253 ± 0.140 ratio units, ($P < 0.7000$)); Figure 3.3.4A) compared to LPI (3 $\mu$M) application alone (0.326 ± 0.157 ratio units) (Figure 3.3.4A-B). However, there was a large degree of variability in both treatment groups, which could have affected the *U* test result.

Due to time constraints, cells were not treated with C390-0219 alone. In future it will be pertinent to treat cells with C390-0219 to observe if the ligand itself causes an increase in $Ca^{2+}$ signal.

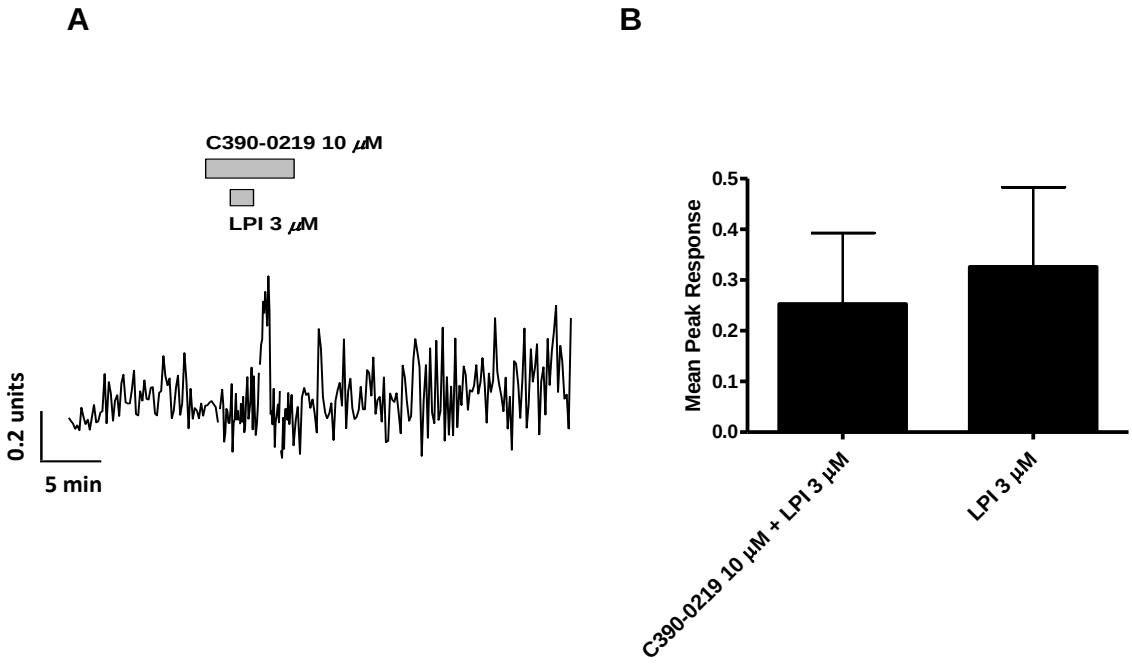

**Figure 3.3.4: The GPR55 antagonist C390-0219 fails to inhibit LPI-induced increases in $Ca^{2+}$ signal in DU145 cells.** (A-C) Representative traces from DU145 cells treated with ligands. These cells were exposed to 100 nM-1 $\mu$M, and 10 $\mu$M C390-0219. LPI was co-perfused over the cells during antagonist exposure. (B) Histogram representing differences in mean peak response between treatment groups. Data is represented as mean ± SEM. A, n = 3, B-C, n =1. Mean peak response measured from 9 cells per experiment. Some data produced by June Penman.

### 3.4.1. The synthetic GPR55 agonist SY-020 fails to induce increases in $Ca^{2+}$ signal in the DU145 prostate cancer cell line.

DU145 cells were stimulated with SY-020 in order to determine if changes in the $Ca^{2+}$ signal were induced via a GPR55-mediated mechanism. An initial concentration of 300 nM SY-020 was chosen because this concentration causes potent increases in fluorescence ratio signal in hGPR55-HEK293 cells. Although endogenous GPR55 expression produces less potent $Ca^{2+}$ responses than overexpressing cells – as discussed previously – we believed that 300 nM SY-020 was a suitable starting concentration. SY-020 (300 nM) did not lead to increases in the fluorescence ratio signal (300 nM SY-020 = 0.103 ± 0.033 ratio units; n = 2; Figure 3.4.1A). This suggests that GPR55 does not mediate intracellular $Ca^{2+}$ release in the DU145 prostate cancer cell line, which is in contrast with previous data (Piñeiro *et al.,* 2011).

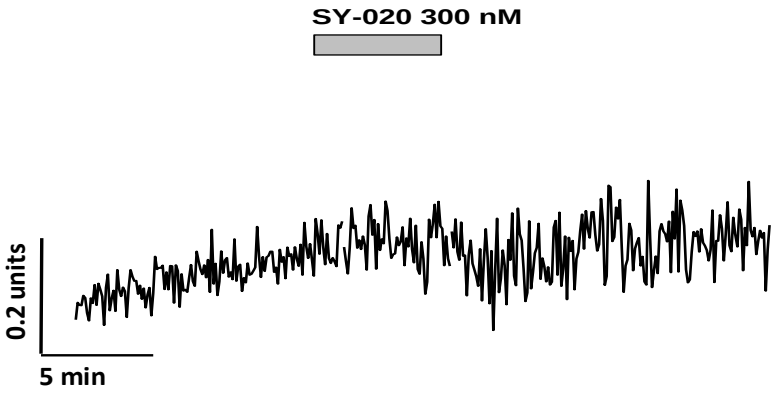

**Figure 3.4.1: The synthetic GPR55 agonist SY-020 fails to induce $Ca^{2+}$ signal increases in DU145 cells.** A representative trace from a DU145 cell treated with (A) 300 nM SY-020. n = 2. Mean peak response measured from 9 cells per experiment.

### 3.4.2. SY-020 induces CREB phosphorylation in the DU145 cell line.

DU145 cells were exposed to increasing concentrations of SY-020 ligand (10 nM-1 $\mu$M). A representative image of cells stimulated with 30 nM of SY-020 can be observed in Figure 3.4.2C (10 nM SY-020 = 1.323 ± 0.595 units; 30 nM SY-020 = 0.444 ± 0.111 units; 100 nM SY-020 = 1.517 ± 1.059 units; 300 nM SY-020 = 0.106 ± 0.073 units; 1 $\mu$M SY-020 = 0.207 ± 0.134 units). Control cells treated with vehicle DMSO (1:1000) showed low levels of CREB phosphorylation (DMSO = 0.721 ± 0.570 units; Figure 3.4.2A), but there was variability in pCREB nuclear fluorescence amongst the experimental groups which altered the fluorescence intensity data. When the cells were treated with 1 $\mu$M TPA it induced CREB phosphorylation (1 $\mu$M TPA = 1.000 units; Figure 3.4.2B).

There were issues in obtaining a concentration-response curve due to variability within the raw data obtained. For instance, pCREB nuclear fluorescence was quite low for TPA-treated cells in one experimental group and this affected the normalised result of that group. Perhaps repeating this assay will aid in decreasing variability.

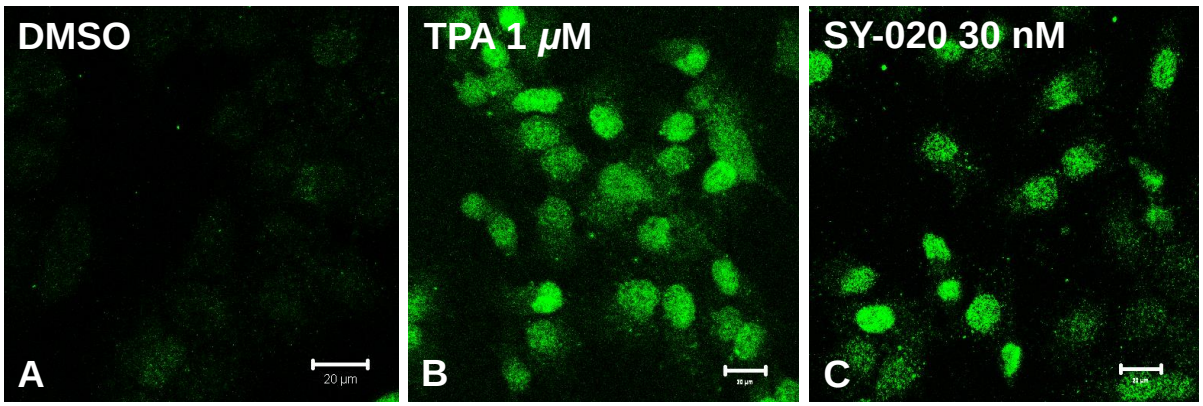

**Figure 3.4.2: SY-020 induces CREB phosphorylation in DU145 cells.** Phosphorylated CREB labelling in DU145 cells treated with (A) DMSO; (B) 1 $\mu$M TPA and (C) 30 nM SY-020. Data presented as mean ± SEM. n = 3. Fluorescence intensity values obtained from 12 cellular nuclei per experiment. Data produced by Cullen McCulloch. Scale bar = 20 μm.

### 3.5.1. LPI has neuroprotective effects against β-amyloid in cortical neurons.

GPR55 mRNA expression has been identified in various regions of the brain e.g. frontal cortex, hypothalamus, striatum, amygdala and cerebellar granule cells (Chiba *et al.,* 2011; Kerr *et al.,* 2013; Ryberg *et al.,* 2007; Sawzdargo *et al.,* 1999) and the regulatory effects of GPR55 have been implicated in the modulation of synaptic transmission (Sylantyev *et al.,* 2011, 2013) and in neuroimmune function, as GPR55 mRNA is expressed in microglia (Pietr *et al.,* 2009). There is increasing interest in the role of GPR55 in neurodegenerative mechanisms however. Cannabinoids e.g. $\Delta^9$-THC and 2-AG, have previously been shown to mediate neuroprotective effects in models of neuronal degeneration (Campbell, 2001; Downer *et al.,* 2007; Gowran *et al., 2*011; Noonan *et al.,* 2010), and the putative GPR55 agonist O-1602 was shown to reduce the formation of aggregated β-amyloid fibrils and reduce the activation of the microglial BV-2 cell line in response to lipopolysaccharide (LPS) in an *in vitro* model of AD. It was therefore of interest to investigate if GPR55 had regulatory effects in degenerating primary cortical neurons exposed to Aβ.

Fixed cortical neurons were stained for caspase-3, NeuN and Hoechst. The neurons were stained for caspase-3 because the analysis of this stain can help to determine if the neurons are undergoing apoptosis or not (Figure 3.5.1Ai, Bi-iv) (Campbell, 2001; Jänicke *et al.,* 1998). The neurons were stained for NeuN because this antibody recognises the protein NeuN which is present in most of the neuronal cell types of vertebrates (Figure 3.5.1Aii) (Wolf *et al.,* 1996). This helped to distinguish cortical neurons from other remaining non-neuronal cells that were present in the culture upon fixation. For instance, in Figure 3.5.1Aii, the blue arrow denotes a glial cell because the NeuN antibody has not stained that cell particularly well compared to the other cells. The shape of the glial cell is rounder and different from that of the surrounding neuronal cells. Hoechst stain was used in order to detect cellular DNA and nuclei (Figure 3.5.1Aiii) (Latt *et al.,* 1975; Latt & Stetten, 1976). All three stains were visualised using a confocal microscope. The wavelength channels from the images taken were combined in order to create a "merged" image (Figure 3.5.1Aiv).

Representative images of caspase-3 activity can be observed in Figure 3.5.1Bi-iv. Upon qualitative analysis, it was observed that neurons looked far less healthy when exposed to amyloid-beta (Aβ)

(1 $\mu$M Aβ = 1781.53 ± 331.28 units; Figure 3.5.1Bii) compared to when they were treated only with normal medium (Control = 995.36 ± 111.25 units; Figure 3.5.1Bi; control). Aβ-treated neurons were shrunken in appearance, possessed distorted and retracted projections and were visibly brighter in fluorescence. When cortical neurons were exposed to LPI in the presence or absence of Aβ however, neuronal fluorescence appeared darker and the condition of the neurons was comparable to that of control neurons (10 $\mu$M LPI = 1026.82 ± 233.70 units; 10 $\mu$M LPI + 1 $\mu$M Aβ = 1137.81 ± 283.60 units; Figure 3.5.1Biii-iv). This suggests that LPI has a protective effect when neurons are exposed to neurotoxic Aβ. A One-Way ANOVA was performed on this data and determined that there was no significant difference in capase-3 fluorescence between each treatment group.

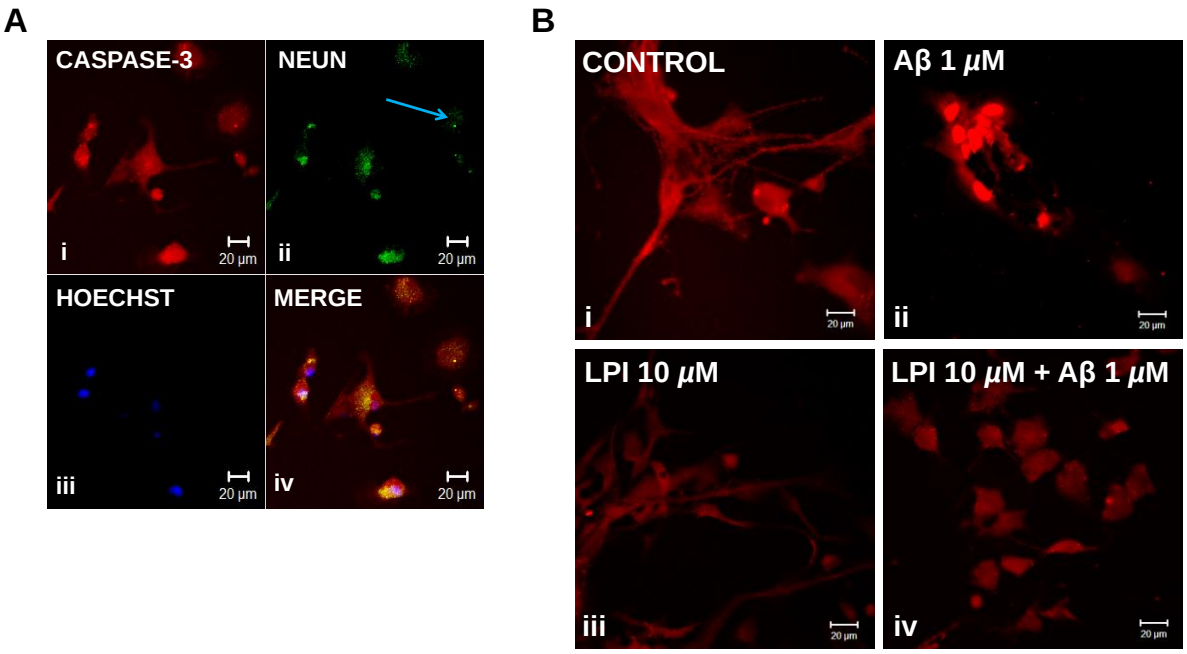

**Figure 3.5.1: LPI has neuroprotective effects against β-amyloid. (A)** Representative images of cortical neurons stained for (i) caspase-3; (ii) NeuN; (iii) Hoechst and (iv) a combination of all three stains. (B) Representative images of caspase-3 activity in cortical neurons exposed to (i) normal medium (control); (ii) 1 $\mu$M Aβ; (iii) 10 $\mu$M LPI; and (iv) 10 $\mu$M LPI in the presence of 1 $\mu$M Aβ. Non-neuronal cells (glia) are denoted by the blue arrow. n = 2. Fluorescence intensities measured from 7 cellular bodies per experiment. Scale bar = 20μm.

### 3.5.2. The GPR55 antagonist D327-0013 does not inhibit the neuroprotective effects of LPI in cortical neurons exposed to β-amyloid.

D327-0013 (3 $\mu$M) did not induce any observable changes to caspase-3 activity in cortical neurons when applied alone (3 $\mu$M D327-0013 = 712.58 ± 341.17 units; Figure 3.5.2Av) but the fluorescence appeared brighter when the cells were co-treated with Aβ (3 $\mu$M D327-0013 + 1 $\mu$M Aβ = 1287.76 ± 111.43 units; Figure 3.5.2Avi). This suggests that D327-0013 was not capable of protecting cortical neurons against neurotoxic Aβ when applied alone. Fluorescence intensity levels of the apoptotic marker, caspase-3, can be observed in Figure 3.5.2B. A One-Way ANOVA was performed to detect any differences in caspase-3 fluorescence intensities between the treatment groups. The ANOVA indicated that there was no significant difference between the groups. It can be observed from the graph that neurons treated with 3 $\mu$M D327-0013 and 10 $\mu$M LPI in the presence or absence of Aβ had fluorescence intensity values and a similar appearance to control neurons (3 $\mu$M D327-0013 + 10 $\mu$M LPI = 1187.206 units; 3 $\mu$M D327-0013, 10 $\mu$M LPI + 1 $\mu$M Aβ = 1320.63 units; Figure 3.5.2Avii-viii). They did not appear shrunken and distorted like neurons treated with just Aβ alone. This suggests that 3 $\mu$M D327-0013 was ineffective at inhibiting the seemingly neuroprotective effects of 10 $\mu$M LPI in the presence of Aβ (Jänicke *et al.,* 1998). However, these latter treatments only consisted of one experimental group each. A concentration of 3 $\mu$M D327-0013 was used in these preliminary experiments in consideration of the data obtained using the other *in vitro* models in this study. This data suggested that a concentration range of 3-10 $\mu$M of antagonist inhibited a working concentration of GPR55 agonist.

**A**

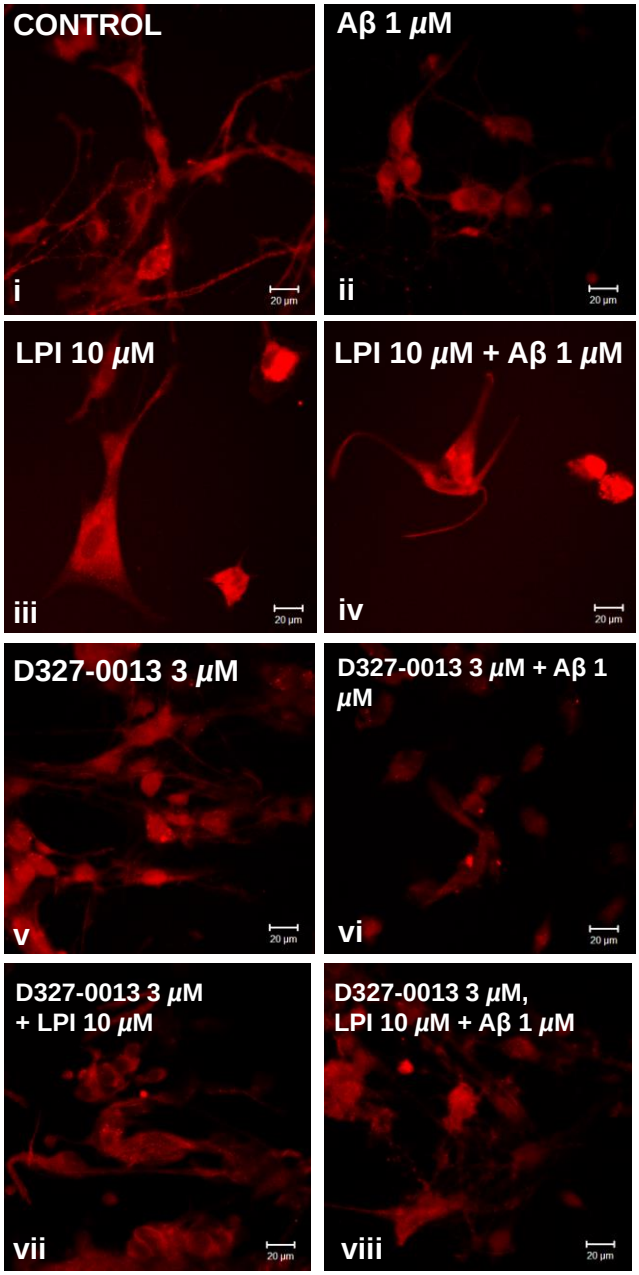
CONTROL
i
20 µm
Aβ 1 µM
ii
20 µm
LPI 10 µM
iii
20 µm
LPI 10 µM + Aβ 1 µM
iv
20 µm
D327-0013 3 µM
v
20 µm
D327-0013 3 µM + Aβ 1 µM
vi
20 µm
D327-0013 3 µM + LPI 10 µM
vii
20 µm
D327-0013 3 µM, LPI 10 µM + Aβ 1 µM
viii
20 µm

**B**

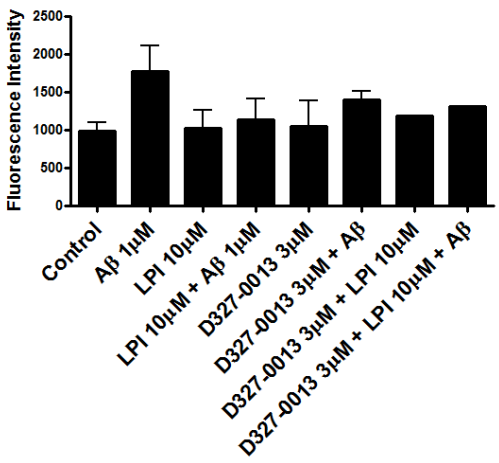
Fluorescence Intensity
2500
2000
1500
1000
500
0
Control
Aβ 1µM
LPI 10µM
LPI 10µM + Aβ 1µM
D327-0013 3µM
D327-0013 3µM + Aβ
D327-0013 3µM + LPI 10µM
D327-0013 3µM + LPI 10µM + Aβ

**Figure 3.5.2: D327-0013 does not inhibit the potential neuroprotective effects of LPI in cortical neurons.** (A) Representative images of caspase-3 activity in cortical neurons exposed to (i) normal medium (control); (ii) 1 $\mu$M Aβ; (iii) 10 $\mu$M LPI; (iv) 10 $\mu$M LPI and 1 $\mu$M Aβ; (v) 3 $\mu$M D327-0013; (vi) 3 $\mu$M D327-0013 and 1 $\mu$M Aβ; (vii) 3 $\mu$M D327-0013 and 10 $\mu$M LPI and (viii) 3 $\mu$M D327-0013, 10 $\mu$M LPI and 1 $\mu$M Aβ. (B) Histogram representing the effects of D327-0013, LPI and Aβ on caspase-3 fluorescence intensity. Data is represented as mean ± SEM. All groups, n = 2, except 3 $\mu$M D327-0013 and 10 $\mu$M LPI; and 3 $\mu$M D327-0013, 10 $\mu$M LPI and 1 $\mu$M Aβ, n = 1. Fluorescence intensities measured from 7 individual neuronal cell bodies per treatment group per experiment. Scale bar = 20μm.

### 3.5.3. The GPR55 antagonist C390-0219 attenuates the neuroprotective effects of LPI in cortical neurons exposed to β-amyloid.

C390-0219 did not induce any observable changes to caspase-3 activity in the neurons when applied alone (3 $\mu$M C390-0219 = 1351.07 ± 160.83 units; Figure 3.5.3Av) but the fluorescence appeared brighter when the cells were co-treated with Aβ (3 $\mu$M C390-0219 + 1 $\mu$M Aβ = 1934.62 units; n =1; Figure 3.5.3Avi). This suggests that C390-0219 was not capable of protecting cortical neurons against neurotoxic Aβ when applied alone. Fluorescence intensity levels of the apoptotic marker, caspase-3, can be observed in Figure 3.5.3B. A One-Way ANOVA was performed to detect any differences in caspase-3 fluorescence intensities between the treatment groups. The ANOVA indicated that there was no significant difference between the groups. It can be observed from the graph that neurons treated with 3 $\mu$M C390-0219 and 10 $\mu$M LPI in the presence or absence of Aβ differed in fluorescence intensity (3 $\mu$M C390-0219 +10 $\mu$M LPI = 735.70 ± 6.58 units; 3 $\mu$M C390-0219, 10 $\mu$M LPI + 1 $\mu$M Aβ = 1126.64 ± 16.6 units). This suggests that 3 $\mu$M C390-0219 was somewhat effective at inhibiting the seemingly neuroprotective effects of 10 $\mu$M LPI in the presence of Aβ. (Figure 3.5.3Avii-viii).

**A**

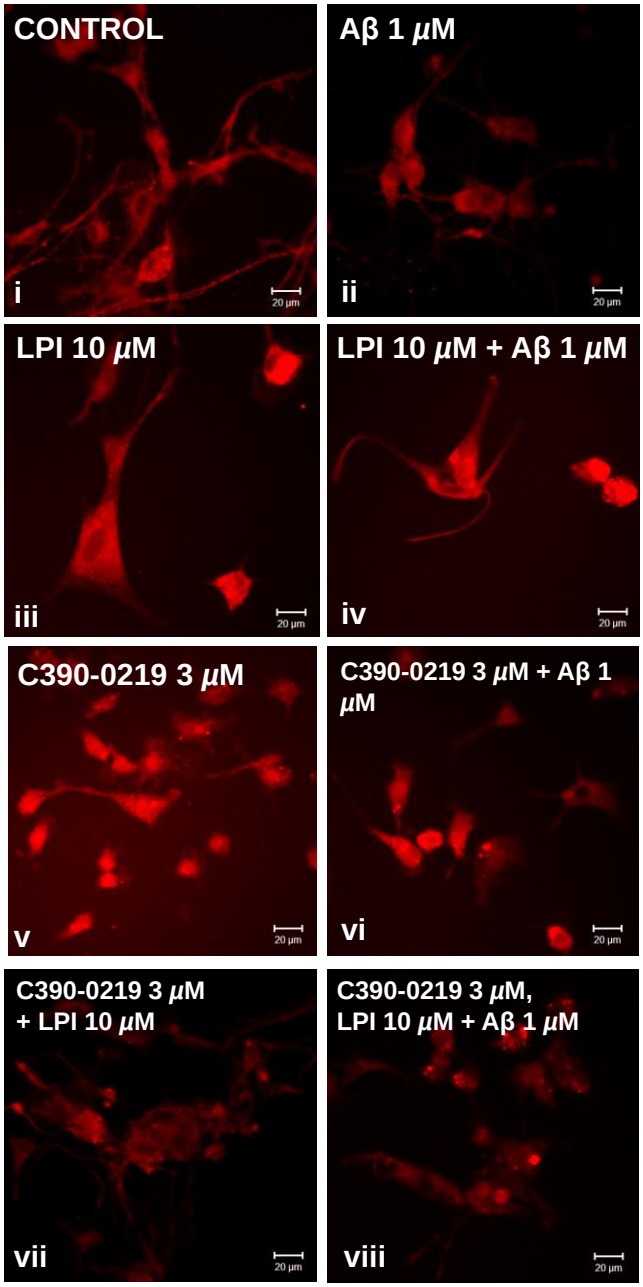
CONTROL
i
20 µm
Aβ 1 µM
ii
20 µm
LPI 10 µM
iii
20 µm
LPI 10 µM + Aβ 1 µM
iv
20 µm
C390-0219 3 µM
v
20 µm
C390-0219 3 µM + Aβ 1 µM
vi
20 µm
C390-0219 3 µM + LPI 10 µM
vii
20 µm
C390-0219 3 µM, LPI 10 µM + Aβ 1 µM
viii
20 µm

**B**

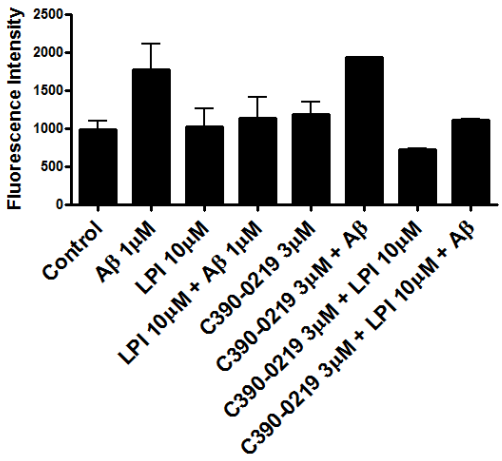
Fluorescence Intensity
2500
2000
1500
1000
500
0
Control
Aβ 1µM
LPI 10µM
LPI 10µM + Aβ 1µM
C390-0219 3µM
C390-0219 3µM + Aβ
C390-0219 3µM + LPI 10µM
C390-0219 3µM + LPI 10µM + Aβ

**Figure 3.4.3: C390-0219 attenuates the potential neuroprotective effects of LPI in cortical neurons.** (A) Representative images of caspase-3 activity in cortical neurons exposed to (i) normal medium (control); (ii) 1 $\mu$M Aβ; (iii) 10 $\mu$M LPI; (iv) 10 $\mu$M LPI and 1 $\mu$M Aβ; (v) 3 $\mu$M C390-0219; (vi) 3 $\mu$M C390-0219and 1 $\mu$M Aβ; (vii) 3 $\mu$M C390-0219 and 10 $\mu$M LPI and (viii) 3 $\mu$M C390-0219, 10 $\mu$M LPI and 1 $\mu$M Aβ. (B) Histogram representing the effects of C390-0219, LPI and Aβ on caspase-3 fluorescence intensity. Data is represented as mean ± SEM. All groups, n = 2, except 3 $\mu$M C390-0219 and 1 $\mu$M Aβ, n = 1. Fluorescence intensities measured from 7 individual neuronal cell bodies per treatment group per experiment.

# Chapter Four

## Discussion

### *4.1. Inhibition of GPR55-mediated signalling using selective antagonists*

To date it has been extremely difficult to delineate the physiological and pathological roles of GPR55 due to a lack of selective pharmacological tools. The data presented herein demonstrates that two novel and selective GPR55 antagonists are capable of inhibiting agonist-induced responses at a concentration of 3 $\mu$M in a HEK293 cell line stably transfected with GPR55 (hGPR55-HEK293). Previous studies have provided evidence which supports certain cannabinoids acting as antagonists at GPR55. The cannabinoid CP55,940 inhibits GPR55 internalization, the formation of β-arrestin GPR55 complexes and the phosphorylation of ERK (Kapur *et al.,* 2009). The $CB_1$ inverse agonist/antagonist SR141716A was previously described as an antagonist of GPR55 when it inhibited the effects of GPR55 agonists in hGPR55-HEK293 cells (Lauckner *et al.,* 2008), but it has since been identified as a GPR55 agonist along with the structurally similar cannabinoid AM251 (Henstridge *et al.,* 2010; Kapur *et al.,* 2009). The phytocannabinoid cannabidiol was suggested to antagonise GPR55-mediated GTPγS binding (Ryberg *et al.,* 2007). The CBD analogue O-1918 is also a proposed GPR55 antagonist and has been shown to inhibit the therapeutic effects of the putative GPR55 agonist O-1602 in a rat model of acute arthritis (Schuelert & McDougall, 2011) and inhibit the attenuating effects of O-1602 on mesenchymal stem cell migration (Schmuhl *et al.,* 2014). The issue with previously reported antagonists however is their lack of selectivity for GPR55 in certain cell types and physiological conditions. The coumarin derivatives PSB-SB-487 and PSB-SB-1203 were found to be potent and selective antagonists however (Rempel *et al.,* 2013). The data described in the current study is therefore very encouraging because it further characterises two effective and selective antagonists for GPR55.

Both D327-0013 and C390-0219 did not induce any effects in hGPR55-HEK293 cells when applied alone. They both significantly inhibited LPI-induced $Ca^{2+}$ responses when applied at a concentration of 3 $\mu$M in hGPR55-HEK293 cells, but only D327-0013 (3 $\mu$M) significantly inhibited SY-020-induced increases in $Ca^{2+}$ signal in these cells. Agonist-induced $Ca^{2+}$ responses were inhibited more effectively by the antagonists than pCREB activation responses. Perhaps the antagonists exhibit ligand bias towards signalling pathways that lead to $Ca^{2+}$ release more-so than CREB phosphorylation signalling pathways in hGPR55-HEK293 cells. Neither antagonist was capable of inhibiting LPI-induced $Ca^{2+}$ release in DU145 cells, but preliminary data indicates that 3-10 $\mu$M of both antagonists inhibit 1 $\mu$M of LPI-induced CREB phosphorylation (Penman, experimental work in progress). However, a control experiment of antagonist treatment alone was

not performed. In future it will be crucial to treat cells with the antagonists to ensure the antagonists are not inducing $Ca^{2+}$ responses themselves in DU145 prostate cancer cells.

$Ca^{2+}$ release from intracellular stores can be induced in DU145 cells using suggested LPI-mediated stimulation of GPR55 (Penman, 2013; Piñeiro *et al.,* 2011). Interestingly, although the specific ROCK inhibitor Y-27632 strongly inhibited LPI-dependent ERK phosphorylation in DU145 cells, it was previously shown not to affect LPI-dependent $Ca^{2+}$ release (Piñeiro *et al.,* 2011). The authors therefore theorised that LPI is capable of inducing increased levels of intracellular $Ca^{2+}$ in a GPR55-dependent mechanism but independently of ROCK involvement. In contrast, hGPR55-HEK293 cells have previously been shown to induce GPR55-mediated $Ca^{2+}$ release via a $G_{\alpha 13}$-RhoA-ROCK pathway (Henstridge *et al.,* 2009a). Prostate cancer cells express GPCRs such as GPR55 (Piñeiro *et al.,* 2011; Raj *et al.,* 2002) and DU145 cells are theorised to signal via a GPR55-$G\alpha_q$ protein mechanism which induces the Rho-mediated downstream activation of ERK (Penman, 2013; Piñeiro *et al.,* 2011). ERK is vital in prostate cancer cell proliferation and advanced prostate tumours express elevated levels of activated ERK (Gioeli *et al.,* 1999; Price *et al.,* 1999).

The data presented herein conflicts with the findings made by Piñeiro *et al.* (2011). It has previously been shown that GPR55-mediated $Ca^{2+}$ release is induced via a ROCK-independent mechanism in DU145 cells (Penman, 2013), which corroborates with the data obtained by Piñeiro *et al.* (2011). However, the current data suggests that in the DU145 prostate cancer cell line, GPR55 does not mediate the release of $Ca^{2+}$ from intracellular stores. Perhaps DU145 cells do not mediate the release of $Ca^{2+}$ through $G\alpha_q$-coupling, which conflicts with previous findings (Piñeiro *et al.,* 2011; Piñeiro & Falasca, 2012; Ruban *et al.,* 2014). Piñeiro *et al.* (2011) also transfected GPR55 siRNA into another prostate cancer cell line (PC-3 cells) which led to subsequent downregulation of *GPR55* expression and prevention of LPI-induced $Ca^{2+}$ release. Only pharmacological tools, i.e. antagonists, were used to validate GPR55-mediated mechanisms in this study. Future work should therefore aim to implement alternative methods, such as the use of siRNA for *GPR55*, in order to confirm ligand selectivity for GPR55.

It is worth noting that when $G\alpha_{13}$-coupled GPR55 is stimulated by an agonist in hGPR55-HEK293 cells, PLCε is activated downstream and cleaves $PIP_2$ into $IP_3$. $IP_3$ subsequently binds to $IP_3$Rs on the ER membrane which induces the release of $Ca^{2+}$ from the ER stores. DU145 prostate cancer cells express PLCβ, so the findings presented herein may suggest that GPR55 only mediates the release of intracellular $Ca^{2+}$ when PLCε is expressed by cells. A diagram representing the potential signalling pathways induced by LPI in DU145 cells is illustrated in Figure 4.1.

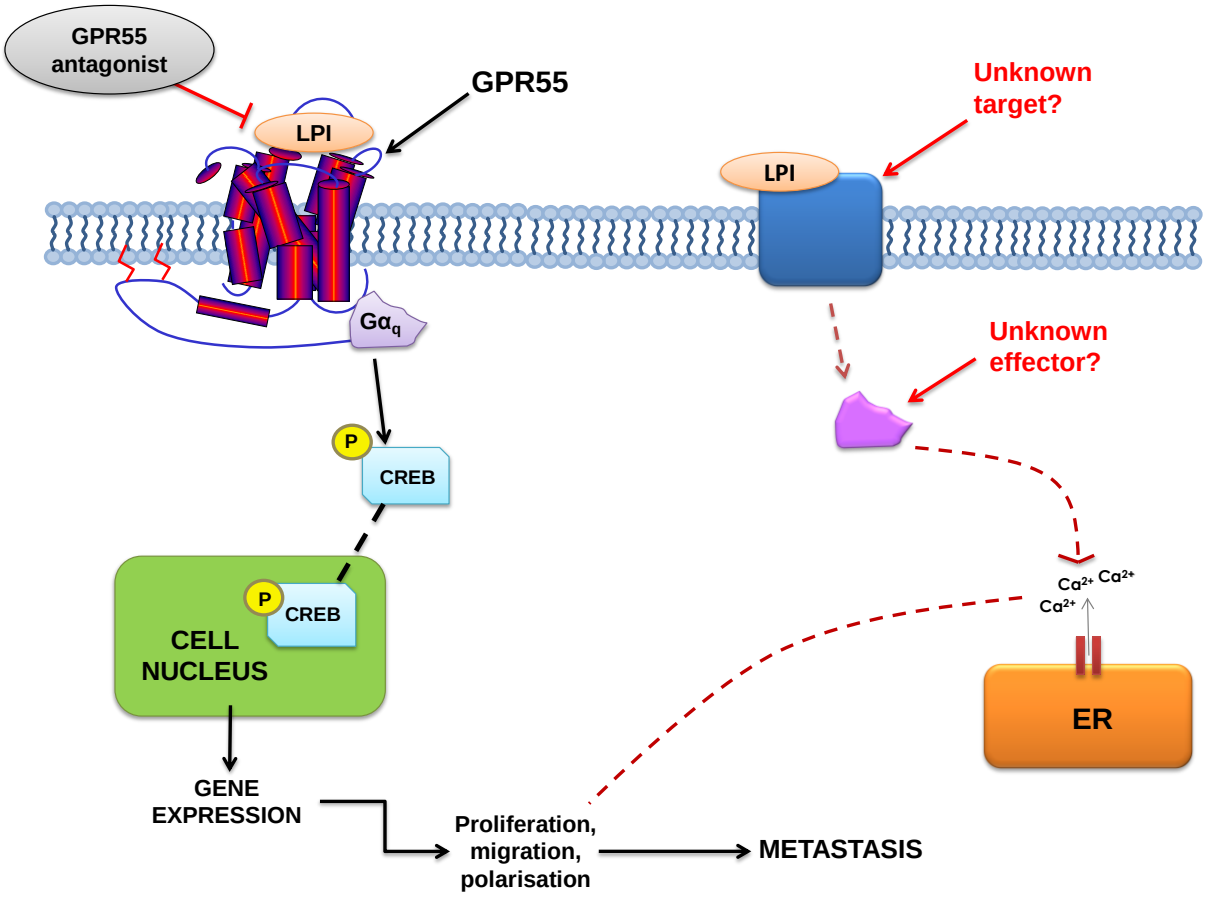


**Figure 4.1. Potential signalling cascades and effects induced by LPI in DU145 prostate cancer cells.** Upon activation of GPR55 by LPI, $G\alpha_q$ protein is activated. The signal transduced leads to phosphorylation of CREB. pCREB translocates to the cell nucleus and induces gene transcription. This gene expression is suggested to contribute to cancer cell proliferation and metastasis. GPR55 antagonists are capable of inhibiting this pathway at the receptor level (Penman, 2013), thus preventing LPI from inducing downstream CREB phosphorylation. However, LPI appears to activate an as yet unknown target in order to induce the release of $Ca^{2+}$ in DU145 cells. This target is not inhibited by GPR55 antagonists. The red dashed arrows indicate a suggested pathway for LPI-mediated $Ca^{2+}$ mobilisation in DU145 cells.

### *4.2. Selective agonism for GPR55*

The selectivity of agonists for GPR55 has long come under scrutiny since the receptor was first identified by Sawzdargo *et al.* (1999). Previous studies proposed that GPR55 could be activated by cannabinoid ligands. Ryberg *et al.* (2007) showed that GPR55 was activated by cannabinoids e.g. CP55,940, $\Delta^9$-THC, AEA, 2-AG, PEA, virodhamine and others, in a GTPγS binding assay. However, other studies have provided contrasting evidence which only replicates some of the data produced by Ryberg *et al.* (2007) (Johns *et al.,* 2007) or does not replicate the data at all (Oka *et al.,*

2007). Furthermore, studies in recent years have provided increasing amounts of evidence identifying LPI as the endogenous agonist for GPR55 (Nevalainen & Irving, 2010; Oka *et al.,* 2007; Piñeiro & Falasca, 2012; Yamashita *et al.,* 2013). The discrepancies surrounding endogenous agonist selectivity for GPR55 have only made the need for selective agonists all the more vital. To date, very few selective agonists have been synthesised. Heynen-Genel *et al.* (2011) identified several potent and selective agonists for GPR55. The agonists ML184 (2440433), ML185 (CID1374043) and ML186 (CID15945391) were ranked in the order ML185 >ML198 >ML184 in terms of potency. Brown *et al.* (2011) identified the benzoylpiperazines, GSK494581A and GSK575594A, as GPR55 agonists, which were initially thought to be inhibitors of glycine transporter subtype 1 (GlyT1). However, these agonists were only selective for human GPR55 and not rodent GPR55. This could present problems when trying to delineate the physiological role of GPR55 in *in vitro* and *in vivo* models.

The data presented herein demonstrates that a novel and selective agonist for GPR55, SY-020, is capable of mediating GPR55-specfic effects in the hGPR55-HEK293 and DU145 prostate cancer cell lines. It did not induce GPR55-specific effects in the control HEK293 cell line in comparison, except for 10 $\mu$M SY-020. It would be worth testing this high SY-020 concentration with the antagonists used in this study to clarify if the increases in $Ca^{2+}$ signal were wholly GPR55-mediated in these control cells. SY-020 was synthesised by the Nevalainen research group. Previous data showed that in a $Ca^{+}$ imaging assay, SY-020 had an $EC_{50}$ = 6 nM in hGPR55-HEK293 cells (Penman, 2013). This was confirmed by the findings presented in the current study, whereby a concentration of SY-020 (30 nM) was capable of inducing increases in $Ca^{2+}$ signal. Although both antagonists attenuated SY-020-induced increases in $Ca^{2+}$ release, only D327-0013 (3 $\mu$M) significantly inhibited this $Ca^{2+}$ release. This suggests that GPR55 mediated this release of $Ca^{2+}$ from intracellular stores. SY-020 was also capable of inducing the GPR55-mediated phosphorylation of CREB in hGPR55-HEK293 cells, and the GPR55 antagonists D327-0013 and C390-0219 both attenuated levels of pCREB fluorescence.

Interestingly, although SY-020 did induce CREB phosphorylation in the DU145 prostate cancer cell line, 300 nM of SY-020 did not induce the release of $Ca^{2+}$. Similarly, GPR55-selective antagonists failed to inhibit LPI-induced increases in $Ca^{2+}$ signal. This data therefore supports the theory that GPR55 activation and coupling to $G\alpha_q$ does not induce the release of $Ca^{2+}$ from intracellular stores in DU145 cells. This suggests that LPI is most likely mediating its effects through another unknown target in this prostate cancer cell line (Figure 4.1).

Due to time constraints, the role of GPR55 in inducing CREB phosphorylation in the DU145 cell line was not fully elucidated. The fact that nanomolar concentrations of SY-020 induced increases in nuclear pCREB fluorescence supports the proposal that GPR55 does mediate the induction of CREB phosphorylation in DU145 cells. This is consistent with the fact that CREB is directly involved in controlling the expression of genes that are essential for cancer cell proliferation and survival (Mitton *et al.,* 2011). Ideally the next actions to take would be to identify if the GPR55 antagonists tested in this study are capable of inhibiting the LPI- and SY-020-induced phosphorylation of CREB. Preliminary data indicates that 3-10 $\mu$M concentrations of both antagonists inhibit pCREB activation induced by 1 $\mu$M LPI (Penman, experimental work in progress).

### *4.3. GPR55 cross-talk mechanisms*

Despite the recent emergence of selective pharmacological tools for GPR55, the selectivity of certain ligands for this orphan receptor is still contentious. For instance, Soga *et al.* (2005) suggested that LPI-induced cellular effects were mediated by the orphan receptor GPR119 in rat hepatoma cells overexpressing human GPR119. In contrast though, Piñeiro *et al.* (2011) found that knockdown of GPR119 in prostate and ovarian cancer cells did not alter LPI-induced cellular effects, which indicated that LPI was signalling via GPR55 instead. The data presented herein suggests that LPI does not induce $Ca^{2+}$ release via GPR55 in the DU145 prostate cancer cell line because selective GPR55 antagonists failed to inhibit LPI-induced increases in $Ca^{2+}$ signal. Similarly, a high concentration of LPI and SY-020 (10 $\mu$M) produced an increase in intracellular $Ca^{2+}$ in control HEK293 cells which conflicts with previous data (Henstridge *et al.,* 2009a). LPI at high concentrations could be signalling through another target in these native cell lines, perhaps GPR119. It is difficult to suggest which target LPI could be signalling through however.

Evidence of GPR55 pharmacological communication with the orphan receptor GPR18 has emerged in recent years. Although LPI is not a putative agonist of the orphan receptor GPR18, it was capable of exerting minimal stimulation of microglial migration that was independent of concentration (McHugh *et al.,* 2010). However, this microglial migration was more than likely induced via GPR55 because microglia also express GPR55 mRNA (Pietr *et al.,* 2009). However, GPR18 is responsive to the agonists O-1602 (Ashton, 2012) and NAGly (Kohno *et al.,* 2006) and both O-1602 (Schmuhl *et al.,* 2014; Schuelert & McDougall, 2011) and NAGly (Penman, 2013) have been implicated in signalling via GPR55. This suggests that GPR18 may participate in cross-

talk mechanisms with GPR55 or may cross-antagonise GPR55. For instance, Schicho *et al.* (2011) found that O-1602 reduced disease severity and inhibited neutrophil recruitment in a model of experimental colitis using a mechanism that was independent of GPR55, $CB_1$ and $CB_2$ receptors. This implicates an additional target of mediating these effects, most likely GPR18. It is worth noting that the putative GPR55 antagonist O-1918 (Schmuhl *et al.,* 2014; Schuelert & McDougall, 2011) is also thought to act as an antagonist at GPR18 (Caldwell *et al.,* 2013), but this theory is controversial because it has recently been found that O-1918 induced an *increase* in MAPK activity and $Ca^{2+}$ mobilisation in GPR18-HEK293 cells (Console-Bram *et al.,* 2014). Interestingly, the $CB_1$ receptor agonists SR141716A and $\Delta^9$-THC induced biased effects at GPR55 and GPR18. SR141716A acted as an agonist at GPR55 and as a weak antagonist at GPR18, whereas $\Delta^9$-THC acted as a weak antagonist at GPR55 and as an agonist at GPR18 (Fuchs *et al.,* 2013). This supports the idea of cross-antagonism occurring between these two receptors. In consideration of previous evidence, this could explain why a single GPR55 receptor antagonist would not be effective. Interfering with the communication between these two receptors, i.e. through the use of pharmacological tools or siRNA, could potentially be a more effective way to inhibit $Ca^{2+}$ release from intracellular stores in native cell lines such as the DU145 prostate cancer cell line.

GPR55 is also thought to participate in cross-talk mechanisms with cannabinoid receptors. Kargl *et al.* (2012) demonstrated that GPR55 formed heteromers with $CB_1$ receptor upon agonist stimulation in GPR55/$CB_1$-HEK293 cells. Both receptors were found to possess a modulatory effect on each other's signalling pathways. Interestingly, although $CB_1$ expression inhibited GPR55-mediated transcription factor activation and ERK activation, the presence of GPR55 enhanced $CB_1$-mediated ERK and NFAT activation in GPR55/$CB_1$-HEK293 cells.

There is increasing amounts of evidence supporting the existence of GPR55-$CB_2$ cross-talk mechanisms (Irving, 2011). Moreno *et al.* (2014) demonstrated that $CB_2$ receptor and GPR55 form heteromers in co-transfected GPR55/$CB_2$-HEK293 cells and in breast and glioblastoma cancer cell lines. These findings are particularly intriguing in consideration of the results observed in the DU145 prostate cancer cells investigated herein. These GPR55/$CB_2$ receptor heteromers displayed cross-talk and cross-antagonism at the level of cAMP and p-ERK pathways. The authors therefore suggested that GPR55/$CB_2$ receptor heteromers drive biphasic signalling responses via cross-antagonism (Moreno *et al.,* 2014). In line with this, Balenga *et al.* (2014) demonstrated that GPR55 and $CB_2$ co-precipitated in the membrane extracts of HEK293 cells and co-localised and formed heteromers in HEK293 cells. Heterodimerisation of these receptors led to attenuation in GPR55-mediated activation of transcription factors e.g. CRE, NFAT, but ERK-MAPK was increased in

the presence of $CB_2$. Balenga *et al.* (2011) also observed that GPR55 expression occurred in neutrophils and GPR55 activation resulted in the recruitment of neutrophils to sites of injury. It was suggested that GPR55 synergised with $CB_2$ receptors in order to recruit neutrophils and GPR55 would prevent the exacerbative inflammatory responses that would occur with $CB_2$-mediated recruitment alone. Schmuhl *et al.* (2014) observed that the $CB_2$ receptor agonist CBD induced migration and p42/44 MAPK phosphorylation in mesenchymal stem cells. These effects were inhibited by AM-630 ($CB_2$ receptor antagonist) and O-1602 (GPR55 agonist). The authors theorised that upstream activation of $CB_2$ receptor as well as inhibition of GPR55 were found to be involved in the activation of p42/44 MAPK which conferred downstream induction of migration.

The potential cross-talk mechanisms described could explain for the contradictory evidence provided on GPR55 pharmacology to date. Perhaps GPR55 interaction with other receptors – GPR18, cannabinoid receptors or otherwise – may be responsible for the differential effects previously reported following GRP55 stimulation in different *in vitro* and *in vivo* systems. This could also aid in the understanding of the results presented in the current study, whereby GPR55 does not appear to be responsible for the induction of $Ca^{2+}$ release in DU145 cancer cells and in control HEK293 cells.

### *4.4. The role of GPR55 in neurodegeneration*

Cannabinoid receptors are expressed in the brain and peripheral nervous system (Cabral & Marciano-Cabral, 2005; Pertwee, 2005) and have long been associated with the regulation of CNS development and synaptic plasticity (Berghuis *et al.,* 2007; Harkany *et al.,* 2008; Mulder *et al.,* 2008). GPR55 mRNA has also been identified in numerous regions of the brain e.g. frontal cortex, hypothalamus, striatum, amygdala and cerebellar granule cells (Chiba *et al.,* 2011; Kerr *et al.,* 2013; Ryberg *et al.,* 2007; Sawzdargo *et al.,* 1999) and GPR55 activity in the brain has been associated with a variety of functions. For instance, GPR55 was suggested to have a modulatory effect on neurotransmitter release from synapses in the brain. GPR55 agonists were found to cause a slow release of $Ca^{2+}$ from intracellular stores, which enabled synaptic transmission to occur. This effect was not seen in $GPR55^{-/-}$ mice (Sylantyev *et al.,* 2011, 2013). However, there is a growing amount of evidence focusing on GPR55 regulation of neuroimmune function. Apoptotic mechanisms have previously been associated with neurodegenerative conditions (Mattson, 2000). The induction of caspase-mediated apoptosis is thought to be implicated in neurodegeneration and aging (Bredesen,

2009; D'Amelio *et al.,* 2011; Friedlander, 2003; Zhang *et al.,* 2003) and cannabinoids e.g. $\Delta^9$-THC, 2-AG and AEA, have been shown to induce neuroprotective effects in neurodegenerative models (Campbell, 2001; Downer *et al.,* 2007; Gowran *et al., 2*011; Noonan *et al.,* 2010). Preliminary findings presented in the current study showed that LPI attenuated the expression of caspase-3 in cortical neurons challenged with β-amyloid. This attenuation appeared to be somewhat reversed by the antagonist C390-0219, but not by D327-0013. This suggests that LPI signalling via GPR55 promotes a protective effect on neurons that are undergoing Aβ-induced degeneration.

Previous studies suggest that GPR55 has a regulatory function in models of neurodegeneration. Janefjord *et al.* (2013) employed the use of an *in vitro* model of AD and reported that the putative ligand for GPR55, O-1602, reduced the formation of aggregated β-amyloid fibrils and reduced activation of the microglial BV-2 cell line in response to lipopolysaccharide (LPS). When LPS-conditioned media was removed from BV-2 cells and applied to neuronal cells, it was found that the application of O-1602 led to decreased neurotoxicity compared to control treatments where no agonists were applied. It is worth bearing in mind though that O-1602 is a putative agonist for both GPR55 and GPR18, as has been discussed previously. Janefjord *et al.* (2013) did not utilise any pharmacological tools or knockout models to elucidate through which receptor O-1602 was signalling. In contrast, Sisay *et al.* (2013) found that GPR55 knockout mice cross-bred onto the C57BL/6 background did not develop experimental autoimmune encephalomyelitis (EAE), the mouse model of Multiple Sclerosis (MS), as severely as their control counterparts. MS is an inflammatory autoimmune disease that is characterised by demyelination and chronic neurodegeneration (Perry *et al.,* 2003). The findings presented by Sisay *et al.* (2013) therefore implicate GPR55 in potentiating neurodegenerative disease progression. Interestingly, C57BL/6.Cnr2tm1Dgen ($CB_2$ receptor knockout) mice exhibited increased disease severity. This alludes to the possible GPR55-$CB_2$ cross-talk mechanism that has been referred to previously. Perhaps GPR55 and $CB_2$ cross-talk alters EAE disease progression. In consideration of the conflicting evidence provided on the regulatory role of GPR55 in neurodegenerative conditions, the results of the current study are therefore promising. The current data suggests that the selective GPR55 antagonist, C390-0219, has a somewhat attenuative effect on LPI-induced neuroprotection, thus implicating GPR55 in mediating a neuroprotective function. However, the findings made by Sisay *et al.* (2013) illustrate the importance of using other models such as siRNA or *in vivo* knockout models when seeking to delineate the (patho)physiological function of GPR55.

Future investigations to conduct should include treating Aβ-challenged cortical neurons with SY-020 and observe if it has any neuroprotective effects, like it does with LPI. If positive effects are observed, tools to block GPR55 function e.g. selective antagonists, siRNA, knockout models, could then be applied to fully validate if GPR55 has a neuroprotective function in a model of AD.

# Conclusion

GPR55 is a putative cannabinoid receptor whose mRNA is widely expressed throughout the body, particularly in the brain and in certain types of tumour. To date it has been extremely difficult to validate the physiological and pathological roles of GPR55 due to an absence of selective pharmacological tools. However, with the recent development of selective antagonists and agonists for GPR55, the delineation of the pathophysiological functions of GPR55 may fast become a reality.

In this study it was shown that two novel and selective antagonists, D327-0013 and C390-0219 (3 $\mu$M), significantly inhibited the induction of $Ca^{2+}$ release by LPI, the endogenous agonist for GPR55, in a HEK293 cell line that stably overexpresses GPR55 (hGPR55-HEK293). Similarly, D327-0013 (3 $\mu$M) significantly inhibited the GPR55-mediated $Ca^{2+}$ release induced by a novel and selective GPR55 agonist, SY-020, in this cell line.

The data presented herein is promising because it demonstrates the effectiveness of selective pharmacological tools for GPR55. The pharmacology of GPR55 has remained a controversial issue ever since its discovery and it is now becoming ever more apparent that GPR55 participates in cross-talk mechanisms with other receptors e.g. GPR18, cannabinoid receptors. In future it will therefore be crucial to use alternative methods to validate the selectivity of ligands for GPR55. For instance, siRNA should be applied in *in vitro* cells, such as the cell lines used in this study, to validate GPR55-mediated signalling pathways. The use of *in vivo* animal models e.g. GPR55 knockouts, would also aid in better understanding the physiological roles of this receptor. The data presented in the current study will serve to advance research into the physiological role of GPR55 and should contribute to the validation of GPR55 as a therapeutic target.

# Chapter Five

## Bibliography

Abood, M. E. (2010). *MLS000675307 - Compound Summary*. Retrieved from http://pubchem.ncbi.nlm.nih.gov/summary/summary.cgi?cid=16020046

Alexander, A., Smith, P. F., & Rosengren, R. J. (2009). Cannabinoids in the treatment of cancer. *Cancer Letters*, *285*(1), 6–12. doi:10.1016/j.canlet.2009.04.005

Andradas, C., Caffarel, M. M., Pérez-Gómez, E., Salazar, M., Lorente, M., Velasco, G., … Sánchez, C. (2011). The orphan G protein-coupled receptor GPR55 promotes cancer cell proliferation via ERK. *Oncogene*, *30*(2), 245–52. doi:10.1038/onc.2010.402

Bailey, J. (2000). Expression of the cyclic AMP-dependent transcription factors, CREB, CREM and ATF2, in the human myometrium during pregnancy and labour. *Molecular Human Reproduction*, *6*(7), 648–660. doi:10.1093/molehr/6.7.648

Balenga, N. A. B., Aflaki, E., Kargl, J., Platzer, W., Schröder, R., Blättermann, S., … Waldhoer, M. (2011). GPR55 regulates cannabinoid 2 receptor-mediated responses in human neutrophils. *Cell Research*, *21*(10), 1452–69. doi:10.1038/cr.2011.60

Balenga, N. A., Martínez-Pinilla, E., Kargl, J., Schröder, R., Peinhaupt, M., Platzer, W., … Franco, R. (2014). Heteromerization of GPR55 and cannabinoid CB2 receptors modulates signaling. *British Journal of Pharmacology*. doi:10.1111/bph.12850

Banwait, S., Galvan, V., Zhang, J., Gorostiza, O. F., Ataie, M., Huang, W., … Bredesen, D. E. (2008). C-terminal cleavage of the amyloid-beta protein precursor at Asp664: a switch associated with Alzheimer's disease. *Journal of Alzheimer's Disease : JAD*, *13*(1), 1–16. Retrieved from http://www.pubmedcentral.nih.gov/articlerender.fcgi?artid=2818039&tool=pmcentrez&rendertype=abstract

Benaud, C., Oberst, M., Hobson, J. P., Spiegel, S., Dickson, R. B., & Lin, C.-Y. (2002). Sphingosine 1-phosphate, present in serum-derived lipoproteins, activates matriptase. *The Journal of Biological Chemistry*, *277*(12), 10539–46. doi:10.1074/jbc.M109064200

Berghuis, P., Rajnicek, A. M., Morozov, Y. M., Ross, R. a, Mulder, J., Urbán, G. M., … Harkany, T. (2007). Hardwiring the brain: endocannabinoids shape neuronal connectivity. *Science (New York, N.Y.)*, *316*(5828), 1212–6. doi:10.1126/science.1137406

Bondarenko, A. I., Malli, R., & Graier, W. F. (2011). The GPR55 agonist lysophosphatidylinositol directly activates intermediate-conductance Ca2+ -activated K+ channels. *Pflügers Archiv : European Journal of Physiology*, *462*(2), 245–55. doi:10.1007/s00424-011-0977-7

Bondarenko, A., Waldeck-Weiermair, M., Naghdi, S., Poteser, M., Malli, R., & Graier, W. F. (2010). GPR55-dependent and -independent ion signalling in response to lysophosphatidylinositol in endothelial cells. *British Journal of Pharmacology*, *161*(2), 308–20. doi:10.1111/j.1476-5381.2010.00744.x

Bredesen, D. E. (2009). Neurodegeneration in Alzheimer's disease: caspases and synaptic element interdependence. *Molecular Neurodegeneration*, *4*(1), 27. doi:10.1186/1750-1326-4-27

Brown, A. J., Daniels, D. A., Kassim, M., Brown, S., Haslam, C. P., Terrell, V. R., … Dowell, S. J. (2011). Pharmacology of GPR55 in yeast and identification of GSK494581A as a mixed-activity glycine transporter subtype 1 inhibitor and GPR55 agonist. *The Journal of Pharmacology and Experimental Therapeutics*, *337*(1), 236–46. doi:10.1124/jpet.110.172650

Bülow, M. H., Bülow, T. R., Hoch, M., Pankratz, M. J., & Jünger, M. A. (2014). Src tyrosine kinase signaling antagonizes nuclear localization of FOXO and inhibits its transcription factor activity. *Scientific Reports*, *4*, 4048. doi:10.1038/srep04048

C. Ashton, J. (2012). The Atypical Cannabinoid O-1602: Targets, Actions, and the Central Nervous System. *Central Nervous System Agents in Medicinal Chemistry*, *12*(3), 233–239. doi:10.2174/187152412802430156

Cabral, G. A., & Marciano-Cabral, F. (2005). Cannabinoid receptors in microglia of the central nervous system: immune functional relevance. *Journal of Leukocyte Biology*, *78*(6), 1192–7. doi:10.1189/jlb.0405216

Caldwell, M. D., Hu, S. S.-J., Viswanathan, S., Bradshaw, H., Kelly, M. E. M., & Straiker, A. (2013). A GPR18-based signalling system regulates IOP in murine eye. *British Journal of Pharmacology*, *169*(4), 834–43. doi:10.1111/bph.12136

Campbell, V. A. (2001). Tetrahydrocannabinol-induced apoptosis of cultured cortical neurones is associated with cytochrome c release and caspase-3 activation. *Neuropharmacology*, *40*(5), 702–709. doi:10.1016/S0028-3908(00)00210-0

Carlezon Jr, W. A., Duman, R. S., & Nestler, E. J. (2005). The many faces of CREB. *Trends in Neurosciences*, *28*(8), 436–445. doi:http://dx.doi.org/10.1016/j.tins.2005.06.005

Chiba, T., Ueno, S., Obara, Y., & Nakahata, N. (2011). A synthetic cannabinoid, CP55940, inhibits lipopolysaccharide-induced cytokine mRNA expression in a cannabinoid receptor-independent mechanism in rat cerebellar granule cells. *The Journal of Pharmacy and Pharmacology*, *63*(5), 636–47. doi:10.1111/j.2042-7158.2011.01250.x

Clapham, D. E. (2007). Calcium signaling. *Cell*, *131*(6), 1047–58. doi:10.1016/j.cell.2007.11.028

Console-Bram, L., Brailoiu, E., Brailoiu, G. C., Sharir, H., & Abood, M. E. (2014). Activation of GPR18 by cannabinoid compounds: a tale of biased agonism. *British Journal of Pharmacology*, *171*(16), 3908–17. doi:10.1111/bph.12746

D'Amelio, M., Cavallucci, V., Middei, S., Marchetti, C., Pacioni, S., Ferri, A., … Cecconi, F. (2011). Caspase-3 triggers early synaptic dysfunction in a mouse model of Alzheimer's disease. *Nature Neuroscience*, *14*(1), 69–76. doi:10.1038/nn.2709

Di Marzo, V. (2008). Targeting the endocannabinoid system: to enhance or reduce? *Nature Reviews. Drug Discovery*, *7*(5), 438–55. doi:10.1038/nrd2553

Downer, E. J., Gowran, A., Murphy, A. C., & Campbell, V. A. (2007). The tumour suppressor protein, p53, is involved in the activation of the apoptotic cascade by Delta9-tetrahydrocannabinol in cultured cortical neurons. *European Journal of Pharmacology*, *564*(1-3), 57–65. doi:10.1016/j.ejphar.2007.02.025

Dupont, S., Morsut, L., Aragona, M., Enzo, E., Giulitti, S., Cordenonsi, M., … Piccolo, S. (2011). Role of YAP/TAZ in mechanotransduction. *Nature*, *474*(7350), 179–83. doi:10.1038/nature10137

Falasca, M., & Corda, D. (1994). Elevated levels and mitogenic activity of lysophosphatidylinositol in k-ras-transformed epithelial cells. *European Journal of Biochemistry / FEBS*, *221*(1), 383–9. Retrieved from http://www.ncbi.nlm.nih.gov/pubmed/8168525

Falasca, M., Iurisci, C., Carvelli, A., Sacchetti, A., & Corda, D. (1998). Release of the mitogen lysophosphatidylinositol from H-Ras-transformed fibroblasts; a possible mechanism of autocrine control of cell proliferation. *Oncogene*, *16*(18), 2357–65. doi:10.1038/sj.onc.1201758

Falasca, M., Silletta, M. G., Carvelli, A., Di Francesco, A. L., Fusco, A., Ramakrishna, V., & Corda, D. (1995). Signalling pathways involved in the mitogenic action of lysophosphatidylinositol. *Oncogene*, *10*(11), 2113–24. Retrieved from http://www.ncbi.nlm.nih.gov/pubmed/7784056

Ford, L. A., Roelofs, A. J., Anavi-Goffer, S., Mowat, L., Simpson, D. G., Irving, A. J., … Ross, R. A. (2010). A role for L-alpha-lysophosphatidylinositol and GPR55 in the modulation of migration, orientation and polarization of human breast cancer cells. *British Journal of Pharmacology*, *160*(3), 762–71. doi:10.1111/j.1476-5381.2010.00743.x

Formosa, R., & Vassallo, J. (2014). cAMP signalling in the normal and tumorigenic pituitary gland. *Molecular and Cellular Endocrinology*, *392*(1-2), 37–50. doi:10.1016/j.mce.2014.05.004

Friedlander, R. M. (2003). *Apoptosis and Caspases in Neurodegenerative Diseases — NEJM*. Retrieved July 27, 2014, from http://www.nejm.org/doi/full/10.1056/NEJMra022366

Fuchs, A., Rempel, V., & Müller, C. E. (2013). The natural product magnolol as a lead structure for the development of potent cannabinoid receptor agonists. *PloS One*, *8*(10), e77739. doi:10.1371/journal.pone.0077739

Gangadharan, V., Selvaraj, D., Kurejova, M., Njoo, C., Gritsch, S., Skoricová, D., … Kuner, R. (2013). A novel biological role for the phospholipid lysophosphatidylinositol in nociceptive sensitization via activation of diverse G-protein signalling pathways in sensory nerves in vivo. *Pain*, *154*(12), 2801–12. doi:10.1016/j.pain.2013.08.019

Gaoni, Y., & Mechoulam, R. (1964). Isolation, Structure, and Partial Synthesis of an Active Constituent of Hashish. *Journal of the American Chemical Society*, *86*(8), 1646–1647. doi:10.1021/ja01062a046

Gasperi, V., Dainese, E., Oddi, S., Sabatucci, a, & Maccarrone, M. (2013). GPR55 and its interaction with membrane lipids: comparison with other endocannabinoid-binding receptors. *Current Medicinal Chemistry*, *20*(1), 64–78. Retrieved from http://www.ncbi.nlm.nih.gov/pubmed/23151004

Gioeli, D., Mandell, J. W., Petroni, G. R., Frierson, H. F., & Weber, M. J. (1999). Activation of mitogen-activated protein kinase associated with prostate cancer progression. *Cancer Research*, *59*(2), 279–84. Retrieved from http://www.ncbi.nlm.nih.gov/pubmed/9927031

Gonzalez, G. A., & Montminy, M. R. (1989). Cyclic AMP stimulates somatostatin gene transcription by phosphorylation of CREB at serine 133. *Cell*, *59*(4), 675–680. doi:10.1016/0092-8674(89)90013-5

Gowran, A., Noonan, J., & Campbell, V. a. (2011). The multiplicity of action of cannabinoids: implications for treating neurodegeneration. *CNS Neuroscience & Therapeutics*, *17*(6), 637–44. doi:10.1111/j.1755-5949.2010.00195.x

Guo, J., & Ikeda, S. R. (2004). Endocannabinoids modulate N-type calcium channels and G-protein-coupled inwardly rectifying potassium channels via CB1 cannabinoid receptors heterologously expressed in mammalian neurons. *Molecular Pharmacology*, *65*(3), 665–74. doi:10.1124/mol.65.3.665

Gupta, V. K., You, Y., Klistorner, A., & Graham, S. L. (2012). Focus on molecules: Sphingosine 1 phosphate (S1P). *Experimental Eye Research*, *103*, 119–120. Retrieved from http://www.sciencedirect.com/science/article/pii/S0014483511002855

Guzmán, M. (2003). Cannabinoids: potential anticancer agents. *Nature Reviews. Cancer*, *3*(10), 745–55. doi:10.1038/nrc1188

Harkany, T., Mackie, K., & Doherty, P. (2008). Wiring and firing neuronal networks: endocannabinoids take center stage. *Current Opinion in Neurobiology*, *18*(3), 338–45. doi:10.1016/j.conb.2008.08.007

Henstridge, C. (2009). The cellular signalling and physiological significance of the orphan receptor GPR55. Published PhD thesis. University of Dundee.

Henstridge, C. M., Balenga, N. A. B., Ford, L. A., Ross, R. A., Waldhoer, M., & Irving, A. J. (2009a). The GPR55 ligand L-alpha-lysophosphatidylinositol promotes RhoA-dependent Ca2+ signaling and NFAT activation. *FASEB Journal : Official Publication of the Federation of American Societies for Experimental Biology*, *23*(1), 183–93. doi:10.1096/fj.08-108670

Henstridge, C., Arthur, S., & Irving, A. (2009b). *Lack of specificity for cannabinoid CB1 receptor antagonists: interactions with GPR55*. 19th Annual Symposium of the International Cannabinoid Research Society. St. Charles, IL: ICRS.

Henstridge, C. M., Balenga, N. A. B., Kargl, J., Andradas, C., Brown, A. J., Irving, A., … Waldhoer, M. (2011). Minireview: Recent Developments in the Physiology and Pathology of the Lysophosphatidylinositol-Sensitive Receptor GPR55. *Molecular Endocrinology* , *25* (11 ), 1835–1848. doi:10.1210/me.2011-1197

Henstridge, C. M., Balenga, N. A., Schröder, R., Kargl, J. K., Platzer, W., Martini, L., … Irving, A. J. (2010). GPR55 ligands promote receptor coupling to multiple signalling pathways. *British Journal of Pharmacology*, *160*(3), 604–14. doi:10.1111/j.1476-5381.2009.00625.x

Heynen-genel, A. S., Dahl, R., Shi, S., Milan, L., Sergienko, E., Hedrick, M., … Abood, M. E. (2011). Probe Report, 1–26.

Heynen-Genel, S. (2011, May 26). Screening for Selective Ligands for GPR55 - Agonists. National Center for Biotechnology Information (US). Retrieved from http://www.ncbi.nlm.nih.gov/books/NBK66152/

Hubbard, K. B., & Hepler, J. R. (2006). Cell signalling diversity of the Gqalpha family of heterotrimeric G proteins. *Cellular Signalling*, *18*(2), 135–50. doi:10.1016/j.cellsig.2005.08.004

Hurowitz, E. H., Melnyk, J. M., Chen, Y.-J., Kouros-Mehr, H., Simon, M. I., & Shizuya, H. (2000). Genomic Characterization of the Human Heterotrimeric G Protein , , and Subunit Genes. *DNA Research*, *7*(2), 111–120. doi:10.1093/dnares/7.2.111

Irving, A. J., Rae, M. G., & Coutts, A. A. (2002). Cannabinoids on the brain. *TheScientificWorldJournal*, *2*, 632–48. doi:10.1100/tsw.2002.139

Iversen, L. L. (2000). *The science of marijuana*. Oxofrd University Press.

Jacobson, M. D., Weil, M., & Raff, M. C. (1997). Programmed cell death in animal development. *Cell*, *88*(3), 347–54. Retrieved from http://www.ncbi.nlm.nih.gov/pubmed/9039261

Janefjord, E., Mååg, J. L. V, Harvey, B. S., & Smid, S. D. (2013). Cannabinoid Effects on β Amyloid Fibril and Aggregate Formation, Neuronal and Microglial-Activated Neurotoxicity In Vitro. *Cellular and Molecular Neurobiology*, (Milton 2002). doi:10.1007/s10571-013-9984-x

Jänicke, R. U., Sprengart, M. L., Wati, M. R., & Porter, A. G. (1998). Caspase-3 is required for DNA fragmentation and morphological changes associated with apoptosis. *The Journal of Biological Chemistry*, *273*(16), 9357–60. Retrieved from http://www.ncbi.nlm.nih.gov/pubmed/9545256

Johannessen, M., Delghandi, M. P., Seternes, O. M., Johansen, B., & Moens, U. (2004). Synergistic activation of CREB-mediated transcription by forskolin and phorbol ester requires PKC and depends on the glutamine-rich Q2 transactivation domain. *Cellular Signalling*, *16*(10), 1187–99. doi:10.1016/j.cellsig.2004.03.009

Johns, D. G., Behm, D. J., Walker, D. J., Ao, Z., Shapland, E. M., Daniels, D. A., … Douglas, S. A. (2007). The novel endocannabinoid receptor GPR55 is activated by atypical cannabinoids but does not mediate their vasodilator effects. *British Journal of Pharmacology*, *152*(5), 825–31. doi:10.1038/sj.bjp.0707419

Josselyn, S. A., & Nguyen, P. V. (2005). CREB, synapses and memory disorders: past progress and future challenges. *Current Drug Targets. CNS and Neurological Disorders*, *4*(5), 481–97. Retrieved from http://www.ncbi.nlm.nih.gov/pubmed/16266283

Kapur, A., Zhao, P., Sharir, H., Bai, Y., Caron, M. G., Barak, L. S., & Abood, M. E. (2009). Atypical responsiveness of the orphan receptor GPR55 to cannabinoid ligands. *The Journal of Biological Chemistry*, *284*(43), 29817–27. doi:10.1074/jbc.M109.050187

Kargl, J., Brown, A. J., Andersen, L., Dorn, G., Schicho, R., Waldhoer, M., & Heinemann, A. (2013). A selective antagonist reveals a potential role of G protein-coupled receptor 55 in platelet and endothelial cell function. *The Journal of Pharmacology and Experimental Therapeutics*, *346*(1), 54–66. doi:10.1124/jpet.113.204180

Kerr, D. M., Downey, L., Conboy, M., Finn, D. P., & Roche, M. (2013). Alterations in the endocannabinoid system in the rat valproic acid model of autism. *Behavioural Brain Research*, *249*, 124–32. doi:10.1016/j.bbr.2013.04.043

Khoury, E., Clément, S., & Laporte, S. A. (2014). Allosteric and biased g protein-coupled receptor signaling regulation: potentials for new therapeutics. *Frontiers in Endocrinology*, *5*, 68. doi:10.3389/fendo.2014.00068

Kohno, M., Hasegawa, H., Inoue, A., Muraoka, M., Miyazaki, T., Oka, K., & Yasukawa, M. (2006). Identification of N-arachidonylglycine as the endogenous ligand for orphan G-protein-coupled receptor GPR18. *Biochemical and Biophysical Research Communications*, *347*(3), 827–32. doi:10.1016/j.bbrc.2006.06.175

Kotsikorou, E., Lynch, D. L., Abood, M. E., & Reggio, P. H. (2011a). Lipid bilayer molecular dynamics study of lipid-derived agonists of the putative cannabinoid receptor, GPR55. *Chemistry and Physics of Lipids*, *164*(2), 131–43. doi:10.1016/j.chemphyslip.2010.12.003

Kotsikorou, E., Madrigal, K. E., Hurst, D. P., Sharir, H., Lynch, D. L., Heynen-Genel, S., … Reggio, P. H. (2011b). Identification of the GPR55 agonist binding site using a novel set of high-potency GPR55 selective ligands. *Biochemistry*, *50*(25), 5633–47. doi:10.1021/bi200010k

Kotsikorou, E., Sharir, H., Shore, D. M., Hurst, D. P., Lynch, D. L., Madrigal, K. E., … Reggio, P. H. (2013). Identification of the GPR55 Antagonist Binding Site Using a Novel Set of High-Potency GPR55 Selective Ligands.

Kotsikorou, E., Sharir, H., Shore, D. M., Hurst, D. P., Lynch, D. L., Madrigal, K. E., … Reggio, P. H. (2013). Identification of the GPR55 Antagonist Binding Site Using a Novel Set of High-Potency GPR55 Selective Ligands. *Biochemistry*, *52*(52), 9456–69. doi:10.1021/bi4008885

Lamkanfi, M., Festjens, N., Declercq, W., Vanden Berghe, T., & Vandenabeele, P. (2007). Caspases in cell survival, proliferation and differentiation. *Cell Death and Differentiation*, *14*(1), 44–55. doi:10.1038/sj.cdd.4402047

Latt, S. A., & Stetten, G. (1976). Spectral studies on 33258 Hoechst and related bisbenzimidazole dyes useful for fluorescent detection of deoxyribonucleic acid synthesis. *Journal of Histochemistry & Cytochemistry*, *24*(1), 24–33. doi:10.1177/24.1.943439

Latt, S. A., Stetten, G., Juergens, L. A., Willard, H. F., & Scher, C. D. (1975). Recent developments in the detection of deoxyribonucleic acid synthesis by 33258 Hoechst fluorescence. *The Journal of Histochemistry and Cytochemistry : Official Journal of the Histochemistry Society*, *23*(7), 493–505. Retrieved from http://www.ncbi.nlm.nih.gov/pubmed/1095650

Lauckner, J. E., Jensen, J. B., Chen, H.-Y., Lu, H.-C., Hille, B., & Mackie, K. (2008). GPR55 is a cannabinoid receptor that increases intracellular calcium and inhibits M current. *Proceedings of the National Academy of Sciences of the United States of America*, *105*(7), 2699–704. doi:10.1073/pnas.0711278105

Leonard, B. E. (2003). *Fundamentals of Psychopharmacology* (3rd ed.). Wiley.

Mackie, K., & Stella, N. (2006). Cannabinoid receptors and endocannabinoids: evidence for new players. *The AAPS Journal*, *8*(2), E298–306. doi:10.1208/aapsj080234

Matsuda, L. ., Lolait, S. J., Brownstein, M. ., Young, A. ., & Bonner, T. . (1990). Structure of a cannabinoid receptor and functional expression of the cloned cDNA. *Letters to Nature*.

Mattson, M. P. (2000). Apoptosis in neurodegenerative disorders. *Nature Reviews. Molecular Cell Biology*, *1*(2), 120–9. doi:10.1038/35040009

Mayr, B., & Montminy, M. (2001). Transcriptional regulation by the phosphorylation-dependent factor CREB. *Nature Reviews. Molecular Cell Biology*, *2*(8), 599–609. doi:10.1038/35085068

McHugh, D., Hu, S. S. J., Rimmerman, N., Juknat, A., Vogel, Z., Walker, J. M., & Bradshaw, H. B. (2010). N-arachidonoyl glycine, an abundant endogenous lipid, potently drives directed cellular migration through GPR18, the putative abnormal cannabidiol receptor. *BMC Neuroscience*, *11*, 44. doi:10.1186/1471-2202-11-44

Mitton, B., Cho, E.-C., Aldana-Masangkay, G. I., & Sakamoto, K. M. (2011). The function of cyclic-adenosine monophosphate responsive element-binding protein in hematologic malignancies. *Leukemia & Lymphoma*, *52*(11), 2057–63. doi:10.3109/10428194.2011.584994

Moreno, E., Andradas, C., Medrano, M., Caffarel, M. M., Pérez-Gómez, E., Blasco-Benito, S., … Sánchez, C. (2014). Targeting CB2-GPR55 Receptor Heteromers Modulates Cancer Cell Signaling. *The Journal of Biological Chemistry*. doi:10.1074/jbc.M114.561761

Mulder, J., Aguado, T., Keimpema, E., Barabás, K., Ballester Rosado, C. J., Nguyen, L., … Harkany, T. (2008). Endocannabinoid signaling controls pyramidal cell specification and long-range axon patterning. *Proceedings of the National Academy of Sciences of the United States of America*, *105*(25), 8760–5. doi:10.1073/pnas.0803545105

Müller, C. E., Schiedel, A. C., & Baqi, Y. (2012). Allosteric modulators of rhodopsin-like G protein-coupled receptors: opportunities in drug development. *Pharmacology & Therapeutics*, *135*(3), 292–315. doi:10.1016/j.pharmthera.2012.06.002

Munro et al., S. (1993). Molecular characterization of a peripheral receptor for cannabinoids. *Nature*, *365*, 61–65.

Nederlof, P. M., van der Flier, S., Raap, A. K., & Tanke, H. J. (1992). Quantification of inter- and intra-nuclear variation of fluorescence in situ hybridization signals. *Cytometry*, *13*(8), 831–8. doi:10.1002/cyto.990130805

Nevalainen, T., & Irving, A. J. (2010). GPR55, a lysophosphatidylinositol receptor with cannabinoid sensitivity? *Current Topics in Medicinal Chemistry*, *10*(8), 799–813. Retrieved from http://www.ncbi.nlm.nih.gov/pubmed/20370712

Noonan, J., Tanveer, R., Klompas, A., Gowran, A., McKiernan, J., & Campbell, V. a. (2010). Endocannabinoids prevent β-amyloid-mediated lysosomal destabilization in cultured neurons. *The Journal of Biological Chemistry*, *285*(49), 38543–54. doi:10.1074/jbc.M110.162040

Oka, S., Kimura, S., Toshida, T., Ota, R., Yamashita, A., & Sugiura, T. (2010). Lysophosphatidylinositol induces rapid phosphorylation of p38 mitogen-activated protein kinase and activating transcription factor 2 in HEK293 cells expressing GPR55 and IM-9 lymphoblastoid cells. *Journal of Biochemistry*, *147*(5), 671–8. doi:10.1093/jb/mvp208

Oka, S., Nakajima, K., Yamashita, A., Kishimoto, S., & Sugiura, T. (2007). Identification of GPR55 as a lysophosphatidylinositol receptor. *Biochemical and Biophysical Research Communications*, *362*(4), 928–34. doi:10.1016/j.bbrc.2007.08.078

Oka, S., Toshida, T., Maruyama, K., Nakajima, K., Yamashita, A., & Sugiura, T. (2009). 2-Arachidonoyl-sn-glycero-3-phosphoinositol: a possible natural ligand for GPR55. *Journal of Biochemistry*, *145*(1), 13–20. doi:10.1093/jb/mvn136

Onaran, H. O., Rajagopal, S., & Costa, T. (2014). What is biased efficacy? Defining the relationship between intrinsic efficacy and free energy coupling. *Trends in Pharmacological Sciences*, *35*(12), 639–647. doi:10.1016/j.tips.2014.09.010

Pacher, P., Bátkai, S., & Kunos, G. (2006). The endocannabinoid system as an emerging target of pharmacotherapy. *Pharmacological Reviews*, *58*(3), 389–462. doi:10.1124/pr.58.3.2

Pacher, P., & Kunos, G. (2013). Modulating the endocannabinoid system in human health and disease--successes and failures. *The FEBS Journal*, *280*(9), 1918–43. doi:10.1111/febs.12260

Pacher, P., & Mechoulam, R. (2011). Is lipid signaling through cannabinoid 2 receptors part of a protective system? *Progress in Lipid Research*, *50*(2), 193–211. doi:10.1016/j.plipres.2011.01.001

Park, M.-H., Lee, H.-S., Lee, C.-S., You, S. T., Kim, D.-J., Park, B.-H., … Kim, E.-G. (2013). p21-Activated kinase 4 promotes prostate cancer progression through CREB. *Oncogene*, *32*(19), 2475–82. doi:10.1038/onc.2012.255

Penman, J. (2013). GPR55 and N-acyl Amino Acids. Unpublished PhD thesis. University of Dundee.

Perry, V. H., Newman, T. A., & Cunningham, C. (2003). The impact of systemic infection on the progression of neurodegenerative disease. *Nature Reviews. Neuroscience*, *4*(2), 103–12. doi:10.1038/nrn1032

Pertwee, R. G. (2005). *Pharmacological actions of cannabinoids. Handbook of experimental pharmacology* (pp. 1–51). Retrieved from http://www.ncbi.nlm.nih.gov/pubmed/16596770

Pertwee, R. G., Howlett, A. C., Abood, M. E., Alexander, S. P. H., Marzo, V. Di, Elphick, M. R., … Kunos, G. (2010). International Union of Basic and Clinical Pharmacology . LXXIX . Cannabinoid Receptors and Their Ligands : Beyond CB 1 and CB 2, *62*(4), 588–631. doi:10.1124/pr.110.003004.588

Pietr, M., Kozela, E., Levy, R., Rimmerman, N., Lin, Y. H., Stella, N., … Juknat, A. (2009). Differential changes in GPR55 during microglial cell activation. *FEBS Letters*, *583*(12), 2071–6. doi:10.1016/j.febslet.2009.05.028

Piñeiro, R., & Falasca, M. (2012). Lysophosphatidylinositol signalling: New wine from an old bottle. *Biochimica et Biophysica Acta (BBA) - Molecular and Cell Biology of Lipids*, *1821*(4), 694–705. Retrieved from http://www.sciencedirect.com/science/article/pii/S1388198112000145

Piñeiro, R., Maffucci, T., & Falasca, M. (2011). The putative cannabinoid receptor GPR55 defines a novel autocrine loop in cancer cell proliferation. *Oncogene*, *30*(2), 142–52. doi:10.1038/onc.2010.417

Porter, A. G., & Jänicke, R. U. (1999). Emerging roles of caspase-3 in apoptosis. *Cell Death and Differentiation*, *6*(2), 99–104. doi:10.1038/sj.cdd.4400476

Potapova, T. A., Sivakumar, S., Flynn, J. N., Li, R., & Gorbsky, G. J. (2011). Mitotic progression becomes irreversible in prometaphase and collapses when Wee1 and Cdc25 are inhibited. *Molecular Biology of the Cell*, *22*(8), 1191–206. doi:10.1091/mbc.E10-07-0599

Price, D. T., Della Rocca, G., Guo, C., Ballo, M. S., Schwinn, D. A., & Luttrell, L. M. (1999). Activation of extracellular signal-regulated kinase in human prostate cancer. *The Journal of Urology*, *162*(4), 1537–42. Retrieved from http://www.ncbi.nlm.nih.gov/pubmed/10492251

Raj, G. V, Barki-Harrington, L., Kue, P. F., & Daaka, Y. (2002). Guanosine phosphate binding protein coupled receptors in prostate cancer: a review. *The Journal of Urology*, *167*(3), 1458–63. Retrieved from http://www.ncbi.nlm.nih.gov/pubmed/11832770

Rempel, V., Volz, N., Gläser, F., Nieger, M., Bräse, S., & Müller, C. E. (2013). Antagonists for the orphan G-protein-coupled receptor GPR55 based on a coumarin scaffold. *Journal of Medicinal Chemistry*, *56*(11), 4798–810. doi:10.1021/jm4005175

Romero-Zerbo, S. Y., Rafacho, A., Díaz-Arteaga, A., Suárez, J., Quesada, I., Imbernon, M., … Bermúdez-Silva, F. J. (2011). A role for the putative cannabinoid receptor GPR55 in the islets of Langerhans. *The Journal of Endocrinology*, *211*(2), 177–85. doi:10.1530/JOE-11-0166

Ruban, E. L., Ferro, R., Arifin, S. A., & Falasca, M. (2014). Lysophosphatidylinositol: a novel link between ABC transporters and G-protein-coupled receptors. *Biochemical Society Transactions*, *42*(5), 1372–7. doi:10.1042/BST20140151

Ryberg, E., Larsson, N., Sjögren, S., Hjorth, S., Hermansson, N.-O., Leonova, J., … Greasley, P. J. (2007). The orphan receptor GPR55 is a novel cannabinoid receptor. *British Journal of Pharmacology*, *152*(7), 1092–101. doi:10.1038/sj.bjp.0707460

Sawzdargo, M., Nguyen, T., Lee, D. K., Lynch, K. R., Cheng, R., Heng, H. H. ., … O'Dowd, B. F. (1999). Identification and cloning of three novel human G protein-coupled receptor genes GPR52, ΨGPR53 and GPR55: GPR55 is extensively expressed in human brain1Sequence data from this article have been deposited with the GenBank Data Library under Accession Nos. . *Molecular Brain Research*, *64*(2), 193–198. Retrieved from http://www.sciencedirect.com/science/article/pii/S0169328X98002770

Schmuhl, E., Ramer, R., Salamon, A., Peters, K., & Hinz, B. (2014). Increase of mesenchymal stem cell migration by cannabidiol via activation of p42/44 MAPK. *Biochemical Pharmacology*, *87*(3), 489–501. doi:10.1016/j.bcp.2013.11.016

Schuelert, N., & McDougall, J. J. (2011). The abnormal cannabidiol analogue O-1602 reduces nociception in a rat model of acute arthritis via the putative cannabinoid receptor GPR55. *Neuroscience Letters*, *500*(1), 72–6. doi:10.1016/j.neulet.2011.06.004

Sharir, H., & Abood, M. E. (2010). Pharmacological characterization of GPR55, a putative cannabinoid receptor. *Pharmacology & Therapeutics*, *126*(3), 301–13. doi:10.1016/j.pharmthera.2010.02.004

Sharir, H., Console-Bram, L., Mundy, C., Popoff, S. N., Kapur, A., & Abood, M. E. (2012). The endocannabinoids anandamide and virodhamine modulate the activity of the candidate cannabinoid receptor GPR55. *Journal of Neuroimmune Pharmacology : The Official Journal of the Society on NeuroImmune Pharmacology*, *7*(4), 856–65. doi:10.1007/s11481-012-9351-6

Shaywitz, A. J., & Greenberg, M. E. (1999). CREB: a stimulus-induced transcription factor activated by a diverse array of extracellular signals. *Annual Review of Biochemistry*, *68*, 821–61. doi:10.1146/annurev.biochem.68.1.821

Sheng, M., Thompson, M., & Greenberg, M. (1991). CREB: a Ca(2+)-regulated transcription factor phosphorylated by calmodulin-dependent kinases. *Science*, *252*(5011), 1427–1430. doi:10.1126/science.1646483

Sisay, S., Pryce, G., Jackson, S. J., Tanner, C., Ross, R. A., Michael, G. J., … Baker, D. (2013). Genetic background can result in a marked or minimal effect of gene knockout (GPR55 and CB2 receptor) in experimental autoimmune encephalomyelitis models of multiple sclerosis. *PloS One*, *8*(10), e76907. doi:10.1371/journal.pone.0076907

Soga, T., Ohishi, T., Matsui, T., Saito, T., Matsumoto, M., Takasaki, J., … Furuichi, K. (2005). Lysophosphatidylcholine enhances glucose-dependent insulin secretion via an orphan G-protein-coupled receptor. *Biochemical and Biophysical Research Communications*, *326*(4), 744–51. doi:10.1016/j.bbrc.2004.11.120

Stevenson, A. S., Cartin, L., Wellman, T. L., Dick, M. H., Nelson, M. T., & Lounsbury, K. M. (2001). Membrane depolarization mediates phosphorylation and nuclear translocation of CREB in vascular smooth muscle cells. *Experimental Cell Research*, *263*(1), 118–30. doi:10.1006/excr.2000.5107

Sylantyev, S., Jensen, T. P., Ross, R. A., & Rusakov, D. A. (2011). The enigmatic receptor GPR55 potentiates neurotransmitter release at central synapses. *Neuroscience Meeting Planner Washington, DC: Society for Neuroscience Online: Program,*, *653*.

Sylantyev, S., Jensen, T. P., Ross, R. A., & Rusakov, D. A. (2013). Cannabinoid- and lysophosphatidylinositol-sensitive receptor GPR55 boosts neurotransmitter release at central synapses. *Proceedings of the National Academy of Sciences of the United States of America*, *110*(13), 5193–8. doi:10.1073/pnas.1211204110

Thompson, C. B. (1995). Apoptosis in the pathogenesis and treatment of disease. *Science (New York, N.Y.)*, *267*(5203), 1456–62. Retrieved from http://www.ncbi.nlm.nih.gov/pubmed/7878464

Walker, W. H., & Habener, J. F. (1996). Role of transcription factors CREB and CREM in cAMP-regulated transcription during spermatogenesis. *Trends in Endocrinology and Metabolism: TEM*, *7*(4), 133–8. Retrieved from http://www.ncbi.nlm.nih.gov/pubmed/18406739

Wolf, H. K., Buslei, R., Schmidt-Kastner, R., Schmidt-Kastner, P. K., Pietsch, T., Wiestler, O. D., & Blumcke, I. (1996). NeuN: a useful neuronal marker for diagnostic histopathology. *Journal of Histochemistry & Cytochemistry*, *44*(10), 1167–1171. doi:10.1177/44.10.8813082

Yamashita, A., Oka, S., Tanikawa, T., Hayashi, Y., Nemoto-Sasaki, Y., & Sugiura, T. (2013). The actions and metabolism of lysophosphatidylinositol, an endogenous agonist for GPR55. *Prostaglandins & Other Lipid Mediators*, *107*, 103–16. doi:10.1016/j.prostaglandins.2013.05.004

Yin, H., Chu, A., Li, W., Wang, B., Shelton, F., Otero, F., … Chen, Y. A. (2009). Lipid G protein-coupled receptor ligand identification using beta-arrestin PathHunter assay. *The Journal of Biological Chemistry*, *284*(18), 12328–38. doi:10.1074/jbc.M806516200

Zhang, J.-H., Zhang, Y., & Herman, B. (2003). Caspases, apoptosis and aging. *Ageing Research Reviews*, *2*(4), 357–366. doi:10.1016/S1568-1637(03)00026-6

Zhang, X., Maor, Y., Wang, J. F., Kunos, G., & Groopman, J. E. (2010). Endocannabinoid-like N-arachidonoyl serine is a novel pro-angiogenic mediator. *British Journal of Pharmacology*, *160*(7), 1583–94. doi:10.1111/j.1476-5381.2010.00841.x